ABSTRACT

Title of Thesis: BRED VECTORS, SINGULAR VECTORS, AND LYAPUNOV VECTORS IN SIMPLE AND COMPLEX MODELS

Adrienne Norwood, Doctor of Philosophy, 2015

Directed by: Professor Eugenia Kalnay, Atmospheric and Oceanic Sciences Department

We compute and compare three types of vectors frequently used to explore the instability properties of dynamical models, Lyapunov vectors (LVs), singular vectors (SVs), and bred vectors (BVs). The first model is the Lorenz (1963) three-variable model. We find BVs align with the *locally fastest growing* LV, which is often the second fastest growing global LV. The growth rates of the three types of vectors reveal all predict regime changes and durations of new regimes, as shown for BVs by Evans et al. (2004). The second model is the toy 'atmosphere-ocean model' developed by Peña and Kalnay (2004) coupling three Lorenz (1963) models with different time scales to test the effects of fast and slow modes of growth on the dynamical vectors. A fast 'extratropical atmosphere' is weakly coupled to a fast 'tropical atmosphere' which is strongly coupled to a slow 'ocean' system, the latter coupling imitating the tropical El Niño–Southern Oscillation. BVs separate the fast and slow modes of growth through appropriate selection of the breeding parameters. LVs successfully separate the fast 'extratropics' but cannot completely decouple the 'tropics' from the 'ocean,' leading to 'coupled' LVs that are affected by both systems but mainly dominated by one. SVs identify the fast modes but cannot capture the slow modes until the fast 'extratropics' are replaced with faster 'convection.' The dissimilar behavior of the three types of vectors degrades the

similarities of the subspaces they inhabit (Norwood et al. 2013). The third model is a quasi-geostrophic channel model (Rotunno and Bao 1996) that is a simplification of extratropical synoptic-scale motions with baroclinic instabilities only. We were unable to successfully compute LVs for it. However, randomly initialized BVs quickly converge to a single vector that is the leading LV. The last model is the SPEEDY model created by Molteni (2003). It is a simplified general atmospheric circulation model with several types of instabilities saturating at different time scales. Through proper selection of the breeding parameters, BVs identify baroclinic and convective instabilities. When the amplitude and rescaling period are further reduced, all BVs converge to a single vector associated with Lamb waves, something never before observed.

BRED VECTORS, SINGULAR VECTORS, AND LYAPUNOV VECTORS IN SIMPLE AND COMPLEX MODELS

By

Adrienne Norwood

Dissertation submitted to the Faculty of the Graduate School of the
University of Maryland, College Park, in partial fulfillment
of the requirements for the degree of
Doctor of Philosophy
2015

Advisory Committee:
Professor Eugenia Kalnay, Chair
Professor James Carton
Professor Brian Hunt
Professor Kayo Ide
Professor Shu-Chih Yang

Acknowledgements

I am sure I am not the only graduate student who has found this to be a very difficult process. Thus I would like to thank God because I am sure it is a miracle that I have made it this far. I would also like to thank my advisor Professor Eugenia Kalnay for all of her kindness, patience, support, and guidance. I have learned so much from working with her, and it has been a great honor. I would also like to thank my other committee members Professors James Carton, Brian Hunt, Kayo Ide, and Shu-Chih Yang for their time, helpful comments, insightful suggestions, and enlightening conversations. I am especially grateful to Dr. Yang for all of her old code and assistance and Dr. Christopher Wolfe, whose code greatly assisted my understanding of the wonderful algorithm he developed with Dr. Roger Samelson.

I greatly appreciate Jeffrey Henrikson, David Yanuk, and everyone at the Physics Helpdesk who have aided me in getting the most from my aging computer. I would also like to thank the members of the Weather Chaos group for their help and suggestions.

Finally, I would like to thank my family for being encouraging, patient, and supportive throughout this process.

Table of Contents

List of Tables

List of Figures

Chapter 1 : Introduction

1.1 Importance and theory of bred vectors, singular vectors, and Lyapunov vectors

Weather and climate forecasts are encumbered with errors originating from inexact observations, numerical methods, and, very importantly, the instabilities inherent in the atmosphere-ocean system. Thus even with exact observations and a perfect model, the instabilities of a system will degrade and limit its predictability (Lorenz 1963, 1965). Much work has been done to characterize this innate chaos (e.g. Benettin *et al.* 1980; Toth and Kalnay 1993; Trevisan and Legnani 1995; Pazó *et al.* 2010) developing and improving upon the goal of identifying the unstable subspace that determines the fastest growing and/or the errors with the largest growing amplitude responsible for the deterioration of forecasts.

In this thesis we compute and compare the three types of vectors frequently used to explore the instability properties of dynamical models, namely Lyapunov vectors (LVs), singular vectors (SVs) and bred vectors (BVs). Of the three types of vectors, the simplest and cheapest to compute are BVs, since they only require running the nonlinear model once for the control run and once for the perturbed solution corresponding to each bred vector. The difference between the perturbed and the control runs is periodically rescaled to the initial amplitude, and added to the control. It is easy to see that, by construction, leading (i.e. fastest growing) bred vectors are related to the (leading) LVs. In fact, for

very small amplitudes and very short rescaling windows, bred vectors align with the leading Lyapunov vector.

SVs for a given time window are computed as the eigenvectors of the matrix representing the Tangent Linear Model (TLM), or propagator, left multiplied by the adjoint (ADJ) of the TLM. This matrix is Hermitian; thus the SVs form an orthogonal basis throughout the time window. The singular values are equal to the square root of the corresponding growth rate, σ^2, since the norm of the initial SV (ISV) propagated forward by the TLM and evolved into the final SV (FSV) grows by σ at the end of the time window; the FSV, integrated backward using the ADJ so that it evolves into the ISV, in turn *also* grows by σ. The ISVs are very sensitive to the choice of both the norm and the optimization window (Errico and Vukicevic 1992). However, as the window length approaches infinity, the FSVs converge to the LVs orthonormalized in decreasing order of their growth rates. Correspondingly, when the window is extended backward toward negative infinity, the ISVs converge to the LVs orthonormalized in increasing order of their growth rates so that the (non-orthogonal) Lyapunov vectors can be computed from the complete sets of FSVs and ISVs (Trevisan and Pancotti 1998). Wolfe and Samelson (2007, WS07) extended Trevisan and Pancotti's approach with a more efficient algorithm (used in this thesis) that computes the leading LVs as a function of the leading FSVs and ISVs only (section 1.4).

Singular and bred vectors have been widely used for the creation of initial perturbations for ensemble forecasting, and their construction algorithms are widely described (e.g., Molteni and Palmer 1993, Toth and Kalnay 1997). Although the leading LV, the leading FSV, and the BVs of a dynamical model are strongly related and rather

easily determined, the non-leading LVs are much more difficult to isolate (see the algorithms of Benettin *et al.* 1980; Shimada and Nagashima 1979; Wolfe and Samelson 2007; and Ginelli *et al.* 2007).

In this thesis we determine the BVs, SVs, and LVs of two simple models using the WS07 algorithm, and compare their evolution in time and their characteristic behavior. The first is the Lorenz (1963) model. It has three degrees of freedom and well-known instability characteristics with one dominant time scale. The second is a toy 'coupled atmosphere-ocean model' with nine degrees of freedom composed of three Lorenz models, with a slow 'ocean' strongly coupled with a fast 'tropical atmosphere,' in turn weakly coupled with a fast 'extratropical atmosphere' (Peña and Kalnay 2004). The second model has two time scales, a slow one associated with 'El Niño' oscillations and a fast one associated with 'extratropical weather.' We then replace the 'extratropical atmosphere' with 'convection' causing the nine-variable model to have three time scales. Next we compute the BVs and SVs for a quasi-geostrophic model developed by Rotunno and Bao (1996) with over 14,000 degrees of freedom and instabilities of one time scale. The SVs fail to converge, rendering the use of the WS07 algorithm impossible, but results with the BVs provide strong evidence to the existence of a leading LV for the model. Finally we examine the BVs of the Simplified Parameterizations, primitivE-Equation DYnamics (SPEEDY) model (Molteni, 2003) which has 135,240 degrees of freedom and instabilities of several time scales, including weather waves, convective instabilities, and inertia gravity waves. Again, results with the BVs lead to strong evidence for the existence of a leading LV, but it corresponds to horizontal inertia sound

waves (Lamb waves), meaning it may not be useful for initializing ensembles in weather forecasting.

Some of the questions we attempt to address using these models are related to real weather and climate problems that have been noted in the past. For example, Lorenz (1996) addressed how to obtain LVs for a system that has more than one time scale and suggested a method very similar to breeding. Boffetta *et al.* (1998) used finite size Lyapunov exponents (which are close in construction to the bred vectors used here) to successfully separate quickly growing fast errors and slowly growing large errors. Toth and Kalnay (1997) computed twenty BVs for the NCEP operational system, each starting from different random initial perturbations, and identified approximately ten independent regions of instability in each hemisphere, where the majority of BVs converged to the same shapes, but with random signs. Since the construction of BVs is a nonlinear, finite time, finite amplitude generalization of the leading LV, it is clear that the BVs do not converge to a single leading LV unless their rescaling amplitude is very small. In fact, we will show that nonlinear BVs, those whose amplitudes and rescaling windows are large enough to cause a separation between them and the leading LV but small enough to remain pertinent to the instabilities of the system, converge to the *locally* fastest growing LV even if it is different from LV1 (that is, the leading Lyapunov vector). We also found that for systems with multiple time scales, it is possible to find BVs, under certain conditions SVs, and, when they can be computed, LVs that are associated with the fast and slow instabilities. More work is needed to ascertain if these results are applicable to a full weather-climate system.

The thesis is organized as follows: In the remainder of chapter 1 we describe the algorithms used to obtain the three types of vectors. Chapter 2 compares the BVs, SVs, and LVs in the classic Lorenz (1963) three-variable model, and discusses what these results imply for a system dominated by a single type of instability. (Many of the results of chapters 1 and 2 have been presented in Norwood *et al.* 2013.) Chapter 3 introduces the nine-variable toy coupled model and the corresponding BVs, SVs, and LVs, and their properties are presented and discussed. Chapter 4 discusses the results with the Rotunno Bao (1996) quasi-geostrophic (QG) model, a more complex model with a single type of instability similar to weather waves. Chapter 5 compares BVs found for the SPEEDY model (Molteni, 2003) and what these results imply for the existence of a leading LV in systems with instabilities of several time scales. Chapter 6 is a summary and discussion of the implications of these results for realistic, large atmospheric and oceanic models.

1.2 Computation of bred vectors

Of the three types of vectors, bred vectors are the easiest and fastest to compute. Toth and Kalnay (1993) first developed BVs as a way to capture the errors present in the initial conditions and how they grow within short- and medium-range weather forecasts. Their objective was to produce ensembles with a strongly growing spread that are representative of the largest instabilities, with minimal computational effort. Thus the nonlinear model is used to obtain these simple yet powerful vectors.

One begins by integrating the nonlinear model, M, for a specified amount of time to obtain the control trajectory, x_c. A perturbation size, δ_0,and an integration window, IW,

are chosen based upon the saturation amplitude and time scale for the mode of growth one wishes to target (see Peña and Kalnay 2004, PK04; S.-C. Yang *et al.* 2006a; and chapters 3 and 5). Nonlinear error growth rates are dominated by instabilities with different time scales, and thus are characterized by different saturation rates. The selection of different perturbation sizes and integration windows allows one to also study the effects of linear and nonlinear disturbances on error growth (see Evans *et al.* 2004 and chapter 2). The initial sizes of the perturbation and integration window are also known as the breeding rescaling amplitude and period, respectively. At every breeding cycle, a perturbation direction is determined, scaled to size δ_0, and added to the initial condition of the control, $x_c(t_i)$. Thus the initial condition for the perturbed trajectory is

$$x_p(t_i) = x_c(t_i) + \delta_0 \frac{p(t_i)}{||p(t_i)||}, \quad (1)$$

where $\frac{p(t_i)}{||p(t_i)||}$ is the direction of the perturbation at time t_i. The nonlinear model is then integrated forward starting from $x_p(t_i)$. At the end of the integration interval, the BV is obtained by subtracting the control trajectory from the perturbed trajectory at time t_{i+IW}:

$$bv(t_{i+IW}) = x_p(t_{i+IW}) - x_c(t_{i+IW}). \quad (2)$$

The process is then repeated from (1) with $p(t_{i+IW}) = bv(t_{i+IW})$ as the perturbation for the next integration interval. BVs can be computed at every time by looping through (1) and (2) beginning at successive initial points. Note that as the

rescaling amplitude $\delta_0 \to 0$, the BVs will converge to the leading Lyapunov vector, which is proportional to the leading asymptotic final singular vector.

The main parameters of interest are the rescaling interval and perturbation amplitude because they directly relate to the dynamics of the system. Pazó *et al.* (2010) demonstrate that the choice of norm used to determine the perturbation size may have important implications on the effectiveness of the ensembles created from the BVs. Here we do not study the effect of the choice of norm on the results and simply use one norm for each model. We compute the local-in-time growth rates as $\frac{1}{dt*IW}\ln(\frac{||bv||}{\delta_0})$, where dt is the integration time period.

1.3 Computation of singular vectors

Singular vectors are a set of perturbations that will maximize the perturbation growth for a chosen norm and optimization period. More precisely, the initial singular vectors are valid at the beginning of the optimization period, and they evolve into the final singular vectors at the end of the optimization period. SVs, although not as simple to compute as bred vectors, have a well-known, fairly simple algorithm for their calculation, and their usefulness in numerical weather prediction has been studied for several years (Buizza *et al.* 1993; Errico and Vukicevic 1992).

With a nonlinear model, M, the tangent linear model (TLM), computed as $\mathbf{M_{ij}} = \frac{\partial M_i}{\partial x_j}$, can be used to evolve perturbations linearly from time t_i to time t_{i+IW}. The leading initial singular vectors are those perturbations that grow fastest during the optimization

period, so that a cost function, defined as the perturbation growth within the period t_i to t_{i+IW}, is

$$J = \frac{\left|\left|\eta(t_{i+IW})\right|\right|_{\mathbf{Q}}^2}{\left|\left|\xi(t_i)\right|\right|_{\mathbf{P}}^2} = \frac{\xi(t_i)^*\mathbf{M}(t_i, t_{i+IW})^*\mathbf{Q}^*\mathbf{Q}\mathbf{M}(t_i, t_{i+IW})\xi(t_i)}{\xi(t_i)^*\mathbf{P}^*\mathbf{P}\xi(t_i)}. \quad (3)$$

$\xi(t_i)$ denotes the ISV at time t_i and $\eta(t_{i+IW})$ denotes the final singular vector at time t_{i+IW} into which $\xi(t_i)$ evolves. Note that in (3), the initial and final perturbation amplitudes are defined with norms **P** and **Q**, respectively. $\mathbf{M}(t_i, t_{i+IW})^*$ is the adjoint model (ADJ) that integrates the perturbations backward from time t_{i+IW} to t_i. Errico and Vukicevic (1992) indicated that the SVs are very dependent on the choice of norm and the length of the optimization period. Also, maximizing (3) is equivalent to finding the leading eigenvector of the matrix $\mathbf{M}^*\mathbf{M}$, where we have dropped the time dependence. This eigenvector, denoted as ξ_1, will be the leading ISV with a growth of σ_1. To calculate all the eigenvectors corresponding to different perturbation growths, we set up the eigen-equation

$$\mathbf{M}^*\mathbf{M}\boldsymbol{\Xi} = \boldsymbol{\Xi}\mathbf{S}. \quad (4)$$

The *j*th column of matrix $\boldsymbol{\Xi}$ corresponds to the *j*th ISV, ξ_j, and the *j*th diagonal element of **S**,contains its corresponding eigenvalue, σ_j^2.

Since $\mathbf{M}^*\mathbf{M}$ is Hermitian, the matrix $\boldsymbol{\Xi}$**,** of right (initial) singular vectors of matrix **M**, is unitary. The corresponding unitary matrix of left (final) singular vectors aligned along the columns of matrix **H** satisfy $\mathbf{M}(t_i, t_{i+IW})\boldsymbol{\Xi}(t_i) = \mathbf{H}(t_{i+IW})\boldsymbol{\Sigma}$, where $\boldsymbol{\Sigma}$ is a diagonal matrix of the singular values, σ_j, in decreasing order. Thus **H** contains the final

singular vectors (FSVs), obtained as the linear evolution of the ISVs contained in $\boldsymbol{\Xi}$, with a growth rate corresponding to their corresponding singular values, σ_j. The *j*th FSV, denoted as η_j, is the *j*th column vector of **H**. We also note that the eigenvalues in (4) are the squares of the singular values. Therefore, by applying $\mathbf{M}^*\mathbf{M}$ to ξ_j, it will grow (or decay) by a factor of σ_j^2.

The conversion between the initial (ξ_j) and final (η_j) SVs for a window from t_i to t_{i+IW} is done applying the TLM and ADJ operators:

$$\mathbf{M}(t_i, t_{i+IW})\xi_j(t_i) = \sigma_j\eta_j(t_{i+IW}), \quad (5)$$

$$\mathbf{M}(t_i, t_{i+IW})^*\eta_j(t_{i+IW}) = \sigma_j\xi_j(t_i). \quad (6)$$

In (5) and (6), the *j*th FSV, η_j, is derived by integrating ξ_j forward in time, while the *j*th ISV is derived by integrating backward in time. From (5) we see transformation under the TLM will rotate ξ_1 to the direction of η_1 and cause its length to grow by σ_1. This gives the exact location of the fastest growing direction and its growth rate. This property is important when attempting to create fast growing perturbations for ensemble predictions.

Since the construction of the TLM for the chosen optimization period depends on the background trajectory, it is not a constant operator for nonlinear dynamics. Thus its influence over a perturbation's behavior is strongly controlled by the integration interval. The interval must be small enough for the tangent linear assumption to remain valid yet large enough to provide dynamically significant results. We note that Legras and Vautard (1996) named the initial SVs, ξ_j , 'forward SVs' (because they are initialized in the future) and the final SVs, η_j , 'backward SVs' (because they are initialized in the past).

The local growth of the initial SV when it is evolved with the TLM to time t_{i+IW} is equal to the growth rate of the final SV when it is evolved with the ADJ to time t_i, and both are given by $\frac{\ln(\sigma_j)}{dt*IW}$ (for their respective times). The growth rates of BVs are slightly smaller than those of the leading SVs, but as the integration time for the SVs increases, the leading final SV, η_1, converges to LV1, the leading Lyapunov vector, which is similar to the BV (see chapter 2).

The computation of the Lyapunov vectors in the following section is based on *asymptotic* initial ($\hat{\xi}_j$) and final ($\hat{\eta}_j$) SVs that were given enough time to converge to a single solution. In other words, the asymptotic SVs are the solutions obtained when computed with an 'infinite' integration window, with the initial state going infinitely far back into the past to obtain the FSVs and infinitely far forward into the future to obtain the ISVs. If the LVs were recurrently orthogonalized they would coincide with the FSVs (when integrating forward in time) and the ISVs (when integrating backward in time) (Trevisan and Pancotti, 1998). This result is the basis of the Wolfe and Samelson (2007) algorithm used to compute Lyapunov vectors, which is described below.

1.4 Computation of Lyapunov vectors

The leading (fastest growing) Lyapunov vector can be obtained by integrating the tangent linear model (TLM) for sufficiently long times starting from a random initial perturbation. Since all perturbations converge to the leading LV as integration time increases, this is a fairly simple and straightforward method to use. Benettin *et al.* (1980) and Shimada and Nagashima (1979) expanded this method to find a set of orthonormal

vectors in the tangent space of the trajectory that span the same subspaces as the LVs by recurrently orthonormalizing initially random perturbations. This orthogonalization, being norm dependent, is not preserved by the tangent linear flow. Thus an orthogonalized set of LVs computed at one time will not evolve into an orthogonalized set of LVs at some future time. For example, if the LVs generated by the Benettin *et al.* (1980) algorithm are integrated backward in time, all (except the first) will rotate toward the most rapidly decaying LVs since orthogonalization starting with the leading LV will produce projections onto the decaying LVs (WS07). Ginelli *et al.* (2007) developed an algorithm for covariant Lyapunov vectors (those which are invariant under the tangent and adjoint linear flow, i.e. LVs computed at a given time evolve into LVs at future and past times) by using the QR algorithm. In the same year, Wolfe and Samelson published their algorithm, building upon the work of Trevisan and Pancotti (1998), which efficiently combines asymptotic initial and final singular vectors to determine the coefficients of covariant LVs. Because we wish to compare LVs to BVs and SVs, it is simpler for us to use the method proposed by Wolfe and Samelson. We briefly describe the WS07 algorithm.

Beginning from the TLM, $\mathbf{M}$, it can be shown (Oseledec 1968) that the Lyapunov exponents, λ_n, are the logarithms of the eigenvalues of

$$S^{+} = \lim_{t_2 \to +\infty} [\mathbf{M}(t, t_2)^{*} \mathbf{M}(t, t_2)]^{\frac{1}{2(t_2 - t)}}, \tag{7a}$$

$$S^{-} = \lim_{t_1 \to -\infty} [\mathbf{M}(t_1, t) \mathbf{M}(t_1, t)^{*}]^{\frac{1}{2(t - t_1)}}, \tag{7b}$$

where $\mathbf{M}^*$ is the adjoint. According to Oseledec's theorem, the norm-independent Lyapunov vectors, ϕ_n, corresponding to these Lyapunov exponents exist. In other words, for almost every time t, integrating forward in time every vector *y* in the tangent space $S_1^+(t)$ of the attractor of the dynamical system grows asymptotically at the rate λ_1 with the exception of any *y* belonging to $S_2^+(t)$. In this case, *y* grows asymptotically at the rate λ_2, unless *y* belongs to $S_3^+(t)$, and so on. As one integrates back in time, for almost every time t, every vector y in the tangent space $S_N^-(t)$ of the attractor of the dynamical system grows asymptotically at the rate λ_N, where N is the number of degrees of freedom of the system, with the exception of any y belonging to $S_{N-1}^-(t)$. In this case y grows asymptotically at the rate λ_{N-1}. One continues in this manner until there are L Lyapunov vectors, ϕ_n, growing (or decaying) at a rate of $\pm\lambda_n$ as $t \to \pm\infty$, where L is the number of distinct Lyapunov exponents. (Kuptsov and Parlitz 2012 discuss an algorithm for the case $L \neq N$, but, like WS07, we shall assume the non-degenerative case.) Using this definition of Lyapunov vectors, one finds vectors that characterize dynamical instabilities both forward and backward in time. This definition most closely relates to that of characteristic Lyapunov vectors (Trevisan and Pancotti, 1998).

The above theorem demonstrates the existence of the Lyapunov vectors and where to find them, but, unfortunately, it does not provide a straightforward algorithm to compute them. From section 1.3 we know singular vectors and their growth rates are computationally expensive but relatively straightforward to compute. Also note that as time approaches infinity in (7a), we obtain asymptotic values of the initial singular vectors, ξ_j. As time approaches infinity in (7b) we obtain asymptotic values of the final

singular vectors, η_j. Since they are asymptotically related to Lyapunov vectors, WS07 exploit this relationship, and use SVs to compute LVs. Let $\hat{\eta}_j$ represent the asymptotic final singular vectors and $\hat{\xi}_j$ represent the asymptotic initial singular vectors. Each set of SVs spans the space of the dynamical system. Thus ϕ_n can be written as a linear combination of either set:

$$\phi_n(t) = \sum_{i=1}^{N} < \hat{\xi}_i(t), \phi_n(t) > \hat{\xi}_i(t), \quad (8a)$$

$$\phi_n(t) = \sum_{j=1}^{N} < \hat{\eta}_j(t), \phi_n(t) > \hat{\eta}_j(t). \quad (8b)$$

As a consequence of errors aligning with the most unstable direction, if a vector is initialized in the distant past, and the model is integrated forward to the present, this vector will align with the most rapidly growing (leading) Lyapunov vector. Thus, $\hat{\eta}_1(t) = c_1^1 \phi_1(t)$ for some constant c_1^1. $\hat{\eta}_2(t)$ is orthogonal to $\hat{\eta}_1(t)$, which means $\hat{\eta}_2(t)$ must have a component that projects onto the second leading Lyapunov vector. Thus, $\hat{\eta}_2(t) = c_1^2 \phi_1(t) + c_2^2 \phi_2(t)$; which implies for coefficients c_i^j, where i is an index corresponding to the LV of interest and j corresponds to the SV of interest,

$$\hat{\eta}_j(t) = \sum_{i=1}^{j} c_i^j \phi_i(t). \quad (9)$$

But $\hat{\xi}_j(t)$, which is initialized in the distant future and evolved back in time, will align with the most rapidly decaying Lyapunov vector, $\phi_N(t)$, where *N* is the degrees of freedom in the model. Thus for coefficients d_i^j, where i is an index corresponding to the LV of interest and j corresponds to the SV of interest,

$$\hat{\xi}_j(t) = \sum_{i=j}^{N} d_i^j \phi_i(t). \qquad (10)$$

Hence $< \phi_i, \hat{\eta}_j > = 0$ for $i > j$ and $< \phi_i, \hat{\xi}_j > = 0$ for $i < j$. Consequently equations (8*a*) and (8*b*) can be rewritten as

$$\phi_n(t) = \sum_{i=n}^{N} < \hat{\xi}_i(t), \phi_n(t) > \hat{\xi}_i(t) \qquad (11a)$$

$$\phi_n(t) = \sum_{j=1}^{n} < \hat{\eta}_j(t), \phi_n(t) > \hat{\eta}_j(t). \qquad (11b)$$

WS07 show that the *n* leading Lyapunov vectors can be found by solving $D^{(n)}y^{(n)} = 0$, where

$$D_{kj}^{(n)} = \sum_{i=1}^{n-1} < \hat{\eta}_k(t), \hat{\xi}_i(t) >< \hat{\xi}_i(t), \hat{\eta}_j(t) > \qquad k, j \leq n,$$

$$y_k^{(n)} = < \hat{\eta}_k(t), \phi_n(t) > \qquad k = 1, \dots, n.$$

The last *n* Lyapunov vectors come from solving $C^{(n)}x^{(n)} = 0$, where

$$C_{ki}^{(n)} = \sum_{j=n+1}^{N} < \hat{\xi}_{k+n-1}(t), \hat{\eta}_j(t) >< \hat{\eta}_j(t), \hat{\xi}_{i+n-1}(t) > \qquad k, i \leq N - n + 1,$$

$$x_k^{(n)} = < \hat{\xi}_{k+n-1}(t), \phi_n(t) > \qquad k = 1, \dots, N - n + 1.$$

Since Lyapunov vectors are characteristic of the instabilities of the system, and because they are invariant under the linearized flow, the above process does not need to be repeated at every time period (Trevisan and Pancotti 1998, WS07). Theoretically one would simply find the Lyapunov vectors once and use the TLM to propagate them forward through time. But in practice small, but inevitable, numerical errors stemming from the chaotic nature of the system cause all the vectors to rotate toward the leading LV, making it necessary to use the complete algorithm periodically. This is done every 0.25 time units for the Lorenz (1963) and the Fast-Slow coupled model (Peña and Kalnay, 2004). The TLM is then used to compute the LVs for the intervening steps. Their local growth rates are computed using a centered difference approximation of equation (48) of WS07 $\frac{1}{||\phi||}\frac{d||\phi||}{dt}$. Using forward or backward difference schemes has little effect on the results.

1.5 Summary

Each of the three types of vectors, bred, singular, and Lyapunov, is very important for studying dynamical instabilities. In general they have rather different characteristics, such as the way they grow. The differences among BVs, SVs and LVs is illustrated through the methods used to derive them. From their derivations one can see each requires the use of different information, to which some of the differences in their behavior can be attributed. For instance, BVs and FSVs require past information about the trajectory for their computation, while ISVs rely upon future information, and LVs require both past and future information. As will be seen, the variations in their calculations lead to slight variations in the spaces they inhabit, the sizes of their growth rates, and, in the case of ISVs, the behavior of their growth rates.

It is still important to keep in mind that although these vectors are all somewhat different, they all describe the instabilities intrinsic in dynamical systems and are equal to one another under various limits. Thus BVs computed using short rescaling windows and small amplitudes align with the leading LV while SVs computed using infinitely long integration windows are orthonormalized LVs (Trevisan and Pancotti 1998). These similarities and differences will be explored more in the following chapters.

Chapter 2 : Results with the Lorenz 1963 Three-Variable Model

2.1 Introduction: Characteristics of the Lorenz (1963) Model

We first compute BVs, SVs, and LVs for the Lorenz (1963) model

$$\begin{aligned} \dot{x} &= \sigma(y - x), \\ \dot{y} &= \rho x - y - x, \\ \dot{z} &= xy - \beta z, \end{aligned} \qquad (12)$$

a simple model exhibiting chaos, whose behavior has been widely studied. We use the standard parameters for the Lorenz model with $\sigma = 10, \rho = 28$, and $\beta = \frac{8}{3}$. The model was integrated for 5000 time periods using a fourth-order Runge-Kutta scheme with a time period of 0.01, so that one unit of time in each of the corresponding graphs corresponds to 100 time periods, allowing sufficient spin-up time for the solution to converge to the attractor.

This model has two regimes, a 'cold' regime, where both *x* and *y* values are negative, and a 'warm' regime, where both *x* and *y* values are positive. Lorenz (1963) indicated that regime changes (where the *x* and *y* variables switch signs) could actually be predicted using large values of the *z* variable while Evans *et al.* (2004) predicted regime changes using large growth rates of bred vectors. In this chapter we will compare properties of BVs, SVs, and LVs, including their ability to predict regime changes (as seen in Norwood *et al.* 2013).

2.2 Regime Change Predictive Power of BVs, SVs, and LVs

There are many works that use Lyapunov vectors to study the hyperbolicity of chaotic systems in general (e.g. H.-l. Yang *et al.* 2009 and Kuptsov 2013) and the Lorenz three-variable model in particular (e.g. Saiki and Kobayashi 2010 and Kobayashi and Saiki 2014). Here we wish to determine if Lyapunov vectors are useful predictors in this simple chaotic model. If they are, there would be reason to continue to study them for more complex systems. Figure 2.1 gives the growth rates of LV1, the leading Lyapunov vector, along the entire trajectory. Regions of fastest growth, anything greater than or equal to 6.4, are represented with red stars. Regions of decay (those with growth rates less than 0) are represented by blue stars. Intermediate values are represented by yellow and green stars. Below we show regions of fast growth are most important for regime change predictions. For clarity of graphical presentations, in the remainder of this section we will focus on the behavior of the trajectory in the interval between times 18 and 30, demarcated with vertical black lines in Figure 2.1; this shortened period includes a long regime as well as a few short regimes. Zooming in on this limited trajectory helps to underscore the details of the behavior of the three types of vectors, making them easier to compare. Clearly the first LV shares the property that large growth rates, indicated by red stars, signal a regime change as found by Evans *et al.* (2004).

Figure 2.2 provides the growth rates for the three LVs, the fastest growing initial and final SVs, corresponding to the largest singular value, and the BVs for the abbreviated trajectory. These are the local growth rates for each of the vectors. Recall

from chapter 1, for integration window IW and integration time period dt, which is 0.01 for this model, these are computed as: $\frac{1}{||\phi(t)||}\frac{d||\phi(t)||}{dt}$ for LV ϕ; $\frac{\ln(\sigma(t))}{dt*IW}$ for singular value $\sigma(t)$; and $\frac{1}{dt*IW}\ln(\frac{||bv(t)||}{\delta_0})$ for initial rescaling amplitude δ_0. The Euclidean norm is used for all three types of vectors. The singular vectors are computed using both a short rescaling time period of 0.02 and a longer one of 0.24 units, corresponding to integration windows of 2 and 24, respectively. With a rescaling time period of 0.02 units, the ISVs and FSVs are very similar (Figure 2.2(*d*) and (*e*)). A time period of 0.24 units provides time for the leading initial and final SVs to sufficiently separate to see a marked difference in their behavior (Figure 2.2(*g*) and (*h*)). Table 2.1 provides the cutoff values for the thresholds for all the vectors of Figure 2.2. These values were tuned for each vector so the growth rates would best predict regime changes. LV1 and the BVs have the same cutoff of 6.4 because their local growth rates are very similar in behavior and size. While most of the thresholds indicate the local growth rate must be greater than or equal to the given value for the growth rate to provide information on regime changes, the given threshold for LV3 signals the rate must be below the given value.

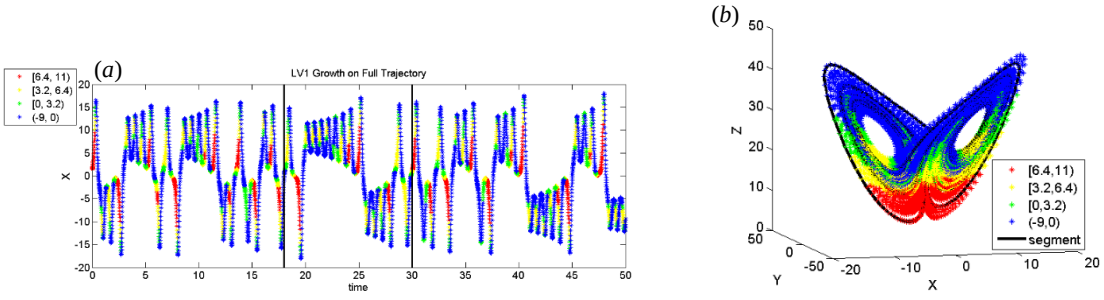

Figure 2.1: Control trajectory of the Lorenz (1963) model. (a) x-variable is plotted overlaid with the growth rates of LV1, the leading LV. The vertical black lines demarcate the time period (time 18-30) focused on

for the graphs in the remainder of the section. (b) The attractor with colored stars indicating the LV1 growth rate range.

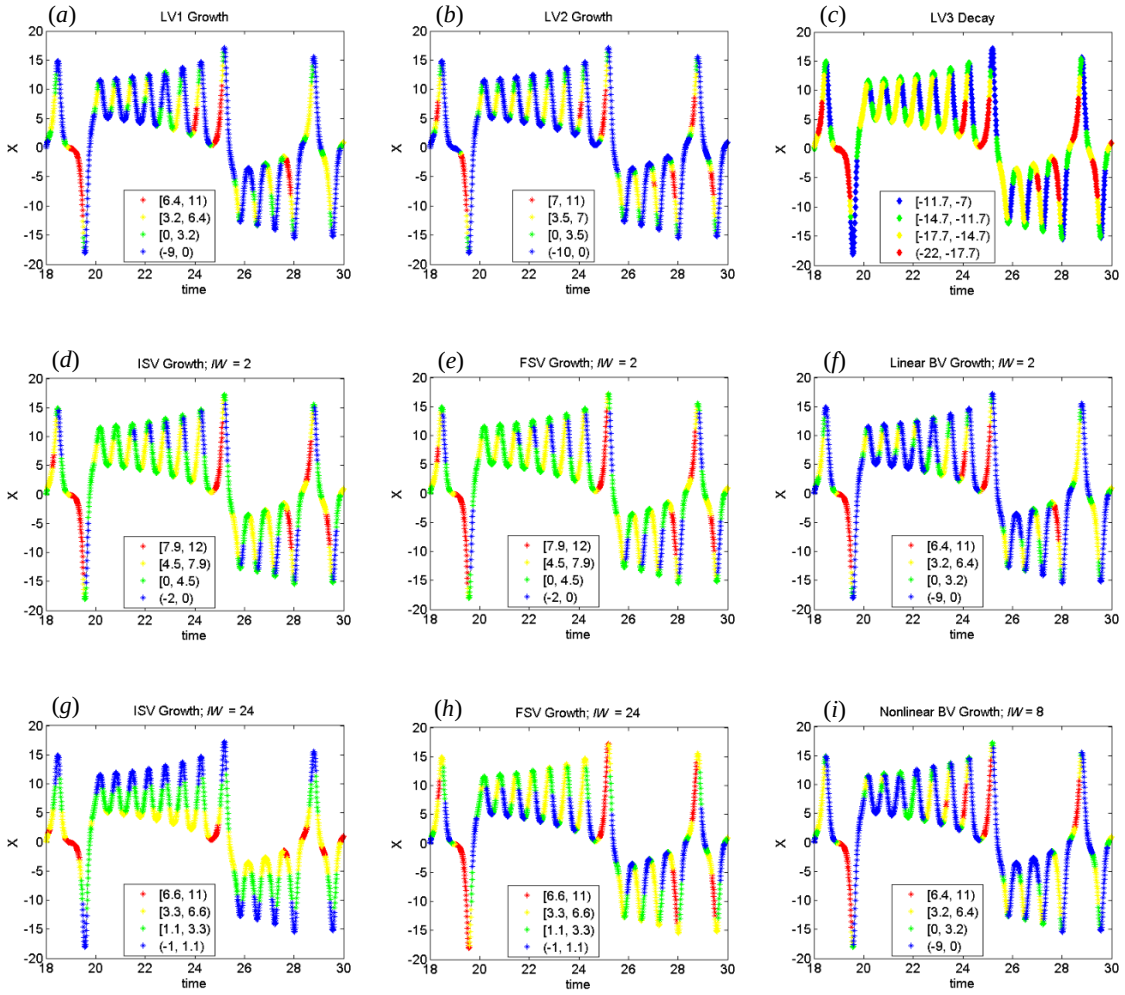

Figure 2.2: Growth rates along the x trajectory of (a) LV1, (b) LV2, (c) LV3, (d) ISV, (e) FSV (both using an integration interval of 0.02 units) , (f) the linear BV rescaled every 0.02 units using an initial perturbation of 0.1, (g) ISV, (h) FSV (both using an integration interval of 0.24 units), and (i) the nonlinear BV rescaled every 0.08 units using an initial perturbation of 1. In general fast growth (decay in the case of LV3) signals a regime change with the SVs providing the best predictions.

Table 2.1: Thresholds for the growth rates of the vectors of Figure 2.2. Values in parentheses are the integration windows (*IW*). Growth rates are tuned to best represent approaching regime changes within the Lorenz (1963) model. Thus rates above (below in the case of LV3) the given threshold typically signal an

approaching regime change. Note LV1 and the BVs have the same thresholds because their local growth rates are very similar in behavior and size.

Vector	LV1	LV2	LV3	BV (2)	BV (8)	ISV (2)	FSV (2)	ISV (24)	FSV (24)
Growth Rate	6.4	7	-22	6.4	6.4	7.9	7.9	6.6	6.6

The bred vectors are first computed using a perturbation of size 0.1 and rescaling interval of 0.02 units. The small amplitude and short resizing interval provide an accurate estimation of the linear evolution of the disturbances, and, as could be expected, these linear BVs are most similar to the leading LV, with an average correlation (cosine between the two vectors) of 0.996 for the entire trajectory. BVs are then computed using a perturbation of size 1 and a rescaling interval of 0.08 units. This provides an indication of the (somewhat) nonlinear evolution of the disturbances without the perturbations being overwhelmed by the nonlinearity of the model. Hence the first set of BVs is referred to as linear BVs while the second set is referred to as nonlinear BVs.

LV1, LV2, the SVs, and the BVs use the same colors to indicate their relative growth rate thresholds used for predicting regime change (e.g. a large growth rate is indicated by red stars; decay is indicated by blue stars) since the behavior of their growth rates are comparable. Notice the values for the growth rates vary (Table 2.1), with the SVs having a slightly larger growth rate than the BVs and LV1. LV3 is a strongly decaying vector, so the opposite colors are used to indicate the intensity of the decay (e.g. slow decay is shown with blue diamonds; fast decay is indicated by red diamonds). Figure 2.2 demonstrates fast growth for LV1, the SVs, and BVs indicates a regime change will take place after the present orbit is completed. In fact LV1 and the linear BV show a ‘false alarm’ at time ~24, whereas the FSV is a superior predictor and has no false

alarms for this particular solution. Thus, although the LVs are valid globally and at all times, they can be used for local, finite time predictions, at least in this simple model. Moreover, the linear BV/LV1, as well as the SVs, also follows the second prediction rule found by Evans *et al.* (2004): longer periods of fast growth (i.e. a larger number of red stars) imply the upcoming regime will be longer. As a result of the time shift for the growth rates of the SVs (see section 1.3) the ISV optimized for 0.24 units has a growth rate that is a function of the absolute value of x: the closer x is to zero, the faster the growth of the ISV. This makes it an early predictor of regime change because it can take advantage of future information. By contrast, the ISV optimized for just 0.02 units has a growth rate essentially identical to the corresponding FSV, which in turn is close to the FSV obtained with an optimization window of 0.24 units.

LV2 (Figure 2.2(*b*)), which is tangent to the attractor and has a global growth rate of zero, has a local growth rate that is very similar to that of LV1 (Figure 2.2(*a*)) and the BVs (linear: Figure 2.2(*f*), nonlinear: Figure 2.2(*i*)), and often grows faster than LV1 locally, as, for example, at times 19 and 29. If the trajectory were extended it would be evident that LV2 begins to grow fastest two orbits before the regime is finished, in multi-orbit regimes (those with more than one extreme value). But it would be difficult to use LV2 as a predictor since one would not know if the present regime has multiple orbits and the warning is in the second to last orbit of the regime or if the regime only has one orbit. Thus LV2 would give too many false predictions to provide a useful warning for regime changes. It would only be useful for predictions if combined with LV1 or a bred vector, which sometimes misses a regime change (such as at time 29) while LV2 never does. Such coupling is not necessary for the FSV which predicts each regime change

without false alarms or misses for this particular solution. Figure 2.2(*c*) provides the decay rate of LV3, whose behavior mirrors that of LV2's growth, in the sense that it does not only decay fastest before a regime change but begins this behavior a couple of cycles before the actual change.

2.3 Correlations among BVs, SVs, and LVs

2.3.1 Comparisons of BVs, SVs, and LVs

It is not surprising that the behavior of the growth rates exhibited by LV1, FSV, and the BVs are very similar. Any perturbation initialized in the past and integrated forward should approximate the same instabilities and errors, represented by LV1, the leading LV. As indicated before, the linear BV is very close to LV1 with an average correlation of 0.996 for the entire trajectory, and the nonlinear BV has a correlation with LV1 of 0.867. By comparison, the FSV computed over a time interval of 0.24 units, shifts toward LV1 but not completely with a correlation coefficient of just 0.757.

The behavior of ISV and FSV are quite different from that of the BVs and the two leading LVs. Having no memory of the previous integration interval, the vectors change directions often and in an inconsistent manner. As the integration interval increases FSV slowly becomes more flow dependent and more aligned to LV1, but, as could be expected, the ISV becomes less correlated with LV1 as the integration interval increases (Table 2.2).

Table 2.2: Mean of the absolute value of the cosines between initial and final SVs with LV1. As expected, as the integration window, increases the FSV moves toward LV1 while the ISV moves away from LV1.

IW	1	2	8	24	48
ISV	0.64	0.63	0.58	0.51	0.45
FSV	0.65	0.66	0.69	0.76	0.79

What is most interesting when examining the correlations among the BVs are the comparisons between the nonlinear BV and the first and second LVs. The BVs become more collinear to the first two LVs preceding a regime change or when any of these vectors grow fastest (Figure 2.3). The linear and slightly nonlinear BVs are more positively correlated to LV1 than to LV2, losing their correlation with LV1 very rarely (Figure 2.3(*a*) and (*d*)). Thus the same patterns of behavior regarding their alignment with respect to the regime being entered also hold. Still, it was not anticipated that the BVs and LV2 would share the same space so frequently. In fact up to a certain point, as δ_0 is held constant at 1 and the integration window increases, the BVs become less aligned with LV1 and more aligned with LV2 (Table 2.3). In addition, whenever LV2 grows faster than LV1 the BVs align themselves more with LV2, as will be further illustrated. The usefulness of BVs is closely linked to the choices of δ_0 and *IW*. If δ_0 is held constant at 1 and *IW* increases beyond 24, the BVs are no longer dynamically significant.

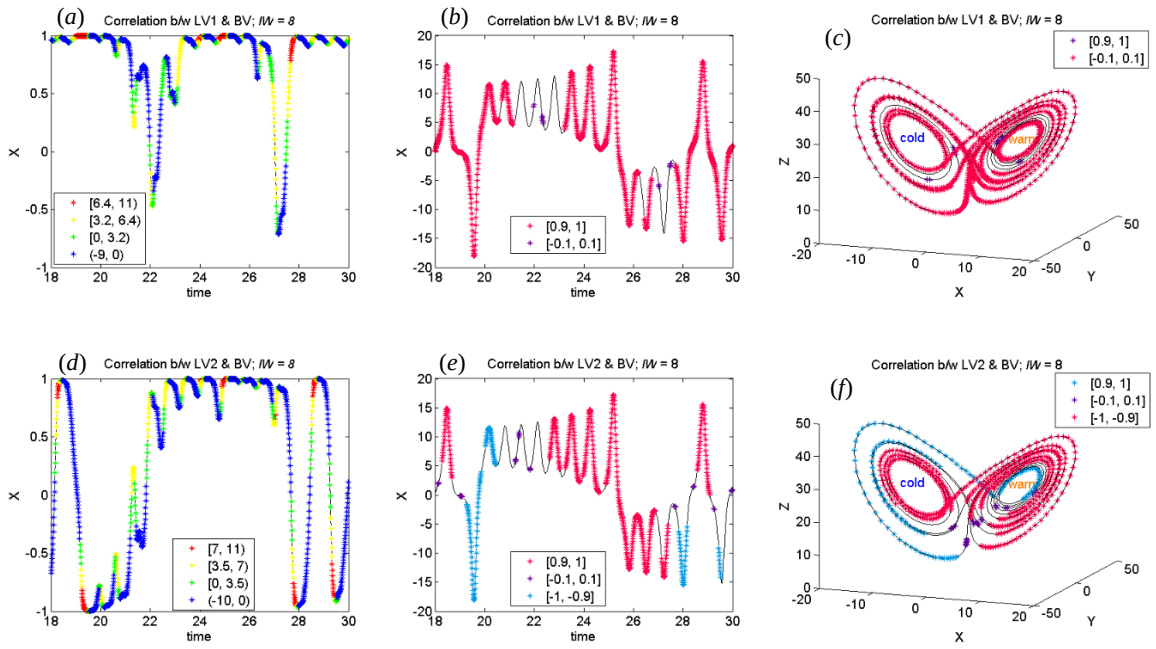

Figure 2.3: Correlations between the nonlinear BV and LV1 and LV2. (a) Cosine between LV1 and the BV. Colored stars represent growth rates of LV1; (b) x-trajectory where pink stars indicate the BV and LV1 and nearly parallel before and after a regime change; (c) like (b) but on the attractor; (d) cosine between LV2 and the BV. Colored stars represent LV2 growth rates; (e) x-trajectory showing correlations between LV2 and the BV; (f) like (e) but on the attractor. The BV aligns with the LVs when the LVs grow fastest and upon entering and leaving a new regime.

Table 2.3: Average absolute correlation between LV1 and LV2 with BVs for increasing integration windows. All have a δ_0 of 1. As IW increases BVs become more aligned with LV2.

IW	2	8	24	48
LV1 and BV	0.98	0.87	0.68	0.70
LV2 and BV	0.75	0.78	0.88	0.83

Finally we address the situation when LV2 and LV1 compete for being the fastest growing vector locally, and the response in the behavior of the BVs, since this competition between different dominant instabilities is very common in complex weather-climate models (e.g. Toth and Kalnay 1997). The construction of BVs suggests

that for small amplitudes and short rescaling intervals they should follow LV1, but what happens for a nonlinear BV when LV2 grows faster than LV1? Figure 2.4 shows, in red, those frequent times in which LV2 grows faster than LV1, and, in blue, the 'expected' behavior of LV1 growing faster than LV2, shown only when both LV1 and LV2 are growing. Figure 2.4(*a*) indicates that most of the time the nonlinear BV closely follows LV1, with an average absolute cosine of 0.87. However, Figure 2.4(*b*) shows that when LV2 grows faster than LV1, the BV gets attracted to the faster growing vector, and becomes more collinear to LV2. As soon as LV2 ceases to grow faster, the BV moves away from it. A similar behavior, although not as clear, can be detected with the BV aligning itself closer to LV1 when its growth dominates (blue stars). In summary, although BVs are created using a nonlinear generalization of the method used to construct the leading LV, they have no 'loyalty' to LV1 and instead will grow closer to the *locally* fastest growing Lyapunov vector.

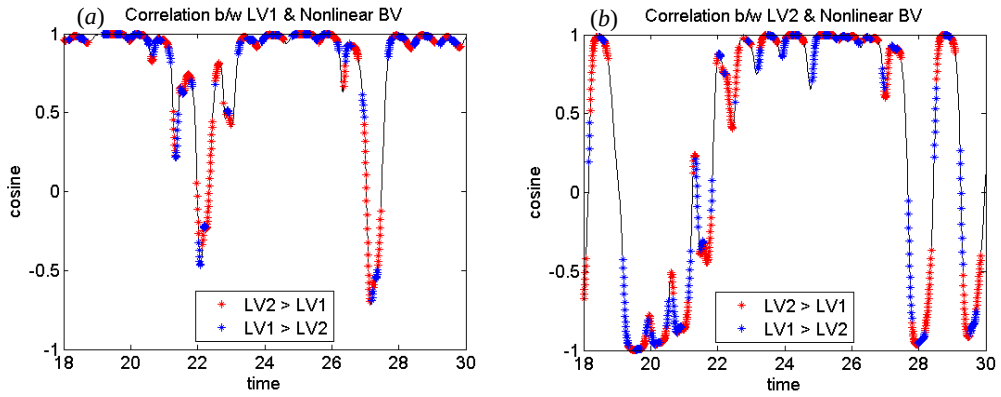

Figure 2.4: Ratio of LV2 and LV1's growth rates. Red stars indicate LV2's local growth rate is larger than LV1's; blue stars indicate LV1's local growth rate is larger than LV2's, only shown when both vectors are growing. (a) Gives the correlation between LV1 and the nonlinear BV, and (b) gives the correlation

between LV2 and the nonlinear BV. BVs align with the fastest locally growing LV. Thus they abandon LV1 to grow closer to LV2 when LV2 grows faster than LV1.

2.3.2 Comparisons among the LVs

The Wolfe and Samelson (2007) algorithm affords us the opportunity to closely examine and compare all of the LVs of this simple model. Figure 2.5(*a*) gives the norms of the LVs, whose global average approximates the Lyapunov exponents (LEs) of the model. Figure 2.5(*b*) shows the typical structure of the LVs. The direction of LV2 is always tangent to the flow while the orientations of LV1 and LV3 change with the flow. Because LV2 is always tangent to the flow, comparing the correlations between LV1 and LV3 with LV2 is the same as comparing the orientations of LV1 and LV3 with the direction of the flow.

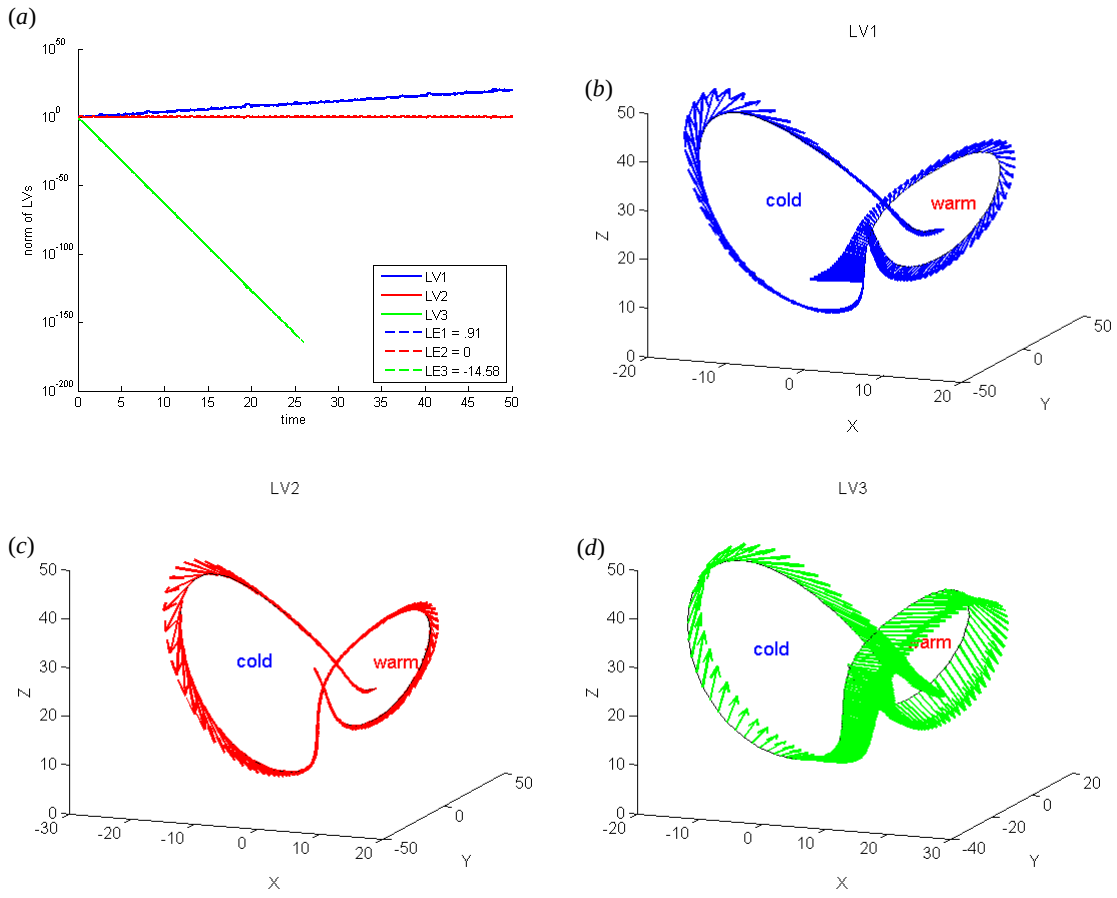

Figure 2.5: (a) Norms of the LVs plotted with the Lyapunov exponents (LEs) of the Lorenz (1963) model. (b) LV1 (c) LV2 (d) LV3 from time 18 to time 20. Flow begins in the center of the plots, travels counterclockwise in the warm regime, crosses the center, and travels clockwise in the cold regime.

LV1 and LV2 often inhabit the same space, and they are most closely aligned when LV2 grows fastest (Figure 2.6(*a*)). They are also approximately collinear before a regime change, and this alignment persists for some time after entering the new regime (Figure 2.6(*b*)). The two vectors are nearly orthogonal near the center of multi-orbit regimes and immediately before the regime change of single orbit regimes (Figure 2.6(*b*) and Figure 2.5(*b*), keeping in mind that orthogonality with LV2 is the same as orthogonality with the attractor).

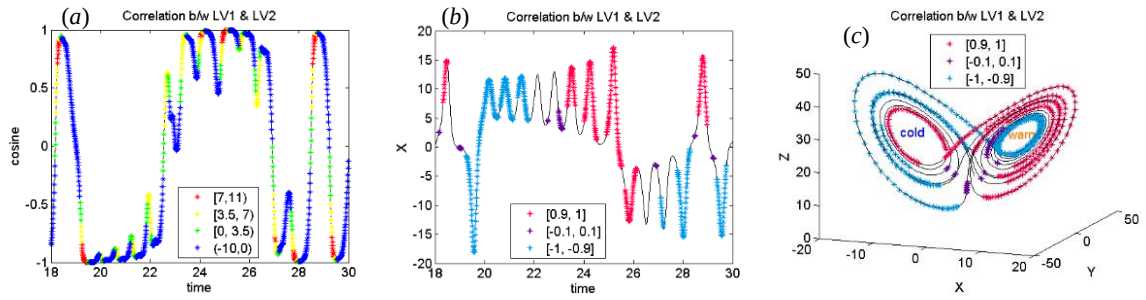

Figure 2.6: Correlations between LV1 and LV2. (a) The cosine between LV1 and LV2 where the colored stars represent the local growth rate of LV2; (b) the stars represent the correlations between the two vectors along the x component; and (c) the correlations between the two vectors along the attractor. They are approximately collinear when LV2 grows fastest and before and after a regime change.

LV3 is very rarely aligned with LV1 or LV2 (Figure 2.7). The rare occasion is when it aligns with LV1 and LV2 upon entering a new regime that will last longer than three cycles. LV3, being the fastest decaying vector, clearly describes the stable subspace, where errors quickly decay, while LV1, being the fastest growing vector, clearly describes the unstable subspace, where errors quickly grow. Thus these rare occurrences when LV1 and LV3 align are times when the unstable and stable subspaces intersect.

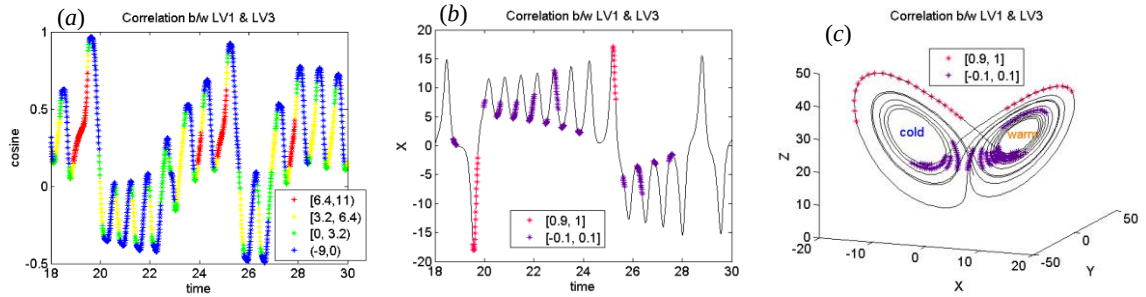

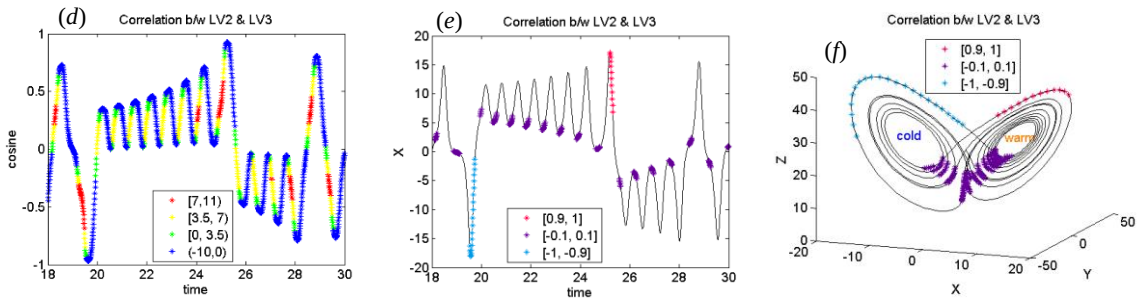

Figure 2.7: Correlations between LV1 and LV3 (top row) and LV2 and LV3 (bottom row). (a) The correlations between LV1 and LV3 with LV1 growth. (b) The correlations between LV1 and LV3 on the x component and (c) the attractor. (d) The correlations between LV2 and LV3 with LV2 growth. (e) The correlations between LV2 and LV3 on the x component and (f) the attractor.

2.4 Summary

The work of Evans *et al.* (2004) showed that the fast growth of bred vectors can be used to predict regime change and duration. From our results it is clear the growth rates of all three types of vectors, bred, singular, and Lyapunov, can be used to effectively predict regime changes within this simple three-variable model. SVs are the best predictors, never missing a regime change and never having a false prediction. ISVs provide earlier warnings than FSVs because they have the advantage of using future information. It is also clear that linear BVs, those with short rescaling windows and small amplitudes, are approximately equal to the leading LV, as they should be since they are linear approximations of LV1. Thus BVs, which are much easier to compute than even the leading LV since they do not require a linearization of the model, can be used to obtain LV1 as long as a small amplitude and short rescaling window are used. But as the rescaling amplitude and window increase enough for the BVs to become nonlinear but

remain dynamically significant, the BVs shed their "allegiance" to LV1 and align with the *locally fastest growing* LV, which is often LV2.

LV2 and LV3 also have growth rates (decay rates in the case of LV3) that are strongly correlated with changes in the flow growing (decaying) fastest two orbits before a regime change. All of the LVs also approximately inhabit the same space at the onset of a long regime. BVs exhibited similar behavior becoming more aligned to the LVs preceding a regime change. Bred and Lyapunov vectors are also closely aligned with one another when any of these vectors grows fastest, which is often at the onset of a new regime. While these are very promising results, they do not guarantee the same effects will be seen in models with more than one mode of growth. Thus we move on to comparisons amongst these vectors in the Fast-Slow Coupled Model developed by Peña and Kalnay (2004).

Chapter 3 : Results with the Fast-Slow Coupled Model (Peña and Kalnay, 2004)

3.1 Description of the Fast-Slow Coupled Model

In 2004, Peña and Kalnay (PK04) developed a coupled model based upon the Lorenz (1963) model to determine the effects of fast and slow modes on the growth of bred vectors. In particular they wished to determine if bred vectors would be able to distinguish between the fast and slow modes, and indeed, they found it is possible to estimate not only the fast but the slow modes by choosing an amplitude and rescaling interval that targets each mode. Here we replicate their success with BVs and study the behavior of SVs and LVs. The equations for the three coupled Lorenz models given by PK04 are

$$\begin{aligned}
\dot{x}_e &= \tau_e\sigma(y_e - x_e) - c_e(Sx_t + k_1) \\
\dot{y}_e &= \tau_e\rho x_e - \tau_e y_e - \tau_e x_e z_e + c_e(Sy_t + k_1) \\
\dot{z}_e &= \tau_e x_e y_e - \tau_e\beta z_e - c_t z_t \\
\\
\dot{x}_t &= \sigma(y_t - x_t) - c(SX + k_2) - c_e(Sx_e + k_1) \\
\dot{y}_t &= \rho x_t - y_t - x_t z_t + c(SY + k_2) + c_e(Sy_e + k_1) \\
\dot{z}_t &= x_t y_t - \beta z_t + c_z Z + c_t z_e
\end{aligned} \tag{13}$$

$$\dot{X} = \tau_o \sigma (Y - X) - c\left(x_t + k_2\right)$$

$$\dot{Y} = \tau_o \rho X - \tau_o Y - \tau_o SXZ + c(y_t + k_2)$$

$$\dot{Z} = \tau_o SXY - \tau_o \beta Z - c_z Z.$$

The lowercase x, y, and z represent the fast modes, with the e and t subscripts designating the quickly varying, small amplitude 'extratropical' and 'tropical' variables, respectively. The uppercase X, Y, and Z represent the slowly varying, large amplitude 'ocean' variables. Here the extratropics and tropics are weakly coupled in the horizontal ($c_e = 0.08$) and vertical ($c_t = 0.08$) directions while the tropics and ocean are strongly coupled in the horizontal and vertical directions ($c = c_z = 1$). τ_o and S are temporal and spatial scaling factors, respectively, for the ocean variables. Here $\tau_o = 0.1$ and $S = 1$. Thus the ocean has a time scale ten times as long as the time scale for the tropics and extratropics (when the extratropical temporal scaling factor, $\tau_e = 1$) but the same amplitude (although a difference in time scale and coupling leads to a difference in the ocean's amplitude, PK04). $k_1 = 10$ and $k_2 = -11$ are 'uncentering' parameters chosen so all the systems are not completely in sync. The model was integrated using a fourth order Runge-Kutta scheme with a time period of 0.01 for 10 000 time periods. Thus one unit of time corresponds to 100 time periods. Such an arrangement leads to a 'tropical' subsystem that is completely dominated by changes in the ocean subsystem. Figure 3.1 gives the typical attractors of this system. Figure 3.2 provides the x-trajectory of the three subsystems. For graphical clarity, the figures in section 3.2 will focus on the region demarcated by the vertical bars in Figure 3.2.

Note that because the extratropical atmosphere is only weakly coupled to the tropical atmosphere, its behavior is similar to the original Lorenz model, and it only introduces 'weather noise' in the strongly coupled ocean-tropical atmosphere subsystems. It is remarkable that although the ocean seems to be the driving system in its coupling with the tropical atmosphere, the coupling with the tropical atmosphere has a profound effect on the ocean: The ocean has 'normal years' with amplitudes that increase every year, and when the ocean x variable becomes larger than approximately 45, there is an abrupt change of regime with a single strong abnormal negative episode which we call an 'El Niño' year because it takes place every 2–8 years (where a 'year' corresponds to roughly $\frac{10}{3}$ time units). Many of the results pertaining to this setup were published in Norwood *et al.* 2013.

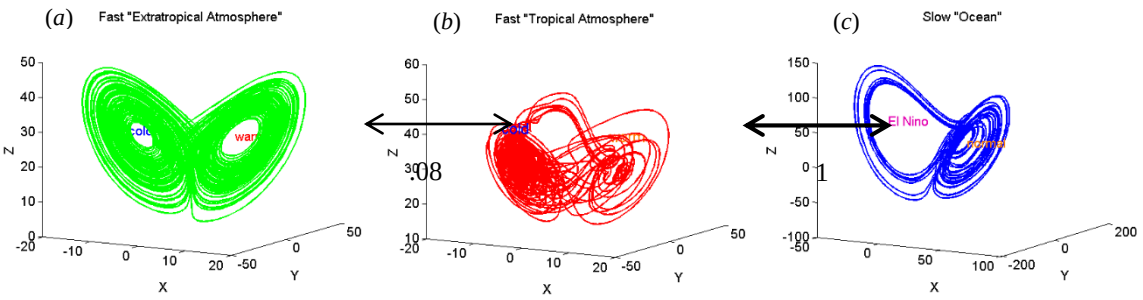

Figure 3.1: Typical attractor for the coupled model. The plots are of the (a) extratropical, (b) tropical, and (c) ocean subsystems. The thickness of the arrows provides a qualitative representation of the strength in the coupling between the systems while the numbers provide the actual coupling parameters.

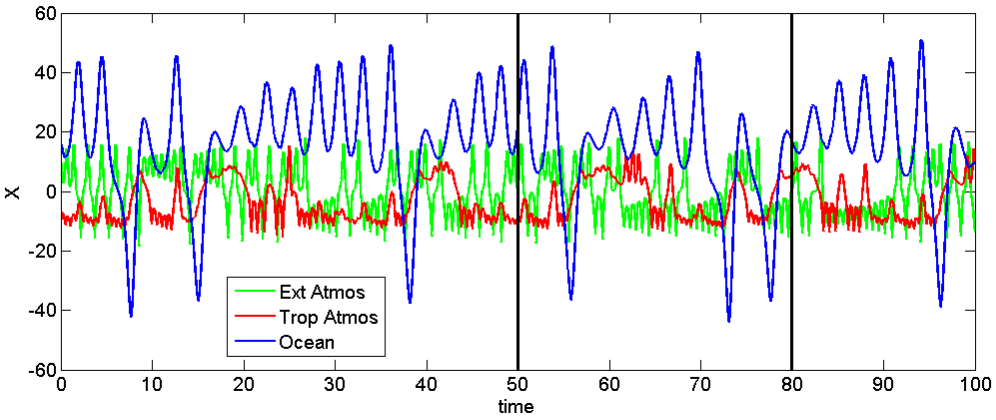

Figure 3.2: X-trajectory of the extratropical, tropical, and ocean subsystems. The black vertical bars mark the section of the trajectories that will be the focus in the figures in section 3.2.

3.2 Results with the Fast-Slow Coupled Model with Weather Noise

3.2.1 Regime change predictive power of BVs, SVs, and LVs

Following Peña and Kalnay (2004), we computed the fast and slow mode BVs by selecting appropriate breeding parameters. To target the fast mode we used a small initial perturbation of 0.05 and a small rescaling interval of 0.05 units. This BV is indeed very similar to LV1. In fact, they are approximately collinear, having an average correlation of 0.99. The SVs are determined for an optimization time of 0.05 time units, and their growth rates (both those of the initial and final SVs) signal regime changes in the fast extratropical atmosphere (Figure 3.3). (Section 2.2 has the formulas for the local growth rates for each vector. Again, the Euclidean norm is used for all three types of vectors with a dt of 0.01.) Interestingly some of the LVs can be assigned to a particular subsystem based upon their local growth rates. LV1, LV4 and LV8 clearly correspond to the

extratropics, with fast growth (decay in the case of LV8) signaling a regime change in this area (Figure 3.4(*a*), (*b*) and (*c*), respectively).

To locate the slow mode bred vector we used a large initial perturbation of 40 (smaller than the amplitude of the ocean but larger than that of the extratropical atmosphere). We chose a long rescaling interval of 0.35 time units, approximately equivalent to one month. With these dynamically appropriate magnitudes, the slow mode BV is a far better predictor of ocean regime changes (Figure 3.5) than its LV counterparts (Figure 3.6), seemingly because it is not influenced by the fast modes of the system, which saturate within a month (S.-C. Yang *et al.* 2006b). The LVs are not able to accomplish this separation. To further demonstrate the lack of influence of the fast modes of the model on the slow mode BV we split its growth rate into its components and compare this to the growth rates of the ocean LVs (Figure 3.7(*a*) and (*b*), respectively). Here the slow mode BV is completely dominated by the slow coupled ocean, while the LVs change on a much faster time scale than the ocean subsystem or the slow mode BV. This is a consequence of the coupling of the system which leads to 'coupled' LVs. Thus the large spikes in the growth of LV2 signals the few times where the tropical subsystem is able to break free of the ocean's influence and begins to behave more like a traditional Lorenz model. The majority of the local minima of LV7 point toward changes in the ocean subsystem. The few false predictions are areas where the tropical subsystem enters a cold regime instead of the warm regime it typically enters as the ocean subsystem returns to normal. SVs were unable to detect the slow growing instabilities. Changing the integration window and even performing the singular value decomposition on only the slow mode did nothing to increase the SVs' usefulness in the slow subsystem.

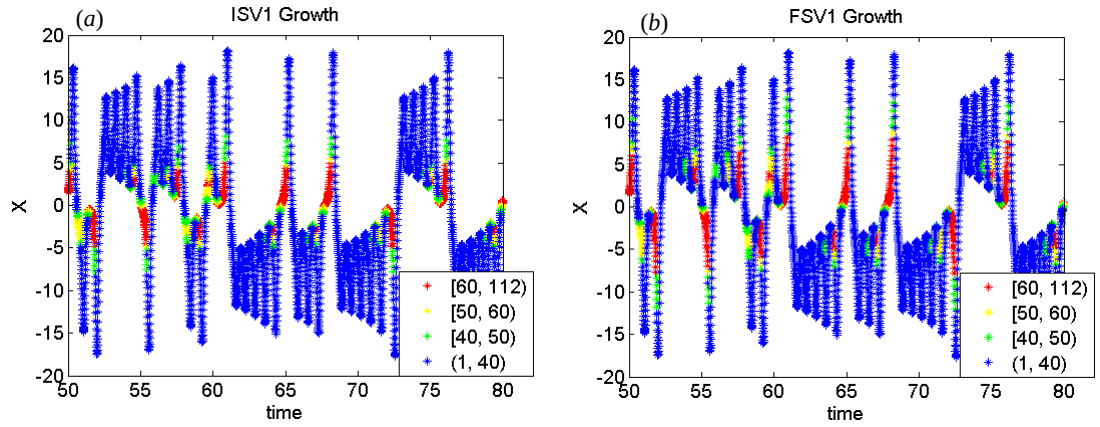

Figure 3.3: Growth rates of (a) the initial SVs and (b) the final SVs signal changes within the fast extratropical subsystem. ISVs offer slightly earlier predictions because they can take advantage of future information.

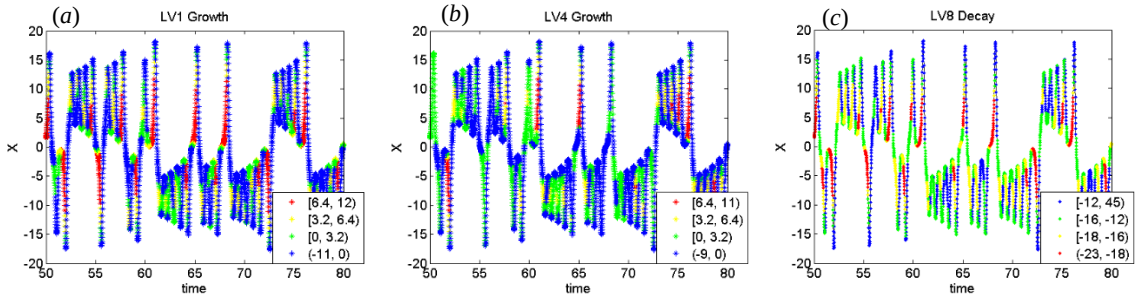

Figure 3.4: Growth rates of (a) LV1, (b) LV4 and (c) LV8 on the x component of the extratropical subsystem. Faster growth (decay in the case of LV8) signals a regime change, but coupling decreases the predictive power of LV4 and LV8.

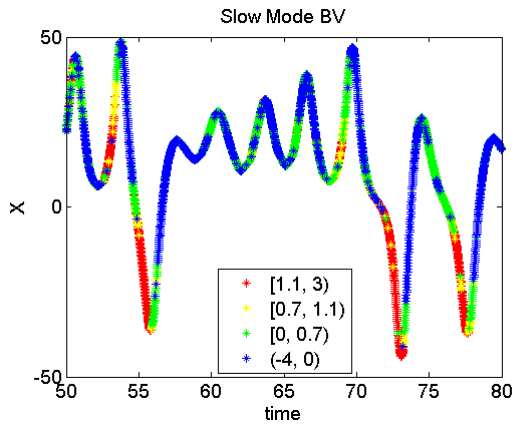

Figure 3.5: Growth rate of the slow mode BV on the x-trajectory of the ocean subsystem. It is obtained using an initial perturbation of 40 and resized every 0.35 units. Its growth rate is most closely related to changes in the ocean subsystem.

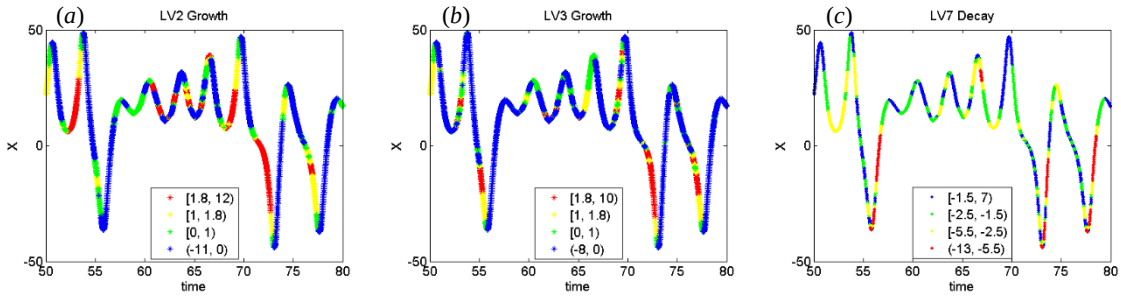

Figure 3.6: (a) LV2 growth, (b) LV3 growth, and (c) LV7 decay on the x component of the ocean subsystem. LV2 and LV3 are complements of one another where fast LV2 growth denotes the beginning of the last cycle of a 'normal' regime and fast LV3 growth denotes the beginning of the last cycle of an El Niño regime. Strong decay of LV7 indicates the coupled ocean subsystem is returning to normal.

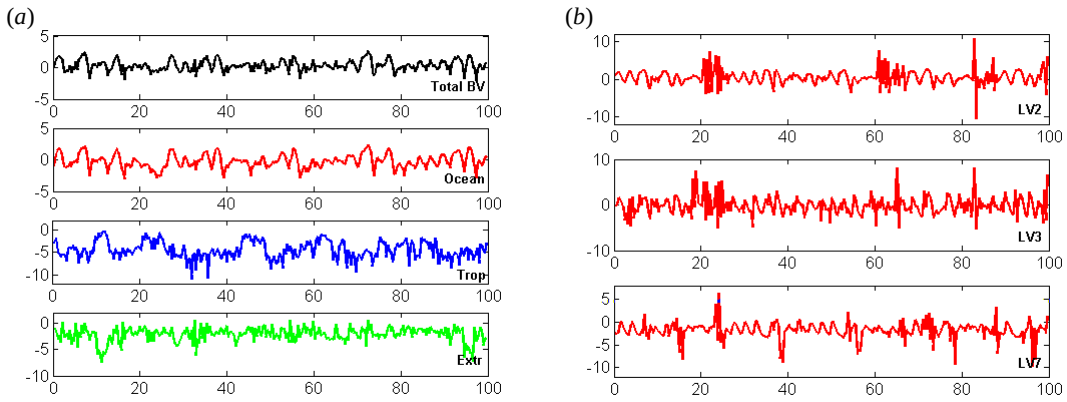

Figure 3.7: (a) Slow mode BV split into its ocean, tropical, and extratropical components, compared to (b) the ocean LVs. The LVs are still highly dependent upon changes in the extratropical and tropical subsystems because of coupling.

The complete coupling of the tropics and ocean means vectors ascribed to these regions often provide information about more than one subsystem, but it is still possible to separate the slow coupled ocean LVs (Figure 3.6) from the LVs of the other two subsystems. Persistent growth of LV2 (Figure 3.6(*a*)) is a strong indicator of when the ocean is to enter an El Niño regime, but there is also short-lasting rapid growth (e.g. for t between 60 and 65) associated with regime changes in the fast atmospheres. Thus only the areas with the longest periods of growth should be considered if this is to be used to predict a cold regime. Note that the 'prediction' of returning to normal at $t \sim 73$ is unusual and most likely predicts the return to an El Niño cycle that follows shortly thereafter. In order to better predict all changes in this system, LV2 should be paired with LV3 whose growth signals the system will soon return to normal (Figure 3.6(*b*)). Areas of rapid decay for LV7 signal that the system is returning to normal (Figure 3.6(*c*)). The growth of LV5, LV6, and LV9 may be useful for changes in the tropics, but this area is so erratic it is difficult to specifically ascertain what their growth rates indicate. Like the

ocean LVs, the tropical LVs also have varying degrees of connection with the ocean subsystem.

LVs were the only ones out of the three types of vectors that were able to identify the existence of the tropical subsystem (Figure 3.8). The growth rates of LV5, LV6, and LV9 correspond to changes within the tropical subsystem. Unlike the LVs that are associated with the extratropical and ocean subsystems, the growth rates of LVs associated with the tropical subsystem do not signal regime changes. Instead fast growth typically indicates a local maximum or minimum value. Again, because of the strong coupling between the tropics and ocean, there are times (like the strong and prolonged growth in LV5 around $t \sim 53$ in Figure 3.8(a)) when the growth rates correspond to changes within the ocean subsystem, but strong growth in these vectors typically corresponds to changes within the tropical subsystem. Table 3.1 provides the thresholds for the growth rates of all of the three types of vectors. The rates for ISV1 and FSV1 are listed as SV1 because they use the same growth rates. The fast mode BV is omitted because it is essentially the same as LV1.

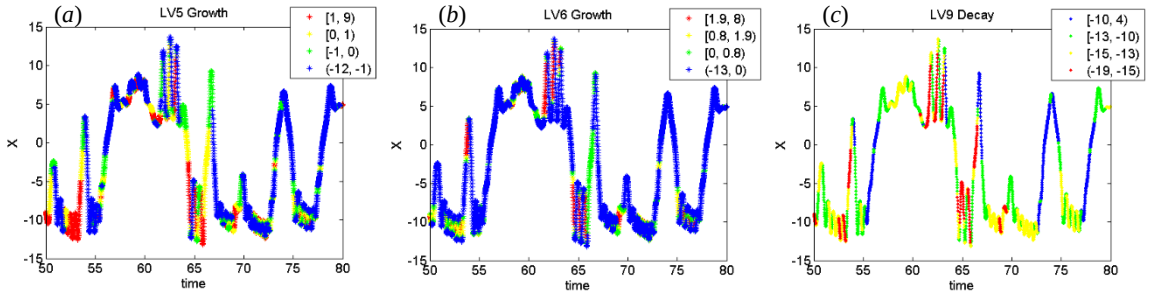

Figure 3.8: (a) LV5 growth, (b) LV6 growth, and (c) LV9 decay all correspond to changes within the tropical subsystem. Fast growth (decay in the case of LV9) typically indicates a local extremum, not a regime change as with the vectors that are associated with the other subsystems.

Table 3.1: Thresholds of the growth rates for the three types of vectors in the coupled nine-variable model with an 'extratropical' subsystem. The growth rates are tuned to best represent changes within a particular subsystem. Green indicates the vectors correspond to changes within the "extratropics," red indicates the "tropics," and blue indicates the "ocean." When growth rates are larger (smaller in the case of negative values) than the given threshold, that typically signals a change within the applicable subsystem.

Vector	SV1	LV1	LV4	LV8	LV5	LV6	LV9	LV2	LV3	LV7	Slow BV
Growth Rate	60	6.4	6.4	-23	1.9	1.9	-19	1.8	1.8	-13	1.1

3.2.2 Correlations among BVs, SVs, and LVs

Having more than one mode of growth somewhat changes the relationship among BVs, SVs, and LVs. Table 3.2 has the subsystem each LV corresponds to as a reference, which will be useful as the correlations between the vectors are discussed. As mentioned before, the average correlation between the fast mode BV and LV1, the leading LV, is 0.99, but, as expected, the fast mode BV only sporadically aligns with LV4 and LV8. Unlike the three-variable model these alignments do not exclusively coincide with fast growth of the BVs or LVs, but there is a relationship between the ratios of LV4 and LV1 growth and the BVs' alignment with LV4. Like it happened with LV2 in the three-variable model, when LV4 grows faster than LV1, the BVs approach LV4 (Figure 3.9). Coupling thwarts the BVs' ability to become completely collinear with LV4 at all times when LV4 grows faster than LV1, but even at these times the correlation between the fast mode BV and LV4 reaches a local extremum. Hence the two become as close to one another as the model will allow. The relationship between the quickly decaying LV8 and

the BVs (and LV1) resembles that of the LV3/BV relationship from the three-variable model. That is LV8 aligns with the BV upon leaving the last orbit of a regime (Figure 3.10 shown using LV1 instead of the BV since they are essentially equal in this case). Even with these patterns, the non-leading LVs and the BVs do not typically inhabit the same subspace.

Although the growth rates of the SVs are able to accurately predict the regime changes of the fast extratropical subsystem (as they do for the Lorenz model, shown in section 2.2), they have very little in common with the BVs and LV1. (ISV has an average absolute correlation of 0.0411 with both; FSV has an average absolute correlation of 0.137 with the fast mode BV and 0.136 with LV1.)

Because of the strong coupling of the ocean and tropical subsystems leading to 'coupled' LVs, the slow mode BV has little correlation with any of the LVs attached to the slower moving ocean, quite unlike the fast mode BV and LV1 which are approximately equal. In fact, the slow mode BV is nearly orthogonal to LV7 having an average correlation of -0.009. There is a slightly higher correlation between the slow mode BV with LV2 during the last cycle before a regime change. There is also a slightly higher correlation between the slow mode BV and LV3 upon entering an El Niño regime. Overall, the slow mode BV and LV2 and LV3 are nowhere near collinear, typically demonstrating a useful pattern with correlations starting upward of 0.75 (or less than -0.75; Figure 3.11).

Table 3.2: Subsystem each Lyapunov vector corresponds to within the nine-variable model with extratropics chosen according to how well their growth rates match changes in the subsystem.

Extratropics			Tropics			Ocean		
LV1	LV4	LV8	LV5	LV6	LV9	LV2	LV3	LV7

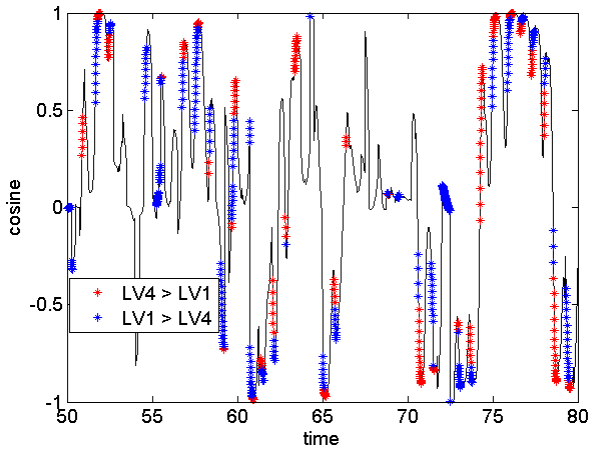

Figure 3.9: Correlation between LV4 and the fast mode BV. Times when LV4's growth rate is greater than that of LV1 are in red. Times when LV1's growth rate is greater than LV4's are in blue. Only times when both vectors are growing are shown. The fast mode BV grows closer to the LV that grows the fastest locally.

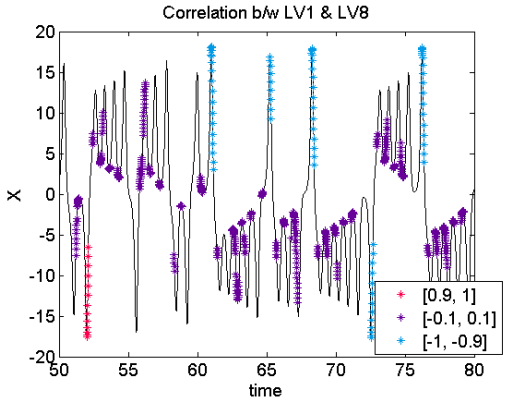

Figure 3.10: Correlations between LV1 and LV8 on the x-trajectory of the extratropical subsystem.

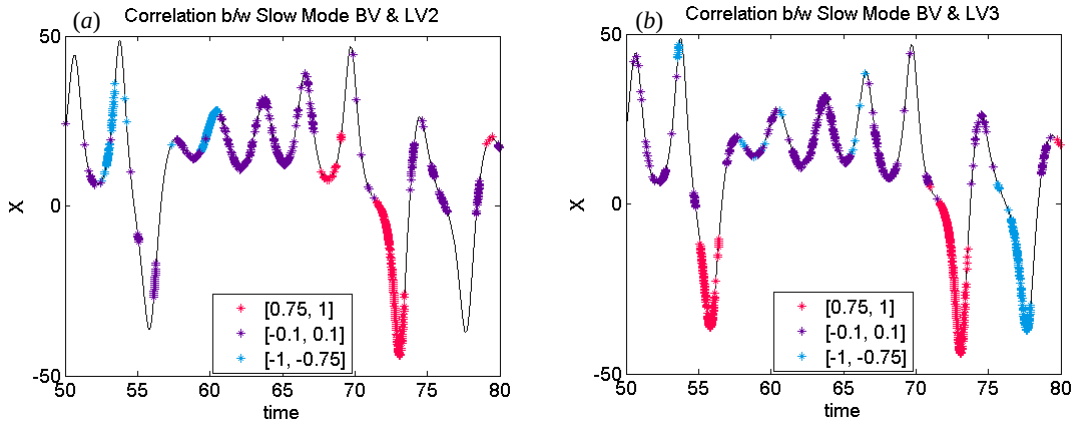

Figure 3.11: Correlations between the slow-mode BV with (a) LV2 and (b) LV3. There is some alignment with LV2 during the last cycle before a regime change. The greatest alignment with LV3 occurs upon entering an El Niño cycle.

3.2.3 Lyapunov vectors in the Fast-Slow Coupled Model

Figure 3.12 shows the norms of the LVs versus time, and Table 3.3 provides the corresponding Lyapunov exponents (LEs, the slopes of the lines in Figure 3.12) for both the Lorenz model, discussed in chapter 2, and coupled models. Rather than replicating the behavior of the original Lorenz model in triplets, the coupling present in this model creates what we have interpreted as coupled LVs. There is one LV of extreme (global) growth that mimics the first LV of the three-variable model, one of moderate growth, one of essentially no growth like LV2 of the three-variable model, four of moderate decay and two of extreme decay like LV3 of the three-variable model. Despite their differences, they mainly behave in a manner similar to that of the LVs of the three-variable model, growing fastest and often aligning with one another before a regime change. The weak coupling between the extratropics and the other two subsystems causes these vectors not to be intensely influenced by changes in the other subsystems, and there is no question as

to which subsystem they correspond. Changes in the local growth rates of LV2, LV3, and LV7, on the other hand, correspond to changes in the ocean subsystem (as seen above in Figure 3.6). Thus the colors of the LVs in Figure 3.12(*b*), appointing the subsystem each vector corresponds to, were assigned according to how well their growth rates could be used as a predictor in said subsystem.

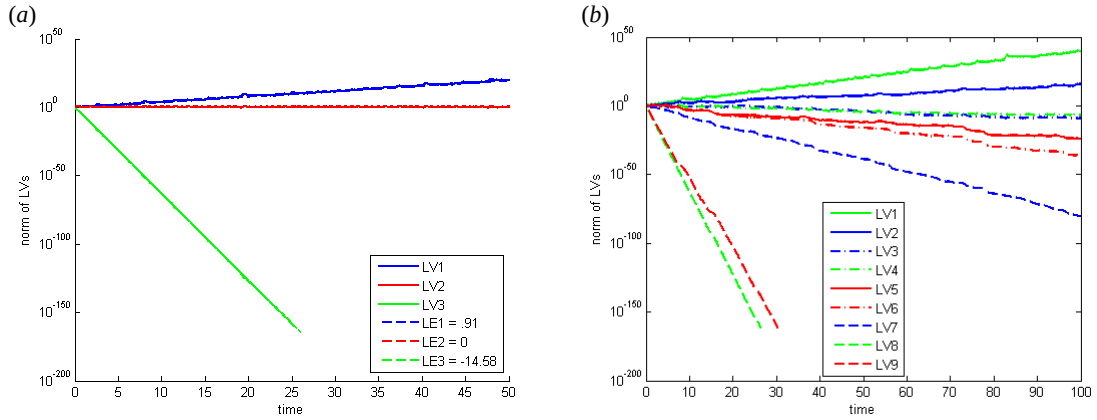

Figure 3.12: (a) Norms of LVs for original Lorenz (1963) model and (b) the nine-variable model based upon 3 coupled Lorenz (1963) models. Green lines indicate LVs associated with the extratropical subsystem, red lines indicate LVs associated with the tropical subsystem, and blue lines indicate LVs associated with the ocean subsystem, separated according to how well their growth rates can be used as predictors for the subsystem. On longer time scales LV3 is neutral while LV4 is slightly decreasing.

Table 3.3: Lyapunov exponents for the Lorenz (1963) and coupled models.

	LE1	LE2	LE3	LE4	LE5	LE6	LE7	LE8	LE9
Lorenz	0.91	0	-14.58						
Coupled	0.91	0.36	0	-0.15	-0.55	-0.82	-1.85	-14.09	-12.27

The alignment of the Lyapunov vectors with one another was also compared (Figure 3.13). As expected there is some alignment of LV1 with LV4 and LV8 during an extratropical regime change but, unexpectedly, very little alignment between LV4 and

LV8. As seen in Figure 3.13, LV1 and LV4 align during the last cycle of a regime and upon entering a new regime. LV1 and LV8 align during the last cycle before a regime of three or more cycles. LV4 and LV8 are most closely aligned upon entering a regime that is four cycles or longer, although this is not true preceding the cycle beginning $t \sim 69$. LV2 and LV3 become aligned when the ocean changes regime (Figure 3.14). LV6 (a tropical LV) and LV8 (an extratropical LV) are collinear with one another in the same areas, approximately, where LV7 (an ocean LV) experiences the fastest decay, that is when entering an El Niño ocean regime or warm tropical cycle (Figure 3.15). Thus, the LVs lack the ability to completely decouple the fast and slow modes when these modes are strongly coupled.

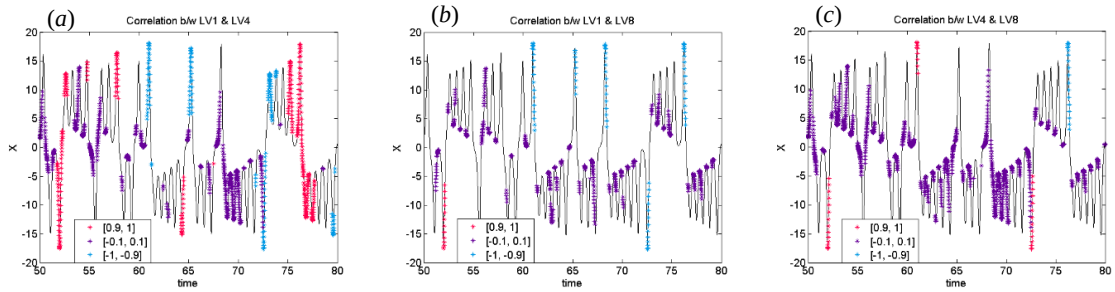

Figure 3.13: Correlations between (a) LV1 and LV4, (b) LV1 and LV8, and (c) LV4 and LV8 shown on the extratropical x-trajectory. LV1 and LV4 align most frequently.

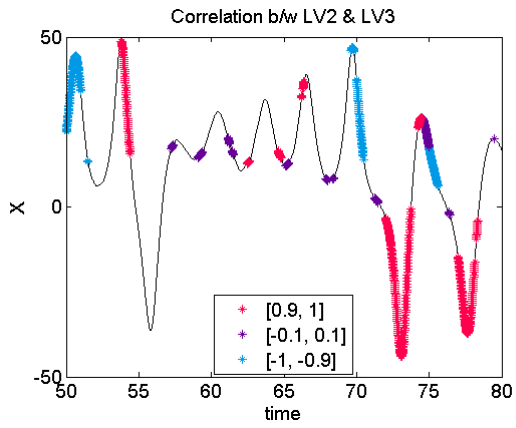

Figure 3.14: Correlation between LV2 and LV3 on the x-trajectory of the ocean subsystem. The vectors align upon entering a new regime.

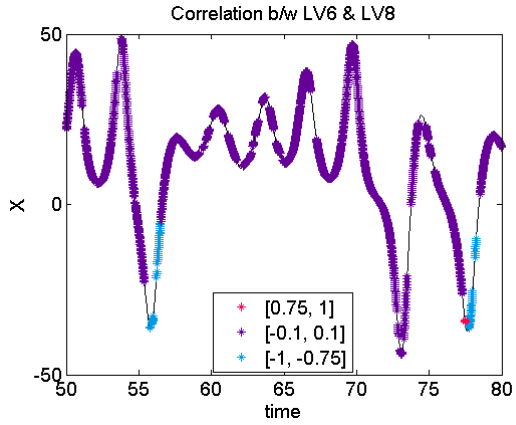

Figure 3.15: Correlation between LV6 (an LV associated with the tropical subsystem) and LV8 (an LV associated with the ocean subsystem. The two are most closely aligned when the ocean returns to normal, which corresponds to regions of fastest decay in LV7 (see Figure 3.6).

3.3 Results with the Fast-Slow Coupled Model with "Convection" Replacing the "Extratropical Atmosphere"

While the above results are interesting, they only focus on a system with two modes of growth while the atmosphere-ocean system has several modes of growth. Thus

we will examine the nine-variable model in the case where the 'weather noise' of the extratropical subsystem is replaced with 'convective noise.' This is done by setting τ_e of equation (13) to 10. Thus the convective subsystem will change with a frequency that is ten times the frequency of changes within the tropical subsystem and 100 times the frequency of changes within the ocean subsystem. We will study the effects of this change with the coupling used to study the effects of 'weather noise' ($c_e = c_t = 0.08$) and with a weaker coupling ($c_e = c_t = 0.008$). The solutions are quite similar, so only the attractors corresponding to the original coupling are shown in Figure 3.16. Figure 3.17 gives the x-trajectory for the three subsystems for both coupling coefficients. The vertical black lines denote the portions of the trajectories that will be the focus in the remainder of the figures of this section.

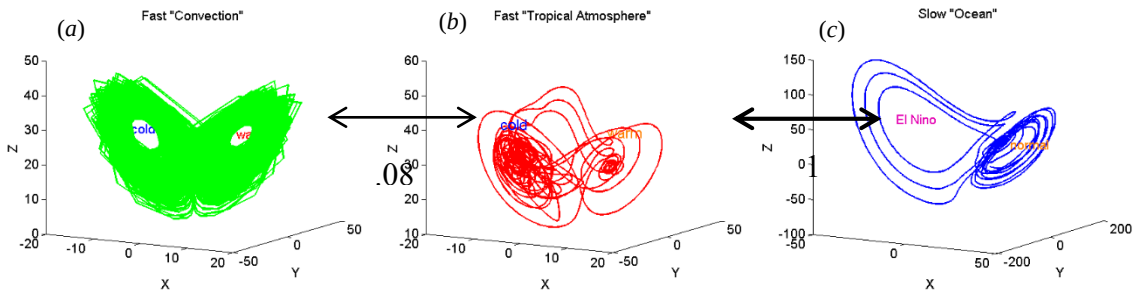

Figure 3.16: The attractors of the nine-variable system with 'convective noise.' Changes within (a) the convective subsystem occur at a rate 10 times faster than changes within (b) the tropical subsystem, which changes at a rate that is 10 times faster than (c) the ocean subsystem.

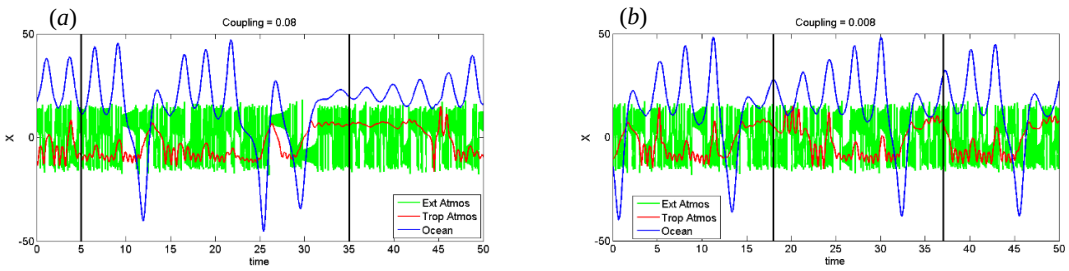

Figure 3.17: X-trajectory of the extratropical, tropical, and ocean subsystems for (a) coupling between the convective with the tropical subsystem equal to 0.08 and (b) coupling equal to 0.008. The black vertical bars mark the section of the trajectories that will be the focus in the figures in the remainder of this section.

3.3.1 Regime Change Predictive Powers of BVs, SVs, and LVs

Just as in the fast-slow coupled model with weather noise, the growth rates of BVs, SVs, and LVs are attributed to changes within the three subsystems of the fast-slow coupled model with convective noise. With the original coupling of 0.08, we targeted the fast mode BVs by using a small perturbation amplitude of 0.1 and a short rescaling window of 0.05 units (Figure 3.18(*a*)). In order to determine the fast mode BV of the nine-variable model using the weaker coupling, the perturbation was cut in half to 0.05 while the rescaling window remained 0.05 (Figure 3.18(*b*)). Their behavior is very similar providing regime change information for the convective subsystem with no perceived influence from the other two subsystems.

We computed the SVs by using an integration interval of 0.05 units. FSV1 growth rates for both convective models signal the end of the current regime (Figure 3.19(*b*) and (*d*)). The ISVs provide a slightly earlier warning since they are able to take advantage of future information (Figure 3.19(*a*) and (*c*)). This time there are only two LVs associated

with the fastest growing mode in both of the convective models. The LVs provide earlier warnings of regime changes than the BVs and FSVs.

We were also able to target the slow mode BV for each of the convective models (Figure 3.21). Both used a rescaling window of 0.35 units, but the slow mode BV for the model using the original coupling required a rescaling amplitude of 30 while the slow mode BV for the model using the weaker coupling required a slightly smaller rescaling amplitude of 25. Both behave in a similar manner, growing fastest and for longer periods of time during the last cycle of the current regime. They both also contain a lot of 'noise,' small areas of large growth within the regimes that do not correspond to changes within the ocean subsystem.

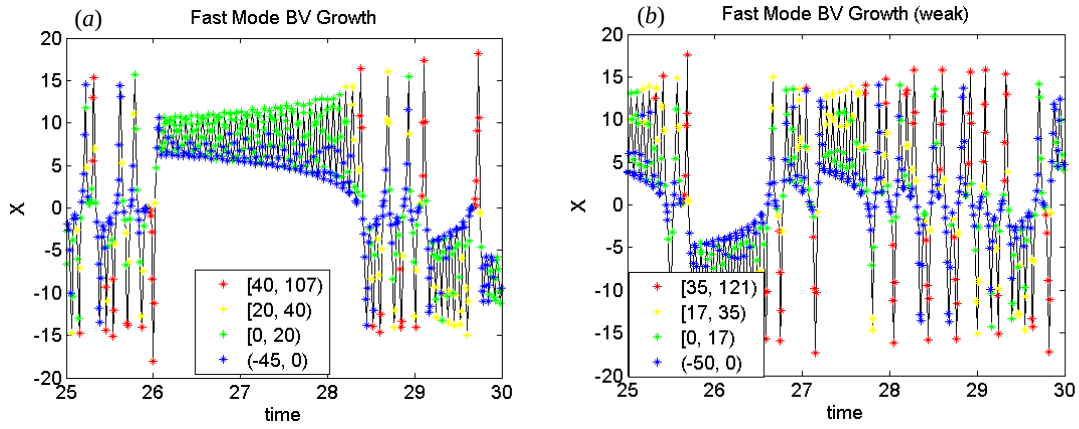

Figure 3.18: Fast mode BV corresponding to changes within the convective subsystem of the nine-variable model with (a) the original coupling of 0.08 and (b) the weaker coupling of 0.008.

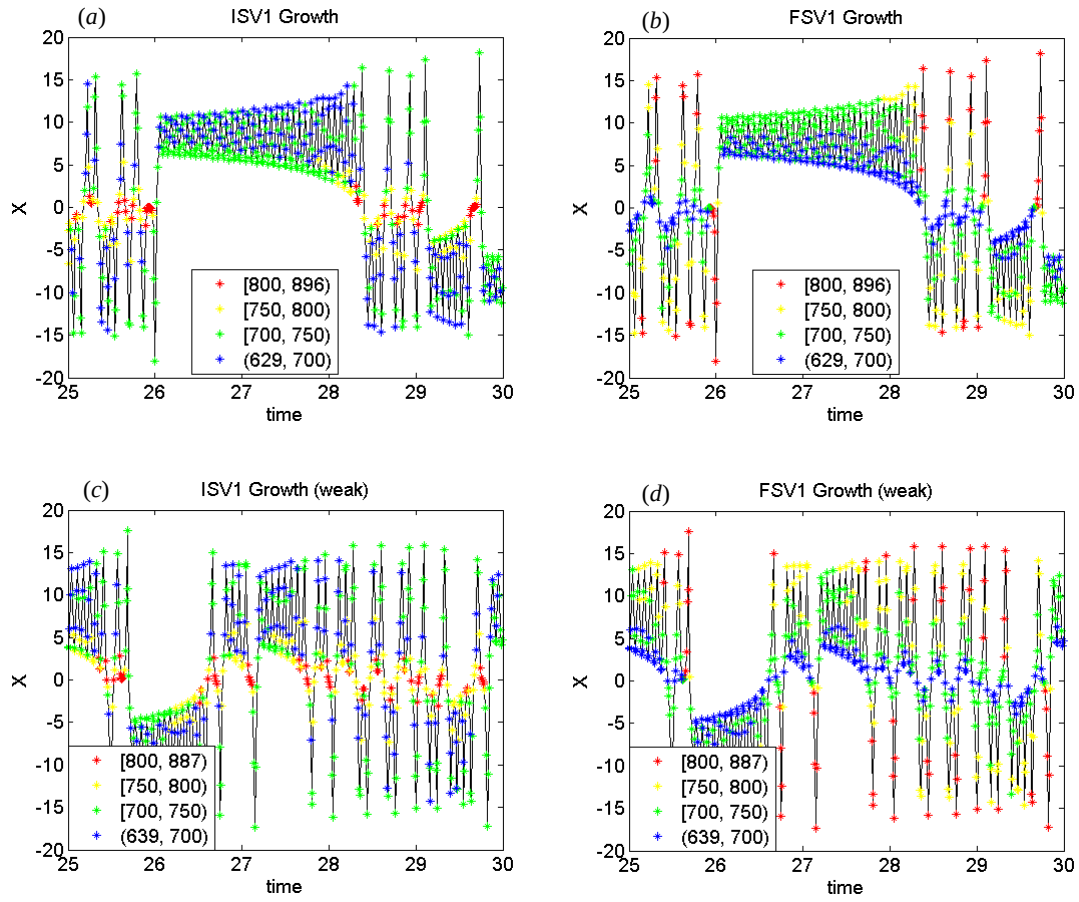

Figure 3.19: Growth rates of (a) the first initial and (b) the first final singular vector for the nine-variable model with the original coupling; growth rates of (c) the first initial and (d) the first final singular vector for the nine-variable model with the weaker coupling. Fast growth rates indicate the regime will change at the beginning of the next cycle. The initial singular vectors benefit from future information, giving earlier warnings than the final singular vectors.

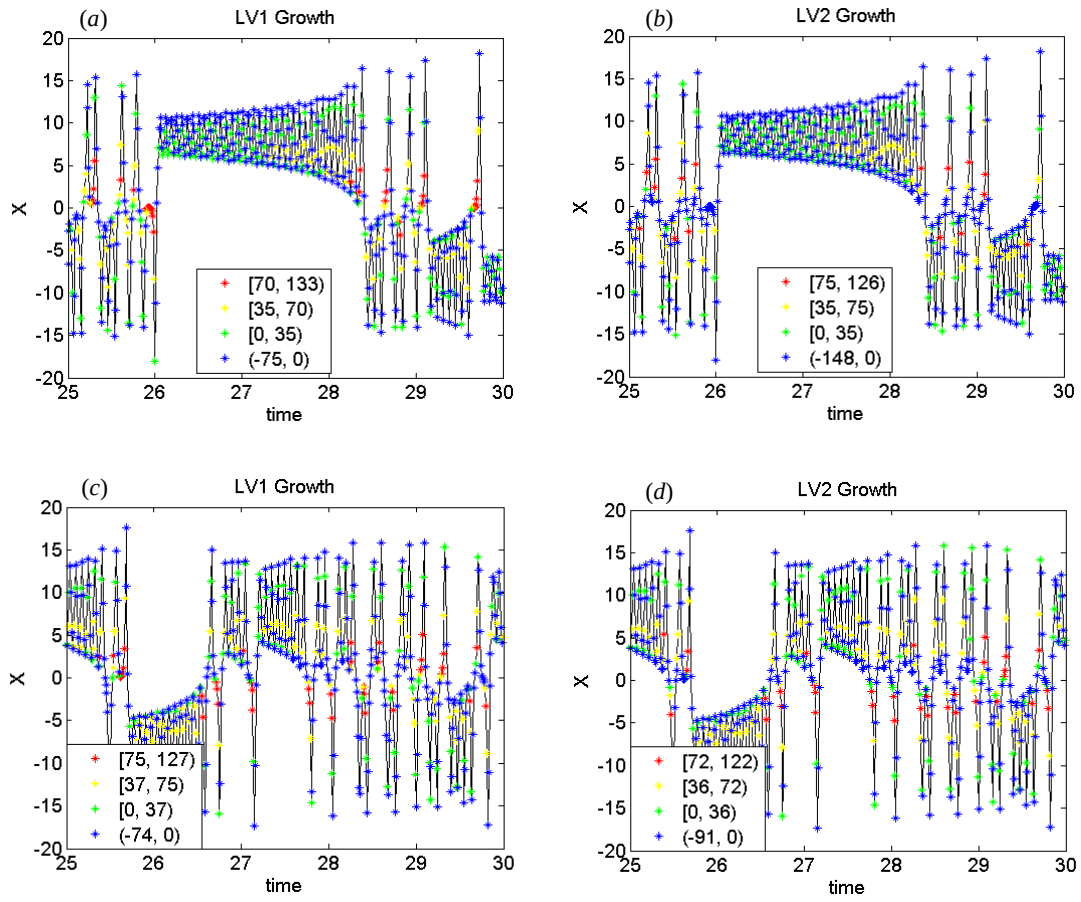

Figure 3.20: (a) LV1 and (b) LV2 of the nine-variable convective model with the original coupling. (c) LV1 and (d) LV2 of the nine-variable model with the weaker coupling. The LVs provide earlier warnings to regime changes in the higher frequency convective subsystems than the BVs and FSVs.

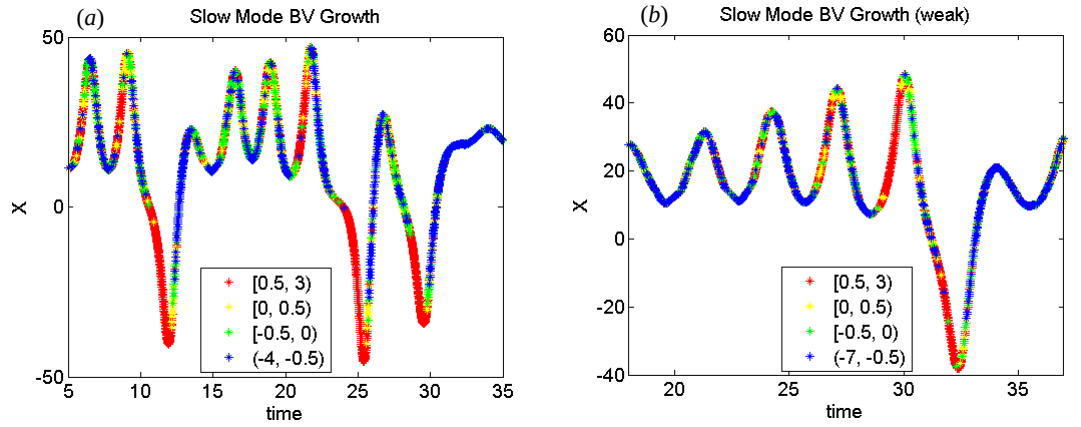

Figure 3.21: Slow mode BV growth for (a) the nine-variable model with the original coupling and (b) the nine-variable model with the weaker coupling. Both grow fastest the last cycle before a regime change.

Surprisingly, replacing the extratropical subsystem with the convective subsystem, enabled us to recognize SVs whose growth rates correspond to changes within the ocean subsystem (Figure 3.22). Three such SVs were found for the model using the original coupling of 0.08, and only one was found when the weaker coupling of 0.008 was used. For the original coupling, the third singular vector grows fastest when entering a new regime. The eighth singular vector decays fastest the final cycle of a regime and throughout an El Niño cycle, while the ninth singular vector decays slowest when the ocean is returning to normal after an El Niño cycle. The eighth singular vector corresponding to the model with the weaker coupling behaves in the same manner as the eighth singular vector corresponding to the model with the original coupling: it decays fastest the last orbit preceding and throughout an El Niño regime. Thus a clear difference

in all the frequencies of growth in a system seems to be required for the SVs to differentiate between the different modes of growth.

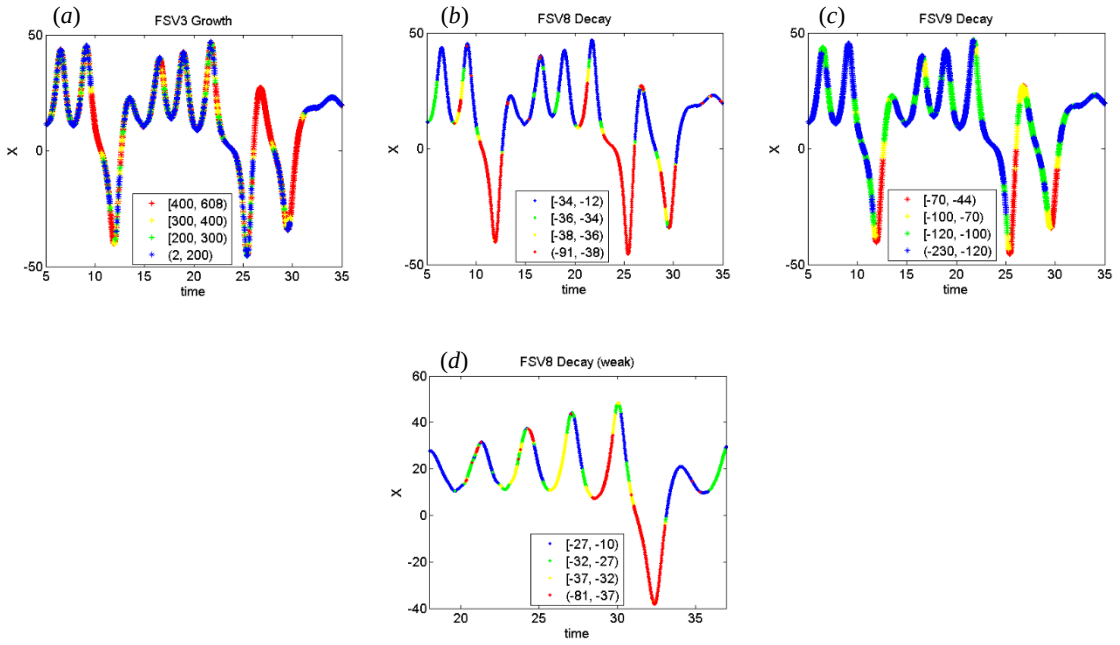

Figure 3.22: The first row gives growth/decay rates of the three FSVs computed for the convective system with the original coupling correspond to changes within the ocean subsystem: (a) FSV3 grows fastest when the ocean subsystem enters a new regime; (b) FSV8 decays fastest the last cycle before and throughout El Niño; and (c) FSV9 decays slowest when going from El Niño back to normal. (d) shows FSV8 decays fastest the last cycle before and during an El Niño event in the convective system with the weaker coupling.

There are also particular LVs whose growth rates correspond to changes within the slow moving ocean subsystem (Figure 3.23). In the convective system with coupling of 0.08 there are three, LV7, LV8, and LV9 (Figure 3.23(*a*), (*b*), and (*c*), respectively). LV7 and LV8 are better predictors, growing fastest and for long periods of time during the last orbit of the current regime. LV9 also grows fastest during the last orbit of the current regime, but it does so for a very short period of time. There is only one LV, LV7

(Figure 3.23(*d*)), associated with the slow moving ocean subsystem in the convective model with coupling of 0.008. It grows fastest upon entering an El Niño cycle, providing a very late warning, and during the last cycle of an El Niño event.

Again, because of the strong coupling between the tropical and ocean subsystems, and the ocean being a driver for changes within the tropical subsystem, we are unable to find a BV whose growth rates correspond to changes within the tropical subsystem. There are, however, SVs and LVs whose growth rates correspond to changes within this system. Figure 3.24 illustrates how the growth and decay rates of these vectors match the tropical subsystem. FSV7 decays fastest for long periods of time when entering a new regime in the convective model with the original coupling of 0.08 (Figure 3.24(*a*)). FSV4, FSV5, and FSV6 grow fastest during local minimum and maximum values (Figure 3.24(*b*), (*c*), and (*d*)). None of the LVs found for either convective system have growth rates that can be used to predict regime changes within the tropical subsystem (Figure 3.25). Instead fast growth typically signals a local extremum.

It was also possible to find 'coupled' SVs (Figure 3.26) and LVs (Figure 3.27), those whose growth rates identify changes in both the tropical and ocean subsystems. Although almost all of the vectors that are assigned to the tropical subsystem show small influences from the ocean subsystem, just as almost all of the vectors that are assigned to the ocean subsystem show small influences from the tropical subsystem, the 'coupled' vectors differ in that their growth rates are not dominated by one subsystem or the other. Instead the length of time of the growth (decay in the case of FSV9 in Figure 3.26(*b*) and (*d*)) typically determines to which subsystem the growth rates refer. Thus the fast growth around $t \sim 6$ and $t \sim 16$ signal local minima in the tropical subsystem with the original

coupling. Prolonged fast growth around $t \sim 21$ signals the approach of El Niño (Figure 3.26(*a*) and (*c*) for FSV4; Figure 3.27(*a*) and (*d*) for LV4). Likewise, in the system with the weaker coupling, prolonged periods of growth (decay) signify changes within the ocean subsystem while shorter periods of growth (decay) indicate changes within the tropical subsystem. Table 3.4 provides a summary of the growth rates of all the vectors of the nine-variable model with "convection" and the original coupling between the convective and tropical subsystems of 0.08. Table 3.5 provides the same for the nine-variable model with the weaker coupling of 0.008.

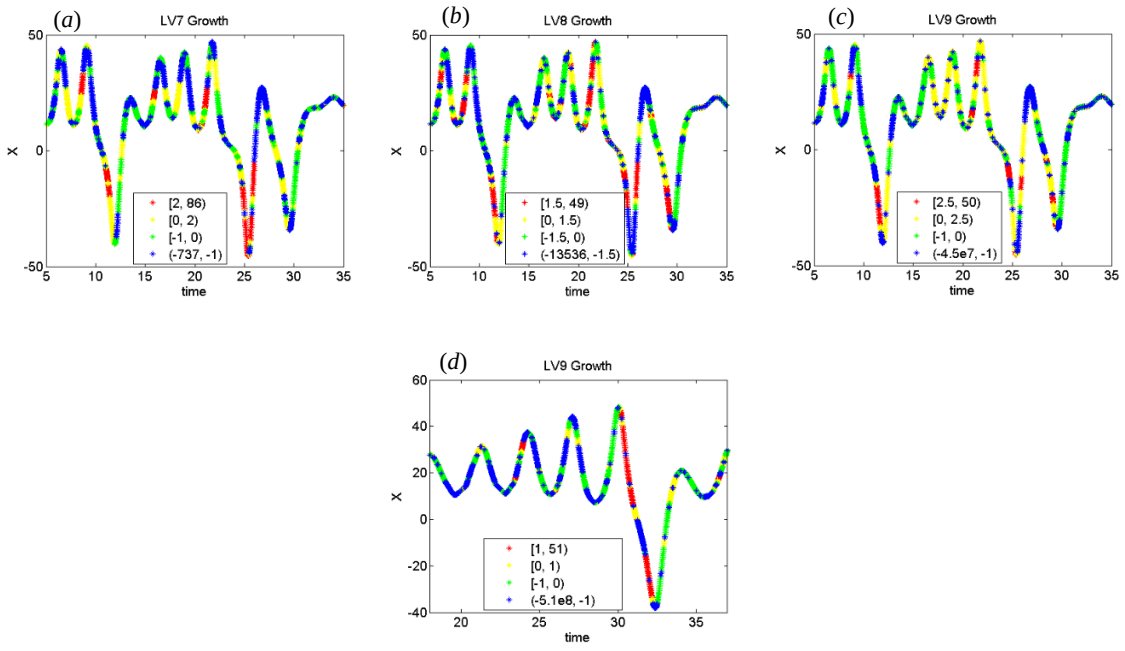

Figure 3.23: LVs whose growth rates correspond to changes within the slow ocean subsystem. For the nine-variable model with the original coupling of 0.08, (a) LV7, (b) LV8, and (b) LV9's prolonged and fast growth rates signal the current cycle will be the last in the regime, with LV7 being a more successful predictor. (c) LV9 growth in the nine-variable model with the weaker coupling of 0.008 gives very late warning for the onset of El Niño.

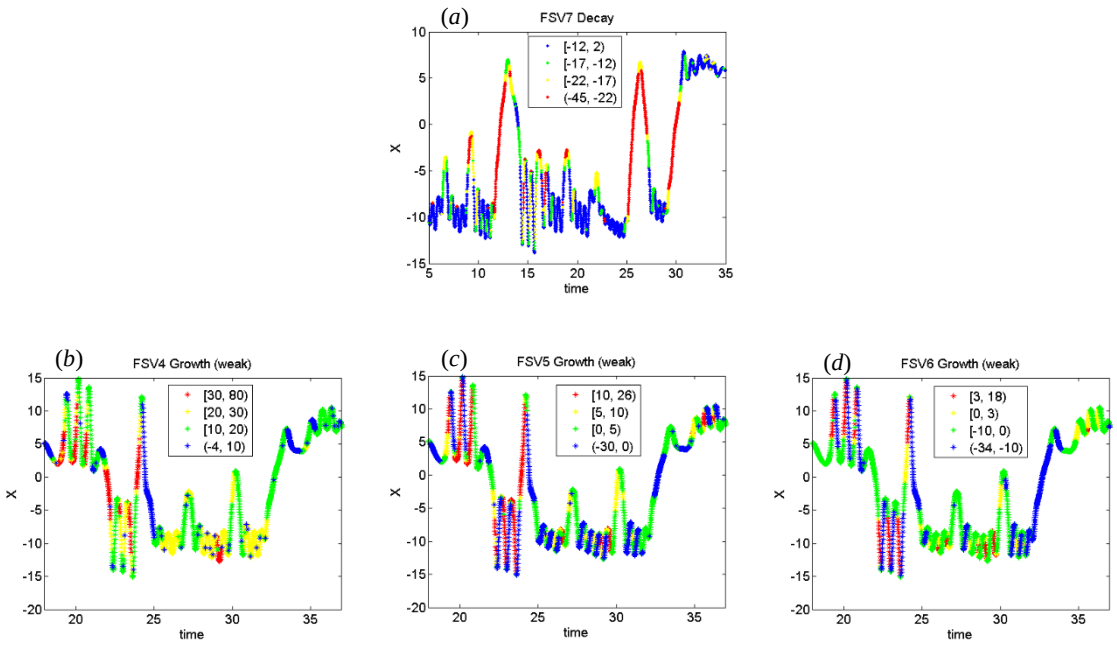

Figure 3.24: FSVs whose growth (decay) rates correspond to changes within the tropical subsystem. (a) FSV7 decay in the nine-variable model with the original coupling of 0.08. Prolonged, fast growth indicates the system is moving into a new regime. Short periods of fast growth often indicate a local maxima or minima. (b) FSV4 growth, (c) FSV5 growth, and (d) FSV6 growth in the nine-variable model with the weaker coupling of 0.008. Fast growth signals a local extremum for all vectors.

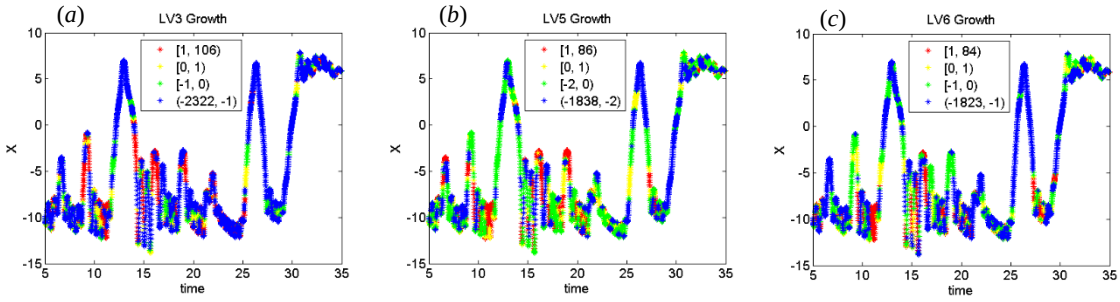

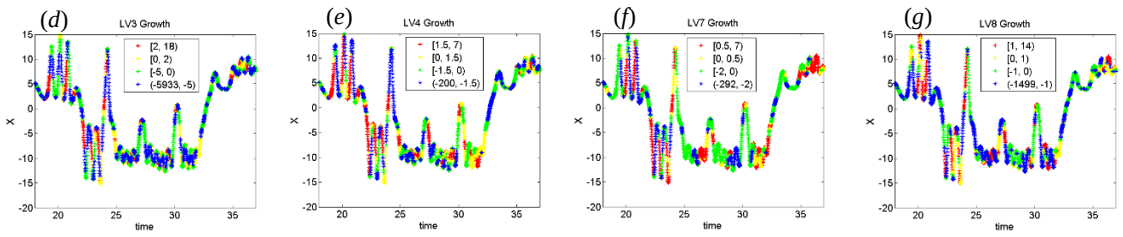

Figure 3.25: (a) LV3, (b) LV5, and (c) LV6 growth in the convective system with coupling equal to 0.08. (d) LV3, (e) LV4, (f) LV7, and (g) LV8 growth in the convective system with coupling equal to 0.008. None of the LVs can be used as predictors of regime change. Fast growth typically indicates a local extremum.

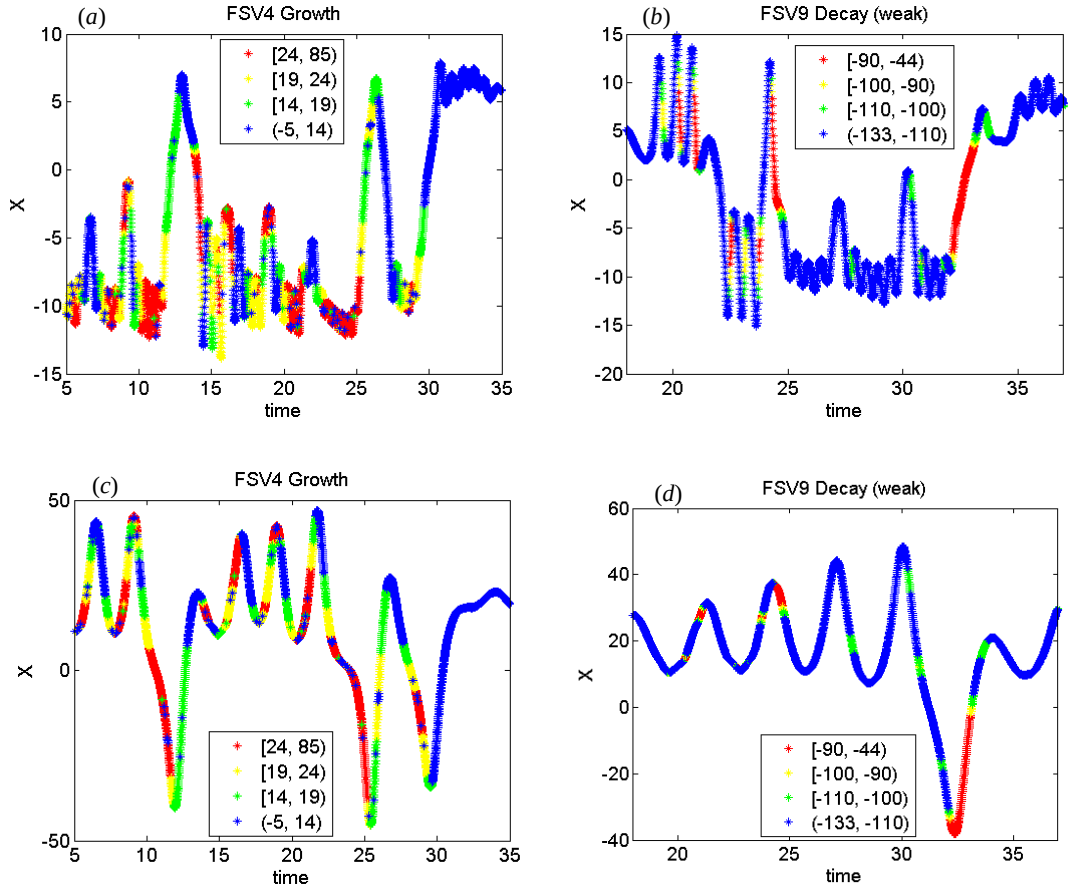

Figure 3.26: The 'coupled' FSV4 of the convective model with the original coupling on the (a) tropical subsystem and (c) ocean subsystem. Very long periods of fast growth signal regime changes in the ocean subsystem. Short periods of fast growth indicate local extremum within the tropical subsystem. The

'coupled' FSV9 of the convective model with the weaker coupling on the (b) tropical subsystem and (d) ocean subsystem are also shown. Very long periods of slow decay indicate a return to normal in the ocean. Shorter periods of slow decay point to changes within the tropical subsystem.

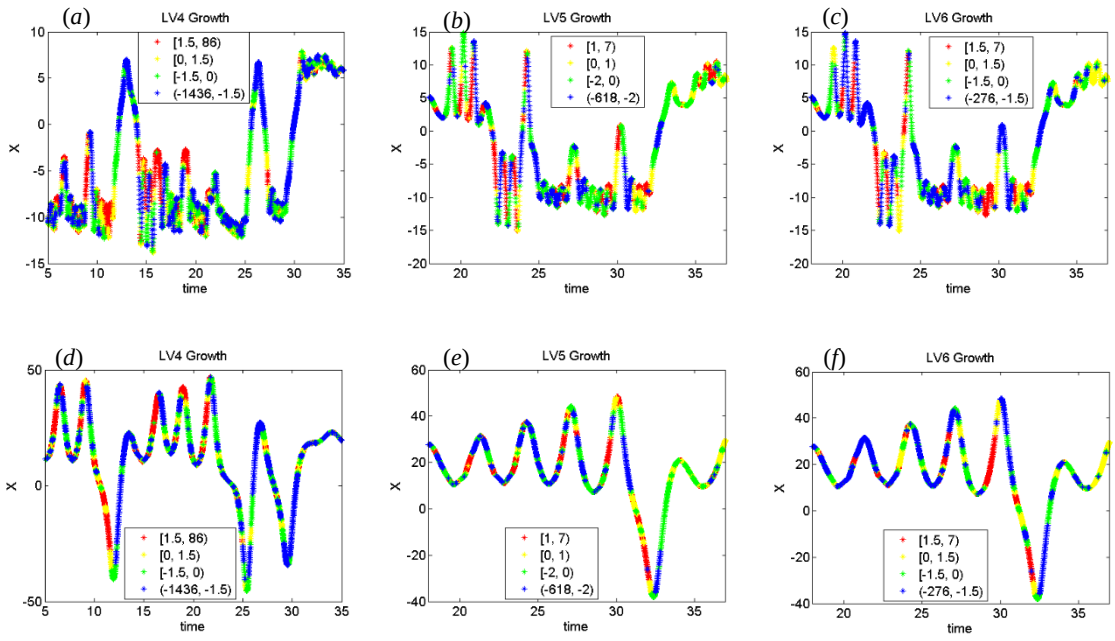

Figure 3.27: The only 'coupled' LV of the convective system with coupling of 0.08 is LV4 shown on (a) the tropical and (d) the ocean subsystems. Fast growth around $t \sim 6$ and $t \sim 16$ signals local minima in the tropical subsystem. Prolonged fast growth around $t \sim 21$ signals the approach of El Niño. LV5 and LV6 are the 'coupled' LVs of the convective system with a coupling of 0.008. Fast growth within the normal regime of the ocean points to local extrema in the tropical subsystem while prolonged fast growth at $t \sim 30$ points to the onset of El Niño in the ocean subsystem.

Table 3.4: Thresholds for the growth rates of the vectors of the nine-variable model with 'convection' and the original coupling of 0.08 between the 'convective' and 'tropical' subsystems. Green is for vectors associated with convection, red for those associated with the tropics, blue the ocean, and purple the coupled vectors associated with both the tropics and ocean. In strictly decaying vectors, typically fastest decay

corresponds to changes within a subsystem, but in the case of FSV9 (the starred vector) slowest decay corresponds to changes within the subsystem.

Vector	LV1	LV2	LV3	LV5	LV6	LV7	LV8	LV9	LV4
Growth Rate	70	75	1	1	1	2	1.5	2.5	1.5
Vector	Fast BV	SV1		FSV7	Slow BV	FSV3	FSV8	FSV9*	FSV4
Growth Rate	40	800		-45	1.1	400	-91	-70	24

Table 3.5: Same as Table 3.4 for the nine-variable model with 'convection' and the weaker coupling of 0.008.

Vector	LV1	LV2	LV3	LV4	LV7	LV8	LV9	LV5	LV6
Growth Rate	75	72	2	1.5	0.5	1	1	1	1.5
Vector	Fast BV	SV1	FSV4	FSV5	FSV6		Slow BV	FSV8	FSV9*
Growth Rate	35	800	30	10	3		0.5	-81	-90

3.3.2 Correlations among BVs, SVs, and LVs

Table 3.6 contains the subsystem each LV and SV corresponds to as a reference. Instead of being almost equal, the leading LV and the fast mode BV often face opposite directions. Thus the average absolute correlation between the two is 0.874 when the coupling coefficient is 0.08 and 0.857 when the coupling coefficient is 0.008. The average absolute correlation between the fast mode BV and LV2 is 0.859 when the coupling coefficient is 0.08 and 0.849 when the coupling coefficient is 0.008. Unlike with the three-variable model, the BV's local loyalty is not contingent upon LV2 growing faster than LV1 (

Figure 3.28(*a*) and (*c*) and Figure 3.29(*a*) and (*c*)) or fast growth of LV1 (

Figure 3.28(*b*) and Figure 3.29(*b*)) or LV2 (

Figure 3.28(*d*) and Figure 3.29(*d*)). Reducing the perturbation to 10^{-5} and the rescaling window to 0.02 units in an attempt to make the BV more linear did nothing to increase the correlation between LV1 and the fast mode BV regardless of the coupling within the system.

When the coupling is 0.08, the slow mode BV is often approximately collinear with LV7, LV8, and LV9, but there is no readily apparent pattern to their alignment. However, when the coupling is reduced to 0.008, the slow mode BV and LV9, which is associated with the ocean subsystem, align slightly during the last cycle before a regime change (Figure 3.30). Thus it seems a marked difference between the frequencies of the instabilities of a system and weak coupling between the fastest changing modes and the slowest changing modes are needed in order for the BVs and LVs corresponding to the slowest instabilities to agree.

There seems to be no obvious reason for the sporadic alignment of the SVs with the fast mode BV, LV1, or LV2 as the SVs continue to change direction often and keep no memory of the previous windows. This is also true when the SVs that are closely related to the ocean subsystem are compared to the slow mode BVs and ocean LVs regardless of the coupling of the subsystems. Comparisons amongst tropical SVs and LVs and the ‘coupled’ SVs and LVs yielded similar results.

Table 3.6: Subsystem each LV and SV corresponds to within the nine-variable model with 'convection' chosen according to how well their growth rates match changes in the subsystem.

	Convection	Tropics	Ocean	Coupled
$c_e =$ 0.08	LV1 LV2 FSV1	LV3 LV5 LV6 FSV7	LV7 LV8 LV9 FSV3 FSV8 FSV9	LV4 FSV4
$c_e =$ 0.008	LV1 LV2 FSV1	LV3 LV4 LV7 LV8 FSV4 FSV5 FSV6	LV9 FSV8	LV5 LV6 FSV9

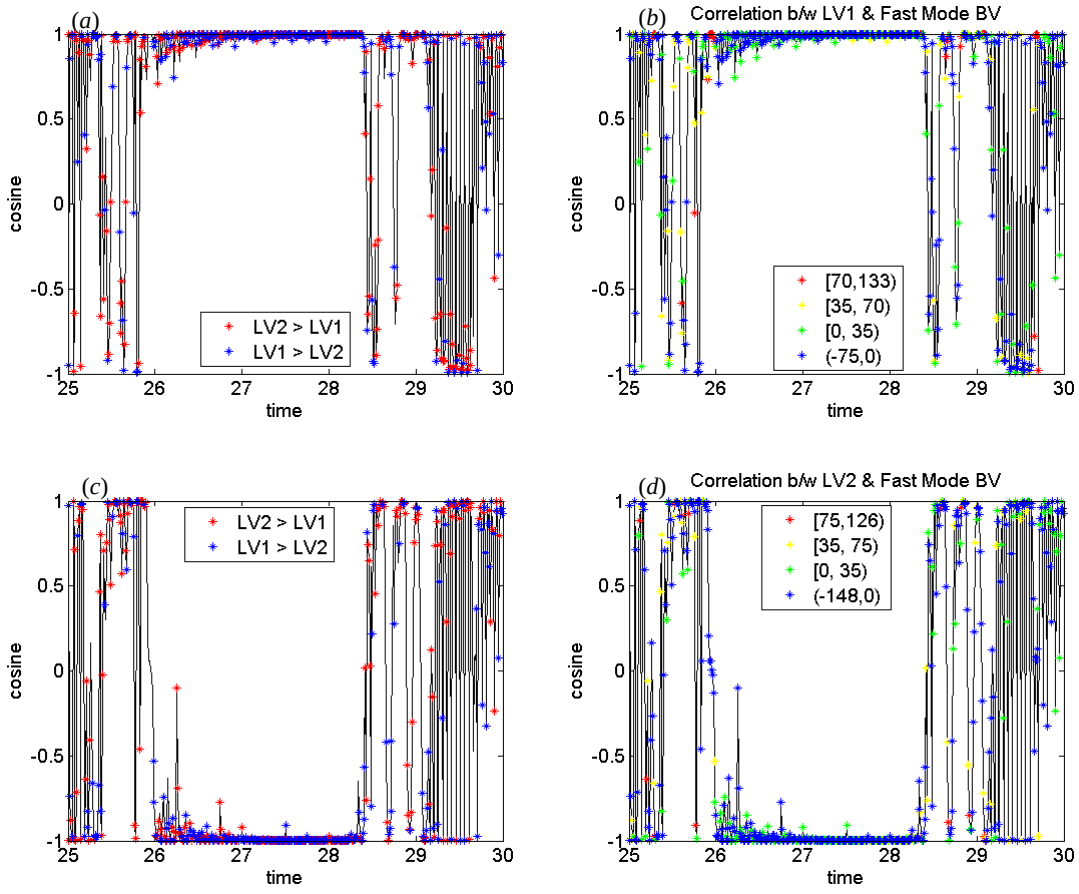

Figure 3.28: The correlation between LV1 and the fast mode BV (with coupling coefficient 0.008) colored with stars indicating (a) when LV2 grows faster than LV1 and (b) the growth rates of LV1. The correlation between LV2 and the fast mode BV colored with stars indicating (c) when LV2 grows faster than LV1 and (d) the growth rates of LV2. The BV does not exclusively align with LV2 when it grows faster than LV1 or when LV2 grows quickly in general.

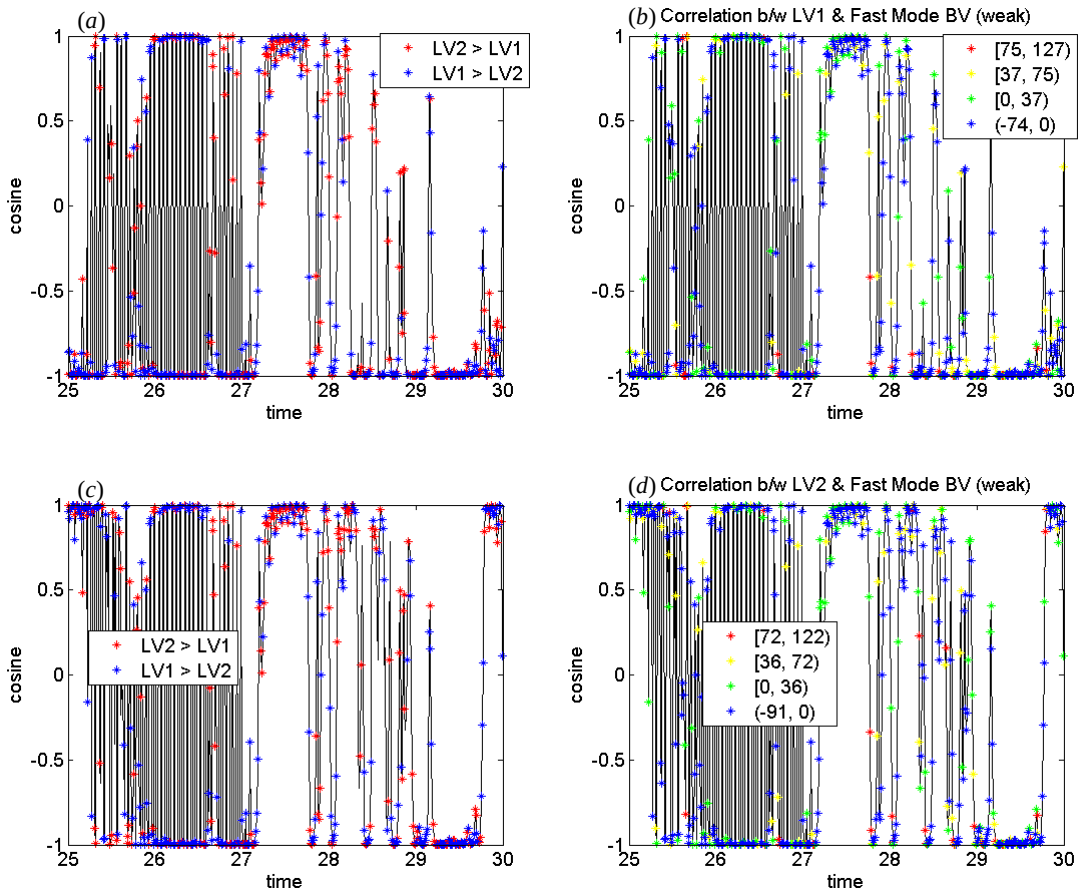

Figure 3.29: The correlation between LV1 and the fast mode BV (with coupling coefficient 0.008) colored with stars indicating (a) when LV2 grows faster than LV1 and (b) the growth rates of LV1. The correlation between LV2 and the fast mode BV colored with stars indicating (c) when LV2 grows faster than LV1 and (d) the growth rates of LV2. LV2 growing faster than LV1 does not imply the BV will become more aligned with LV2. The BV is more aligned with LV1 and LV2 when either grows fast, but this is not the only time the BV is aligned with either.

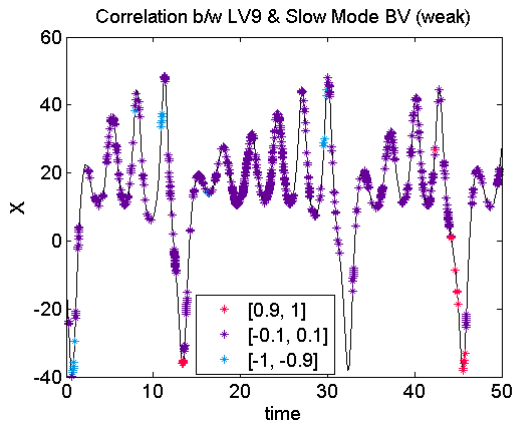

Figure 3.30: Correlation between the slow mode BV and LV9 when the coupling coefficient is 0.008 along the entire x-trajectory of the ocean subsystem. There is some alignment between the vectors during the last cycle before a regime change. When the nine-variable model had the 'extratropical' subsystem instead of 'convection,' there was no significant agreement among LVs associated with the slow modes (which were slightly influenced by changes within the 'tropical' and sometimes 'extratropical' subsystems) and the slow mode BV.

3.3.3 Correlations among LVs

Figure 3.31 gives the norms of the LVs for the nine-variable model using a coupling of 0.08 (Figure 3.31(*a*)) and 0.008 (Figure 3.31(*b*)) while Table 3.7 provides the corresponding Lyapunov exponents. Both have two growing vectors, but unlike the three-variable Lorenz (1963) model and the coupled model with an extratropical subsystem, there are no vectors with zero global growth. All of the other vectors are decreasing. Also note LV8 and LV9 should be the fastest decaying vectors, but LV3 and LV9 are actually the fastest decaying vectors.

LV1 and LV2 are often collinear, having an average absolute correlation of 0.884 for the nine-variable model with a coupling of 0.08 between the convective subsystem and the tropical subsystem and an average absolute correlation of 0.895 when the coupling is 0.008. Many of the LVs often share the same space, but there is no useful or readily discernible pattern to their correlations.

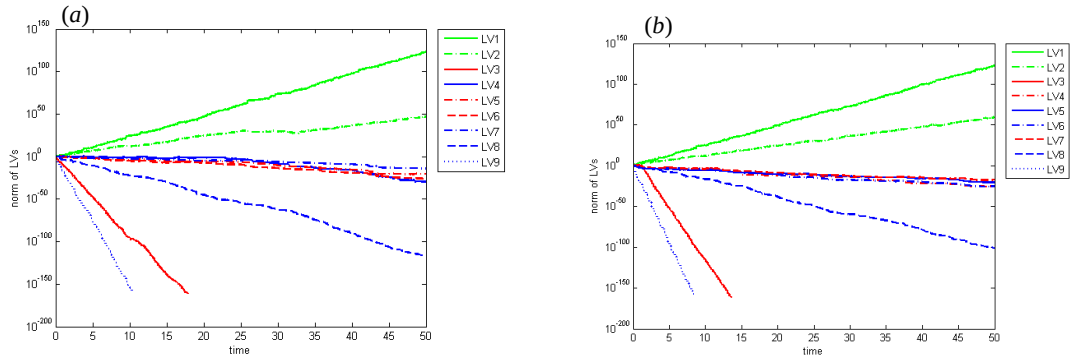

Figure 3.31: Norms of LVs for the nine variable model with the coupling between the convective and tropical and ocean subsystems equal to (a) 0.08 and (b) 0.008. Green lines mark LVs associated with the convective subsystem, red lines mark LVs associated with the tropical subsystem, and blue lines mark LVs associated with the ocean subsystem, separated according to how well their growth rates can be used as predictors for the subsystem. Oddly, LV3 is the second fastest decaying vector; LV3 and LV9 presumably decay faster with the weaker coupling because the effects of the fast convective system are lessened.

Table 3.7: Lyapunov exponents for the nine-variable model with a convective subsystem with two different couplings between the convective and tropical subsystems. While the values are similar to one another, they are very different from the LEs of the nine-variable model with an extratropical subsystem (see Table 3.3).

	LE1	LE2	LE3	LE4	LE5	LE6	LE7	LE8	LE9
$c_e = 0.08$	6.82	3.06	-23.40	-1.84	-1.30	-1.53	-0.82	-14.32	-5.25e4
$c_e = 0.008$	6.86	3.74	-36.70	-1.33	-1.06	-1.19	-0.86	-8.46	-5.87e5

3.4 Summary

Extending the work of Evans *et al.* (2004) and Peña and Kalnay (2004) it is clear the growth rates of BVs, SVs, and LVs can be used to predict regime changes and the three types of vectors can be used to target specific modes of growth with varying degrees of success. Regardless of the frequency of the fastest modes of growth in relation to the slowest modes, BVs can target each through careful selection of the perturbation amplitude and rescaling window (PK04). They are unable to recognize the existence the tropical subsystem, but this is because it is strongly coupled to the ocean subsystem, which completely governs the changes within the tropical subsystem. SVs are only able to recognize the tropical and ocean subsystems when the frequencies of each subsystem are different, as in the case when the weather noise is replaced with convection. LVs, on the other hand, are always able to spot each of the three subsystems. Unlike the BVs, they are unable to completely decouple the various modes of growth. Thus LVs whose growth rates strongly relate to changes within the ocean subsystem are sometimes influenced by changes within the tropical subsystem. Also, the LVs and SVs that are linked to the tropical subsystem cannot be used as predictors of regime changes, but only local extrema, at best. Interestingly, there are also 'coupled' LVs and SVs when the frequencies of each subsystem are different. These are vectors whose growth rates correspond to both the ocean and tropical subsystems while being dominated by neither. While this is an interesting trait of the SVs and LVs, BVs may be more useful in weather prediction because of their unique ability to isolate a particular mode of growth.

Although each of the three types of vectors, bred, singular, and Lyapunov, has slightly different behaviors, because they describe the same instabilities they often align with one another. In general the alignments between BVs and LVs occur near regime changes in the subsystem to which they correspond. Hence, for example, the approximate alignment of the slow mode BV in the nine-variable model with weather noise with LV2 and LV3. The same is true when LVs are compared to other LVs. The SVs sometimes align with the LVs, but these alignments are not directly related to changes within the subsystem.

In the standard three-variable Lorenz (1963) model we saw that BVs will align more with the locally fastest growing Lyapunov vector, which was often LV2. This is not true in the coupled model. With an extratropical subsystem, the fast mode BV will align as close to LV4 as the model will allow during those times when LV4 grows faster than LV1, but the BV does not fully break its loyalty to LV1. With a convective subsystem the nearly parallel alignment of the fast mode BV to LV2 does not appear to rely upon the growth rates of LV2 at all.

Now that we have an idea of the behavior of bred, singular, and Lyapunov vectors in simple models, we want to see how they behave in a more complex case. We move now to a quasi-geostrophic model. While this model has many more degrees of freedom, like the Lorenz (1963) model, it has only a single mode of growth, in its case associated with baroclinic instability.

Chapter 4 : Experiments with a Quasi-Geostrophic Model

4.1 Description of the Quasi-Geostrophic Model

The quasi-geostrophic (QG) model provides a simplification of extratropical synoptic scale motions by making approximations in the primitive equations that govern fluid motions. In particular, winds are approximated by their geostrophic values in the continuity equation and in the acceleration and advection terms of the momentum and thermodynamic equations, respectively. Also the static stability of the thermodynamic equations is replaced by basic state static stability (Holton 2004, pp. 147-151). With these approximations in place, the QG model presents a relatively realistic approximation of synoptic scale motions that contains advection, diffusion, relaxation, and Ekman pumping at the bottom level. The model described by Rotunno and Bao (1996) has 7 levels on a 65 x 33 grid leading to 15,015 total degrees of freedom. The nondimensional form of the equation for a Boussinesq fluid on a β-plane is

$$q_t + \beta\psi_x q_y - \psi_y q_x = 0$$

where potential vorticity, q, is given by

$$q = \psi_{xx} + \psi_{yy} + \left[\frac{\psi_z}{S(z)}\right]_z .$$

ψ is the geopotential, and $S(z)$ is the stratification parameter. Snyder *et al.* (2003) describe the forcing and dissipation included in the model. There is a single mode of growth for this system, baroclinic instability. This instability is associated with weather waves that transport heat poleward, compensating for the positive net radiative heating in the tropics and net cooling in high latitudes.

When solving these equations, it is assumed there are walls at the northern and southern boundaries, a frictionless lid at the upper vertical boundary, a well-mixed Ekman layer, and the x direction is periodic. These assumptions bring the total degrees of freedom down to 14,336. The variables for the model are potential vorticity in the 5 inner layers and potential temperature at the top and bottom layers. This particular QG model has been used in several studies (e.g. Snyder *et al.* 2003; Snyder and Hamill 2003; S.-C. Yang *et al.* 2009a) and has even been considered in the context of data assimilation in the unstable subspace (Uboldi *et al.* 2005; Carrassi *et al.* 2007; Carrassi *et al.* 2008a, 2008b). Here we will study the dominant modes of growth in the "true" (sans the effects of model and observational errors) trajectory only.

4.2 BV and SV Behavior

For this particular model, the dynamically relevant mode of growth (baroclinic instability) is best targeted with bred vectors. A range of perturbation amplitudes and rescaling windows can be used; here we use a rescaling amplitude of 1 and a rescaling window of 24 hours. Although the choice of norm changes some properties of the singular vectors (Palmer *et al.* 1998; Snyder and Joly 1998; S.-C. Yang *et al.* 2015), a

kinetic energy norm is used for all vectors. Figure 4.1(*a*) shows two of the five BVs computed using these parameters, one shown by color shading and the other by black contours. At the initial time these are simply random perturbations. Figure 4.1(*b*) gives the local ensemble dimension of all five BVs for this first time period, which is approximately five in the center of the domain and smaller near the walls that impose a constraint. Although the vectors are global, the ensemble dimension is computed locally, on a 5 x 5 grid using the method of Patil *et al.* (2001). The equation of the local ensemble dimension, ED, is given by

$$ED = \frac{\left(\sum_{i=1}^{k} \sigma_i\right)^2}{\sum_{i=1}^{k} \sigma_i^2}.$$

σ_i is the i^{th} singular value of the matrix $B^T B$, where the columns of B are the bred vectors, and k is the total number of vectors, five in this case. Because we are interested in the local dimension, the entire BV was not used in matrix B; only the portion of the BV that was within two grid points of the point of interest was included.

All 5 bred vectors quickly collapse into a single vector (Figure 4.2). By the fifth day the BVs have coalesced into a single vector, corresponding to the results of Corazza *et al.* (2003), but the tenth day is shown. It is clear there is only one vector describing the shape and growth of the instability. We also computed BVs using a rescaling window of 24 hours and amplitudes of 0.25, 0.5, and 2. The growth rates for all three have the same general behavior, converging to an (approximate) constant value after the first few days (Figure 4.3(*a*)). The growth rates (whose computation is given in section 1.2, here using an integration of thirty minutes) are constrained by the overall growth of the system. Thus the bred vectors with larger amplitudes, being closer to the saturation level of the

QG system, have a smaller growth rate than the bred vectors with smaller amplitudes. Also, the growth rates approach a constant value because they are global rates. Locally the growth rates would vary greatly, but globally the total energy is constant, thus the growth rates converge to a constant value after merging. Figure 4.3(*b*) gives the local dimension of these four vectors. Again, they all converge to the same vector. There is only one type of instability for this model, and all small perturbations will eventually align with the leading LV (Oseledec 1968); thus this is the leading Lyapunov vector for this model.

To compute the SVs, the Lanczos algorithm was used to solve the eigensystem (4) for the ISVs. Then (5) was used to compute the FSVs. The first final singular vector, FSV1, should align with the bred vectors/leading LV as the integration window is extended. Unfortunately the SVs for this model fail to converge. Figure 4.4 shows the first final SV computed using optimization windows of 96, 120, and 144 hours. The FSV computed using 120-hour window is shaded; those computed using 96- and 144-hour integration windows are the contours of Figure 4.4(*a*) and (*b*), respectively. These integration windows were chosen because the BVs converge within 5 days of the start of the breeding process. We had hoped the SVs would follow suit and converge within the first week. Unfortunately they do not. We extended the integration to eight days, always increasing in increments of 24 hours, but this did not improve the results. Although there are local regions of agreement among these vectors, in particular the region from 0° to 2°E and the equator to 2°N, it is clear these are all different vectors. Note the opposite signs of the vectors in regional areas of agreement is unimportant since they were found by simply extending the integration window. If the WS07 algorithm were used successive

vectors would use previous information to ensure they are pointing in the same general direction. We also computed the second leading final singular vector, FSV2, and they also fail to converge within a week (Figure 4.5).

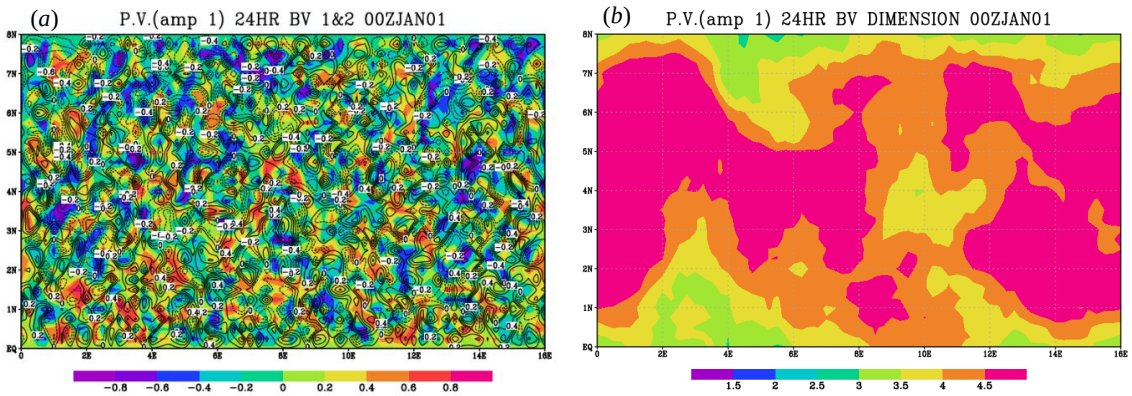

Figure 4.1: (a) Potential vorticity at level 1 (where level 0 is the surface) for two random initial perturbation vectors. (b) The dimension of the five BVs initialized at this time.

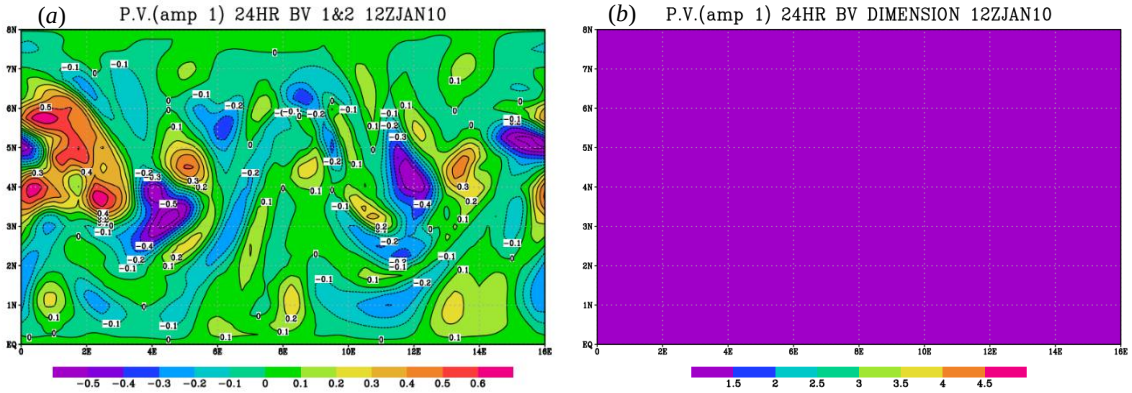

Figure 4.2: (a) Two of the five potential vorticity BVs computed using a perturbation amplitude of 1 and rescaling window of 24 hours the 10th day after initialization. (b) The local dimension of the five BVs is approximately 1 because the BVs converged to the single growing Lyapunov vector.

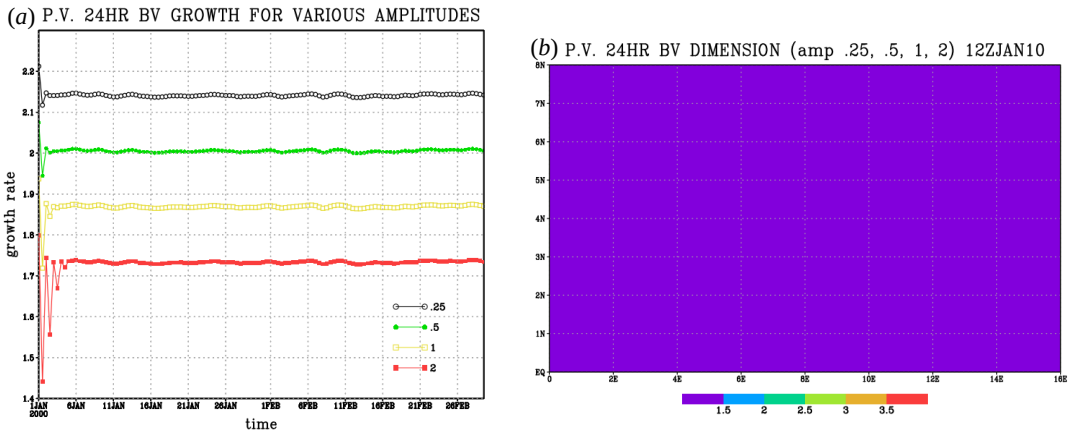

Figure 4.3: (a) Growth rates computed with a rescaling window of 24 hours and perturbation amplitudes of 0.25, 0.5, 1, and 2. Growth rates are different because larger amplitudes are closer to nonlinear saturation, but they have the same general behavior. (b) Local dimension for these BVs is approximately 1, meaning they all converge to the leading LV.

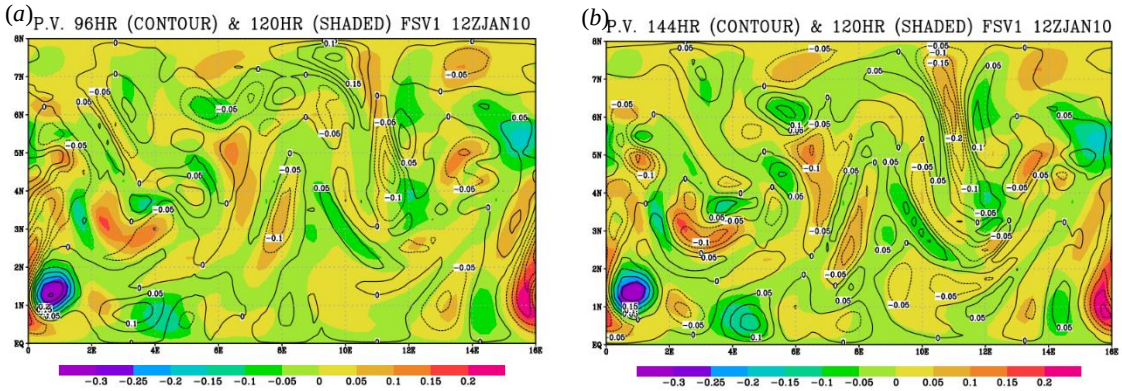

Figure 4.4: The first final SV on the 10th day. Shaded regions for both are FSV1 computed using a 120-hour integration window. (a) Contours are FSV1 computed with a 96-hour integration window. (b) Contours are FSV1 computed using a 144-hour integration window. Unlike the bred vectors (Figure 4.2), FSV1 fails to converge within the first 10 days.

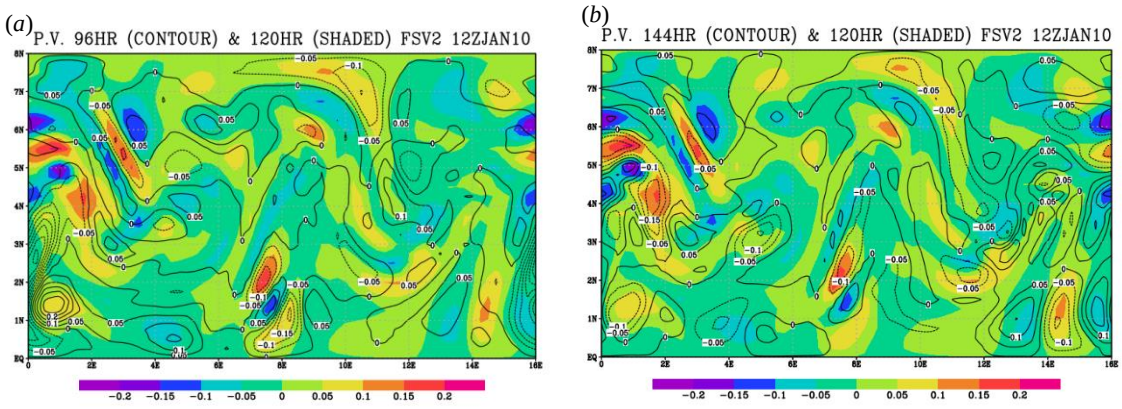

Figure 4.5: The second leading final SV on the 10th day. Shaded regions for both are FSV2 computed using 120-hour integration windows. (a) Contours are FSV2 computed using a 96-hour integration window. (b) Contours are FSV2 computed using a 144-hour integration window. FSV2 does not converge within this time frame.

4.3 Summary

Pires *et al.* (1996) showed, with the Lorenz (1963) model, that errors aggregate on the unstable subspace of the model. This is the reason for the development of data assimilation in the unstable subspace (Trevisan and Uboldi 2004), which is exactly as it sounds: instead of doing the assimilation on the entire space, observation locations and updates to the analysis are restricted to the unstable subspace. Before this restriction can be accomplished one must first define the unstable subspace. Many of the studies using data assimilation in the unstable subspace use breeding (e.g. Carrassi *et al.* 2008a, 2008b) or orthogonal Lyapunov vectors (e.g. Trevisan and Uboldi 2004; Trevisan *et al.* 2010). Orthogonal Lyapunov vectors are relatively easy to compute but less physically meaningful than LVs which are invariant under the linearized flow (H.-l. Yang *et al.*

2010; Bosetti and Posch 2013; Posch 2013). Thus it would be useful if one could compute the more physically meaningful LVs. Unfortunately we did not have the computational resources to do so.

It is clear the quasi-geostrophic model of Rotunno and Bao (1996) has a single leading Lyapunov vector. All of the bred vectors corresponding to the main mode of growth for the system coalesce into a single vector within the first 5 days of the integration. Even BVs computed using different perturbation amplitudes converge to this same vector (with the growth reduced for larger amplitudes by nonlinear saturation). The SVs fail to converge within this time period. It is possible that testing for convergence at different intervals, i.e. every 72 hours instead of every 24 hours, may aid convergence. It may also be that the SVs require a much longer integration time to allow for convergence. If they need time to experience most of the possible phase space, 6 days is much too short of an integration window to permit convergence. Regrettably longer integration windows are beyond the computational capabilities currently available to us. It is also possible that this particular reference state is making it difficult for the SVs to converge (S.-C. Yang 2005). Even though, theoretically, the choice of norm is unimportant as the integration window extends to infinity (Ginelli et al. 2007; WS07), numerically it is possible SV convergence may be sensitive to this choice, especially when more complex models are being considered. Consequently, because the singular vectors fail to converge within this time frame, it was impossible for us to use the WS07 algorithm to compute the LVs. Ginelli *et al.* (2007) also developed an algorithm to compute physically relevant LVs, but it requires more memory than WS07 if one wants the actual LVs (and not just the angle between them; Ginelli *et al.* 2013).

Although the SVs did not converge in the allotted time, the BVs' convergence offers an interesting result that warrants an examination of a more complex model. Here we have shown that the quasi-geostrophic model has a single leading LV because of the behavior randomly initialized BVs exhibit, something that could be expected from the fact that the QG model has only one type of instability, baroclinic, associated with weather waves. Is it possible to achieve similar results with a more complex model that contains not only baroclinic instability but other types of instabilities associated with convective and Lamb (sound waves) instabilities?

Chapter 5 : BVs and LVs with the SPEEDY Model

5.1 Description of the SPEEDY Model

While the quasi-geostrophic model is a simplification of the atmospheric flow that only includes synoptic (weather) scale motions, the Simplified Parameterizations primitivE-Equation DYnamics (SPEEDY) model is an efficient but realistic hydrostatic general circulation model of the atmosphere. It was developed by Molteni (2003) and includes convection, clouds, large scale condensation, short- and longwave radiation, surface fluxes, and vertical diffusion. Hence SPEEDY has several types of instabilities triggered and saturating at different time scales. The full dynamic equations are solved on a 96 x 48 grid with 7 levels. Horizontal wind, temperature, and specific humidity are defined at all levels while precipitation and pressure are defined at the surface. This leads to 138,240 degrees of freedom. A result of the ease with which this highly realistic model can be run is its use in many studies seeking to improve upon or compare different aspects of the data assimilation process such as localization (e.g. Greybush *et al.* 2011), the assimilation of asynchronous observations (Harlim and Hunt 2008), methods to address model errors (e.g. Li *et al.* 2009b), the simultaneous estimation of observation errors and covariance inflation (e.g. Li *et al.* 2009a), and adaptive inflation (Miyoshi 2011 and the sources therein). We are still interested in targeting the fastest growing instabilities of the model itself. Thus data assimilation techniques are not considered. We did not compute the SVs or LVs for this model because of computational constraints. Instead we focused on the study of the behavior of the BVs in order to elucidate basic

characteristics of the instabilities of this model, and the behavior of BVs in models with multiple types of instabilities, more representative of the real atmosphere. Just as with the quasi-geostrophic model, the kinetic energy norm was used to compute all of the bred vectors.

5.2 Bred Vectors in the SPEEDY Model

Miyoshi (2005) computed bred vectors for this model to study the "errors of the day" (the day-to-day atmospheric variability and resulting errors introduced because of them). This was useful to check the reliability and accuracy of ensemble members. Here we are interested in the dynamics of a complex model, with more than one type of instability, itself. In chapter 3 we were able to use a fast-slow toy atmosphere-ocean model to take advantage of the nonlinear computation of BVs, which allows saturation of fast instabilities, to target fast or slow instabilities through the proper choice of the perturbation amplitude and rescaling window. By contrast, SVs and LVs are linear; so they can only completely isolate the fastest instability of the model.

This is not an exclusive property of simple models. In this chapter we show that we are able to replicate the results with this more complex and realistic model. For the following, we calculated 5 global bred vectors, all beginning from different random perturbations, for each set of breeding parameters. The local dimensions were computed using the method of Patil et al. (2001) as in Chapter 4.

5.2.1 Baroclinic Instabilities

We located the baroclinic instabilities by using an amplitude of 1 m/s (if using winds) or 1 K (if using temperatures) and a rescaling window of 24 hours. These BVs capture best disturbances associated with baroclinic instability within the mid-latitudes. Figure 5.1 shows the results for the 500mb zonal wind (using an amplitude of 1 m/s) and temperature (using an amplitude of 1 K) while Figure 5.2 displays the results for the surface wind and temperature. Figure 5.2(*a*) and (*c*) display two of the five vectors that were computed for the zonal wind and temperature fields, respectively. Figure 5.2(*b*) and (*d*) provide the local ensemble dimensions. The lower the ensemble dimension, the closer the BVs are to converging. Toth and Kalnay (1997) found that in areas of great instability a set of BVs will locally converge and most BVs typically have the same shape, even if they have opposite signs. For both variables displayed in Figure 5.1 and Figure 5.2, the ensemble dimension is highest in the tropics, because the tropics do not have baroclinic instability, and lowest in the extratropics, the Southern Hemisphere in particular. The Southern Hemisphere is much more zonally symmetric than the Northern Hemisphere, aiding the development of clearly defined waves and the growth of instabilities with regular shapes. This facilitates the convergence of BVs with locally low ensemble dimensions as we see at the 500mb and surface levels for the temperature (Figure 5.1(*b*) and Figure 5.2(*b*), respectively) and zonal wind fields (Figure 5.1(*d*) and Figure 5.2(*d*), respectively). In the Northern Hemisphere, orographic forcing and the land-sea contrast distort the shape of the waves, hindering the ability of bred vector convergence. This is pronounced in the temperature fields at the 500mb level. There is a disturbance off the

northeast coast of the United States (Figure 5.1(*a*)); the ensemble dimension in that area is generally lower than that of the tropics but not as low as the Southern Hemisphere ensemble dimension (Figure 5.1(*b*)).

Like the zonal wind fields, the temperature BVs have a higher local dimension around the equator and a lower local dimension in the Southern Hemisphere, although they exhibit more general agreement than the zonal wind BVs. There is a somewhat low local dimension in the winter hemisphere where there is a disturbance off the northeast coast of Canada. The same patterns generally hold at the 500mb level as well (Figure 5.1). Overall there is slightly more agreement among the temperature BVs (a scalar value) than the zonal wind BVs (a portion of a vector value) and the ensemble dimension is higher in the tropics and lowest in the Southern Hemisphere. There is also a slight reduction in the local dimension of the 500mb zonal winds compared to the surface zonal winds.

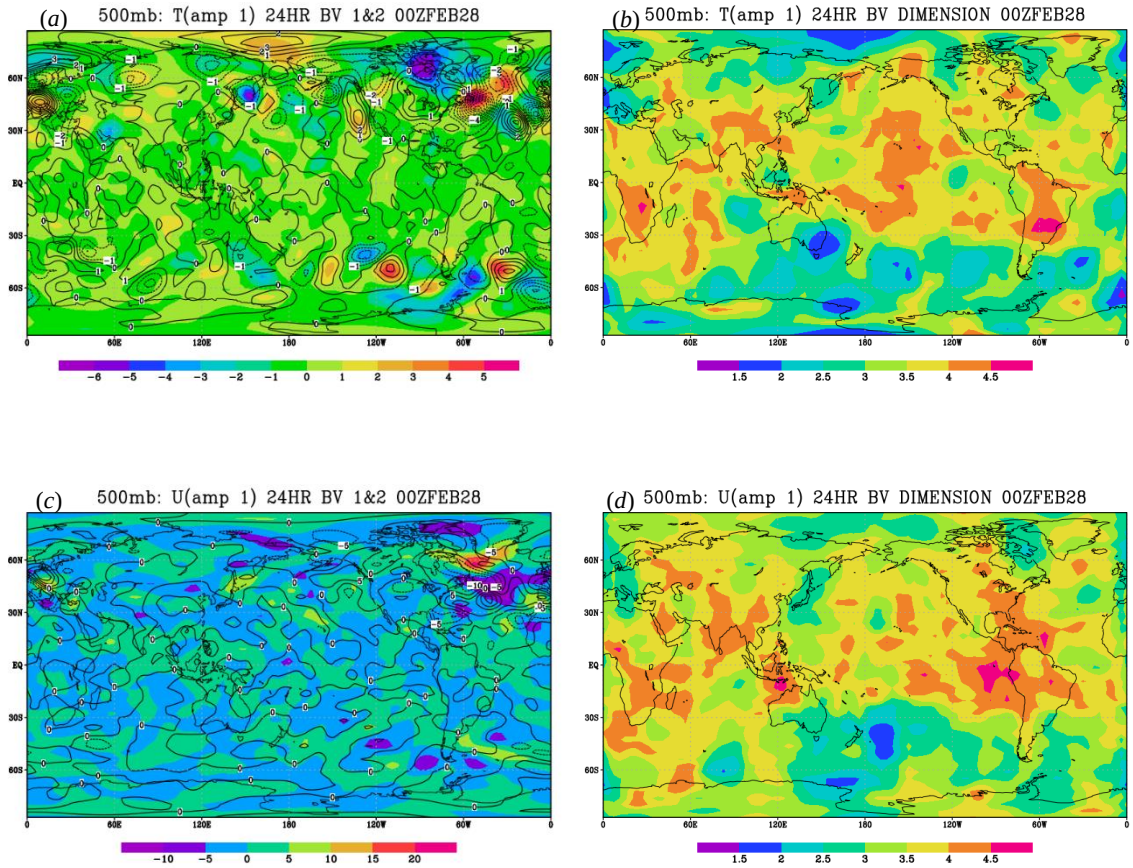

Figure 5.1: (a) Two temperature BVs computed using $\delta_0 = 1$ K and $IW = 24$ hours represented by shading and contours respectively. (b) Dimension of the five temperature BVs computed using $\delta_0 = 1$ K and $IW = 24$ hours. (c) Two of the five zonal wind BVs computed using $\delta_0 = 1$ m/s and $IW = 24$ hours. (d) Dimension of the five zonal wind BVs computed using $\delta_0 = 1$ m/s and $IW = 24$ hours. All vectors are shown at the 500mb level. The BVs exhibit the greatest agreement in the Southern Hemisphere.

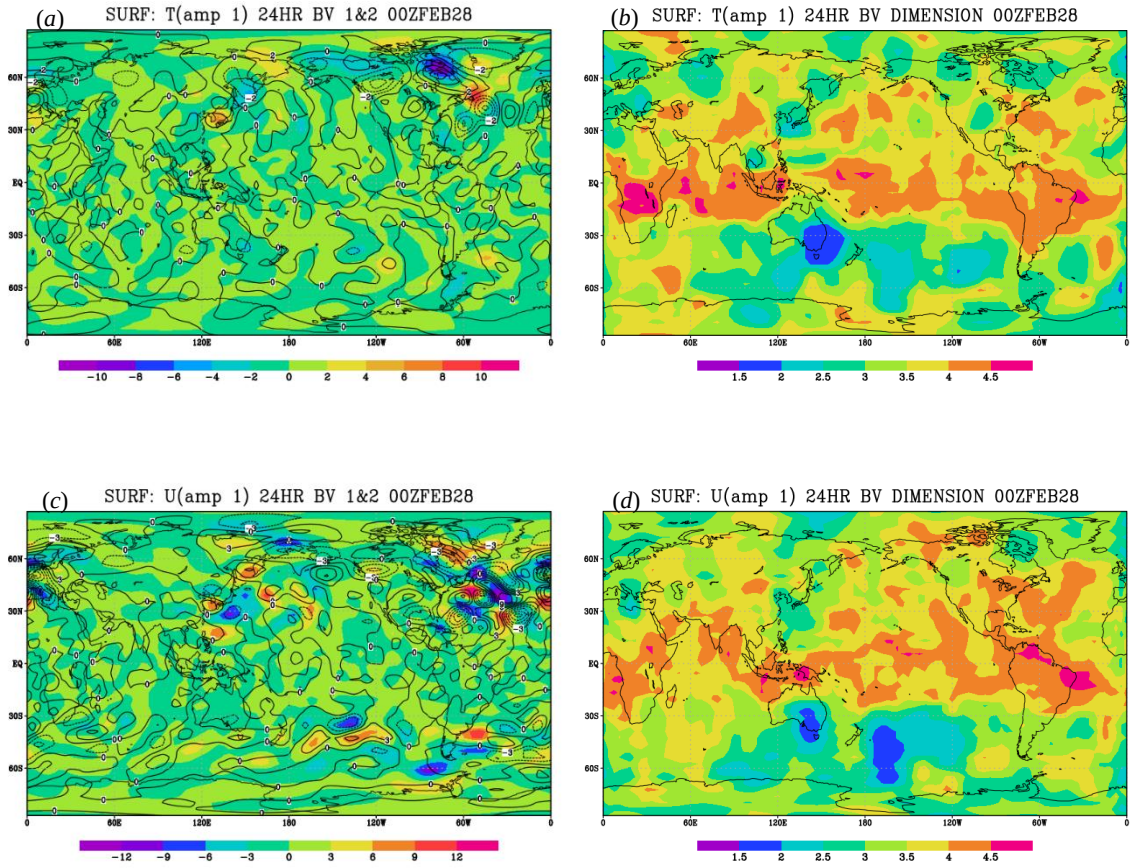

Figure 5.2: Same as Figure 5.1 but at the surface. Thus (a) two temperature BVs computed using $\delta_0 = 1$ K and $IW = 24$ hours. (b) Dimension of the five temperature BVs computed using $\delta_0 = 1$ K and $IW = 24$ hours. (c) Two zonal wind BVs computed using $\delta_0 = 1$ m/s and $IW = 24$ hours. (d) Dimension of the five zonal wind BVs computed using $\delta_0 = 1$ m/s and $IW = 24$ hours. The greatest agreement is in the Southern Hemisphere.

5.2.2 Convective Instabilities

We used BVs to locate the convective instabilities by choosing a perturbation amplitude of 0.01 and a rescaling window of 6 hours. These BVs best capture the disturbances of the tropics where convection is most prominent. Again, there is very little

agreement among the five vectors computed using this combination (Figure 5.3 and Figure 5.4). There is some agreement of all vectors at both the 500mb and surface levels around the 180th meridian, where there are only regionally small disturbances within the model. The 500mb temperature BVs show the lowest ensemble dimension in this area. It is interesting to note that, in general, the local dimension of these vectors is lowest in the tropics and higher in the mid-latitudes which is attributed to the fact that convection is dominant in the tropics (Toth and Kalnay, 1997). This contrasts with the BVs used to target baroclinic instabilities which had greater general agreement in the mid-latitudes, in the Southern Hemisphere in particular, than in the tropics. The same basic pattern holds at the surface (Figure 5.4).

Also, these BVs attain some of their lowest local dimensions in areas of atmospheric disturbances (Toth and Kalnay, 1997). This is especially true of the temperature BVs in relation to the disturbance off the northeast coast of Australia (Figure 5.3(*c*) and (*d*) at the 500mb level; Figure 5.4(*c*) and (*d*) at the surface). Thus the ensemble dimensions of the BVs associated with baroclinic instability and the BVs associated with convective instability achieve their respective minima in the regions of the instabilities they target.

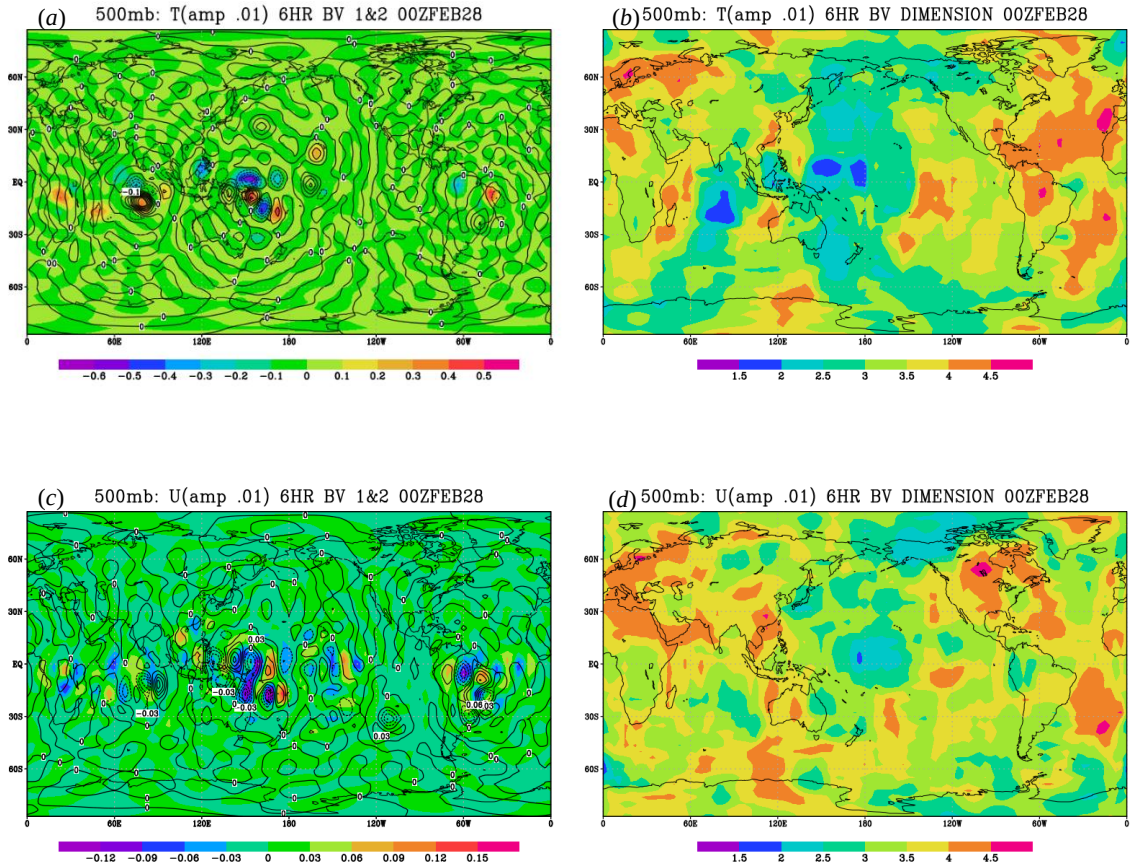

Figure 5.3: (a) Two temperature BVs computed using $\delta_0 = 0.01$ K and $IW = 6$ hours. (b) Dimension of the five temperature BVs computed using $\delta_0 = 0.01$ K and $IW = 6$ hours. (c) Two zonal wind BVs computed using $\delta_0 = 1$ cm/s and $IW = 6$ hours. (d) Dimension of the five zonal wind BVs computed using $\delta_0 = 1$ cm/s and $IW = 6$ hours. All vectors are shown at the 500mb level. The vectors agree most in the tropics.

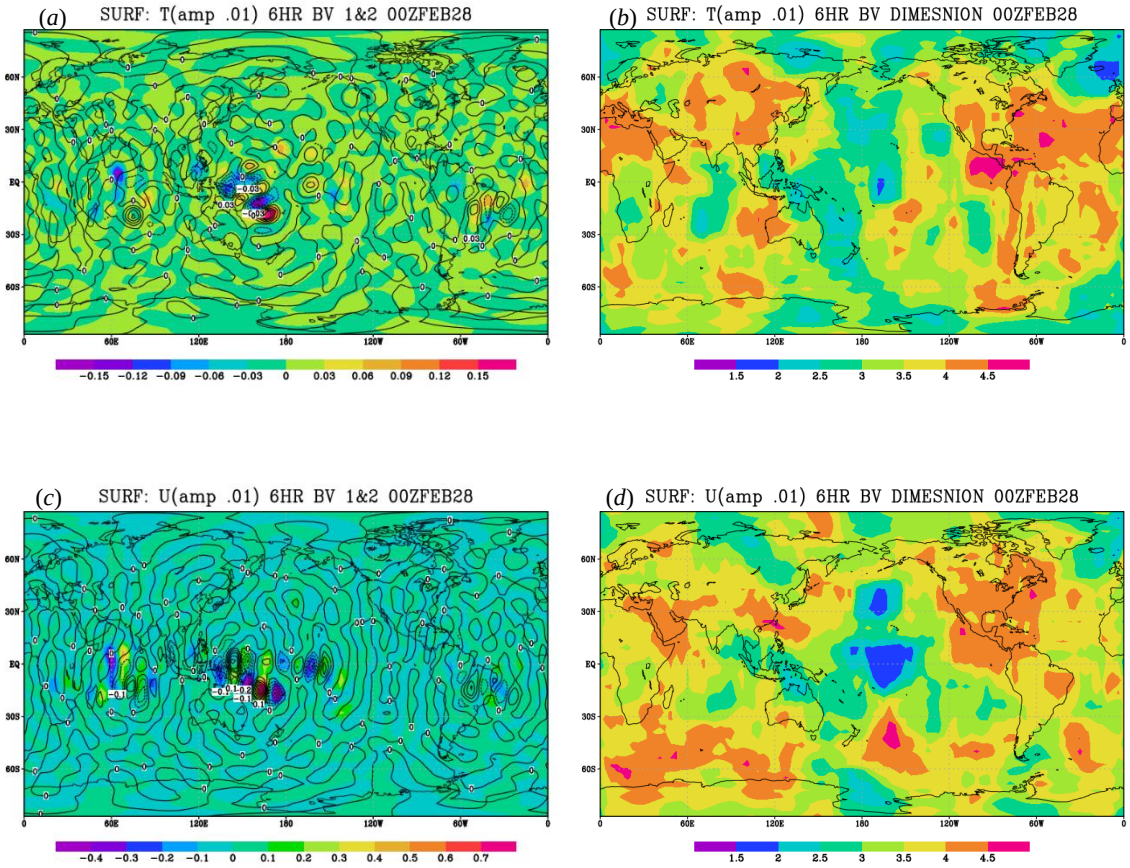

Figure 5.4: Same as Figure 5.3 but at the surface. Thus (a) two temperature BVs computed using $\delta_0 = 0.01$ K and $IW = 6$ hours. (b) Dimension of the five temperature BVs computed using $\delta_0 = 0.01$ K and $IW = 6$ hours. (c) Two zonal wind BVs computed using $\delta_0 = 1$ cm/s and $IW = 6$ hours. (d) Dimension of the five zonal wind BVs computed using $\delta_0 = 1$ cm/s and $IW = 6$ hours. The ED reaches its minimum in the tropics.

5.3.3 Convection Coupled with Lamb Waves with Very Small Amplitudes

Recall BVs are finite time approximations of the leading LVs, and with very small perturbation amplitude and rescaling window, they should become equal to the leading LV. Thus, we took a small amplitude of 0.001 and the minimum possible

rescaling window for this model of 40 minutes (one time period) in an attempt to find the leading Lyapunov vector. Figure 5.6(*a*) and (*c*) displays two of the five surface wind and temperature BVs, respectively, computed using this combination of breeding parameters. Figure 5.6(*b*) and (*d*) give the local dimensions of the five vectors. By the end of the second day, the vectors have indeed merged into a single vector. While the surface temperature BVs require two more breeding cycles to combine, it is clear the 500mb temperature BVs have merged into a single vector at this time (Figure 5.5(*d*)). This provides strong evidence that this is the leading LV for this model. It corresponds to the inertia gravity waves (equivalent to external inertia-gravity waves) excited by strong convection centered at the Warm Pool in the West Pacific. The instability that gives rise to the LV is the intense convection in the warm Maritime continent, which triggers Lamb (sound) waves, akin to external inertia gravity waves that propagate horizontally with the speed of sound (~300 m/s) so that they travel around the world in about one day. Because they propagate so quickly, they create a global leading LV.

Inertia-gravity waves are not the customary targets of weather prediction models, but they are the fastest growing instabilities of the system, exactly what the leading LV detects. It is unlikely that this vector would be useful in the creation of ensembles in weather forecasting applications, but it may be useful in some other application.

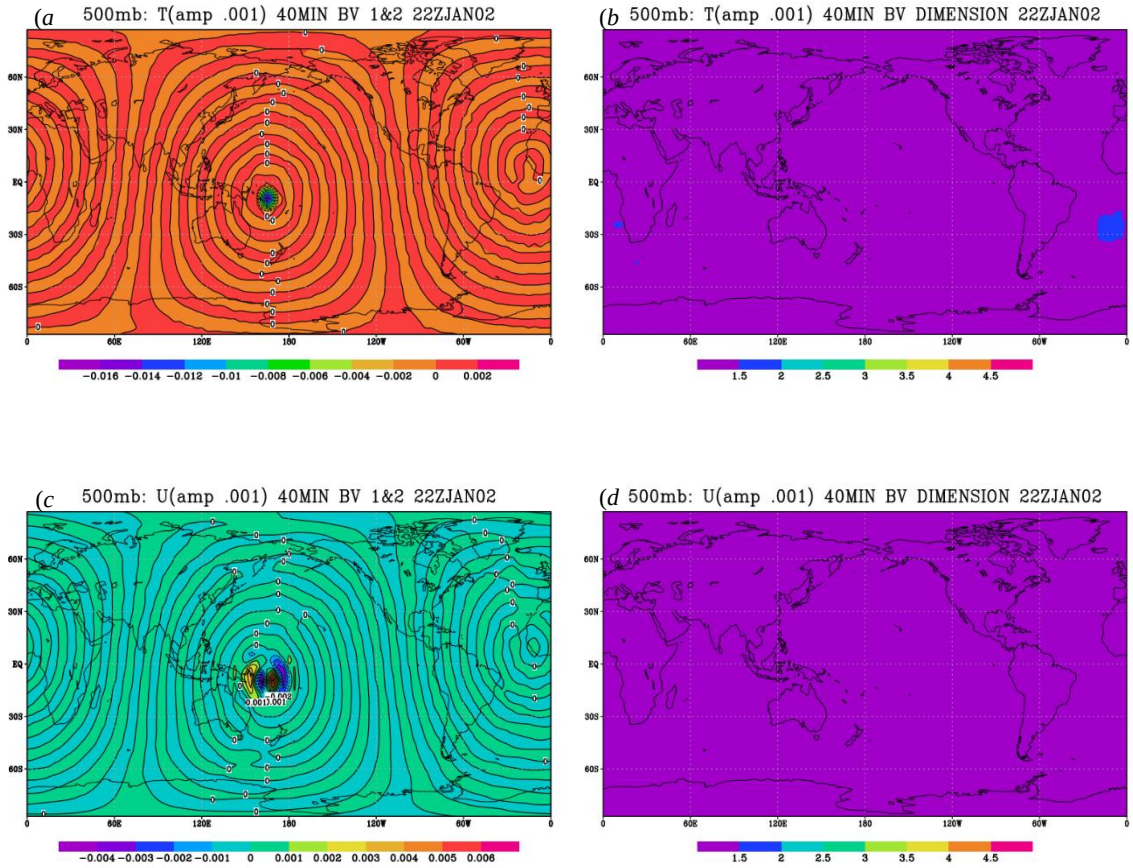

Figure 5.5: (a) Two temperature BVs computed using $\delta_0 = 0.001$ K and $IW = 40$ minutes. (b) Dimension of the five temperature BVs computed using $\delta_0 = 0.001$ K and $IW = 40$ minutes. (c) Two zonal wind BVs computed using $\delta_0 = 1$ mm/s and $IW = 40$ minutes. (d) Dimension of the five zonal wind BVs computed using $\delta_0 = 1$mm/s and $IW = 40$ minutes. All vectors are shown at the 500mb level. The BVs converge by the end of the second day.

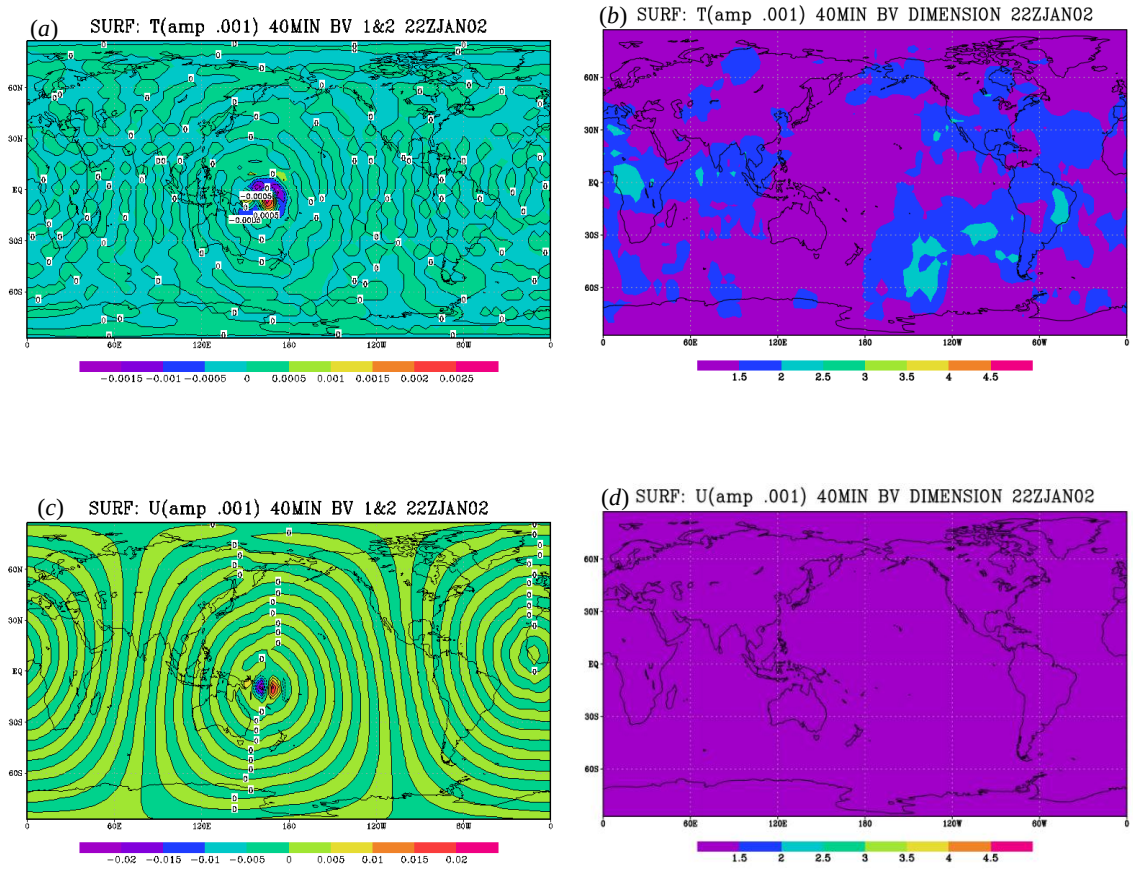

Figure 5.6: Same as Figure 5.5 but at the surface. Thus (a) two temperature BVs computed using $\delta_0 =$ 0.001 K and $IW =$ 40 minutes. (b) Dimension of the five temperature BVs computed using $\delta_0 = 0.001$ K and $IW =$ 40 minutes. (c) Two zonal wind BVs computed using $\delta_0 = 1$ mm/s and $IW =$ 40 minutes. (d) Dimension of the five zonal wind BVs computed using $\delta_0 = 1$ mm/s and $IW =$ 40 minutes. The BVs merge into a single vector, the leading LV for this system.

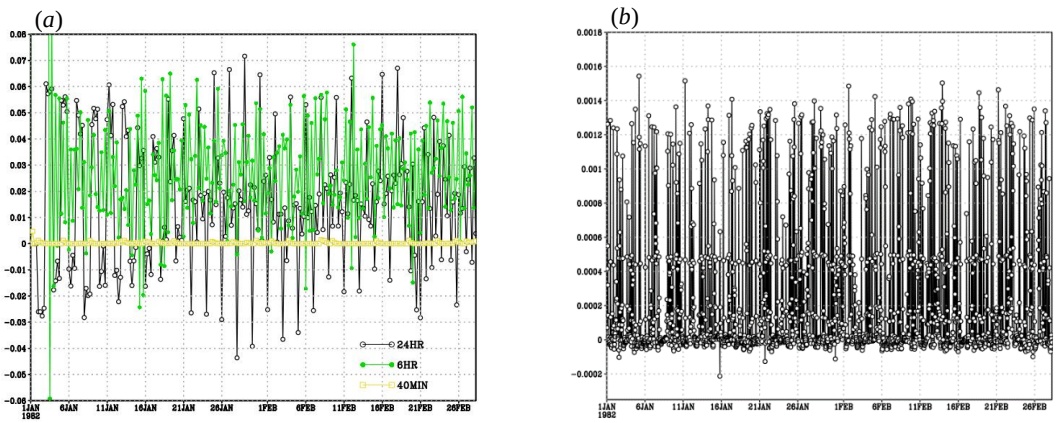

Figure 5.7: (a) Growth rates for the vectors associated with baroclinic instabilities (24HR), convection (6HR), and inertia gravity waves (40MIN). Although the global growth rate appears constant for the gravity waves, (b) demonstrates that it is not. This value is small relative to the other growth rates because in most regions around the world, the vector is not growing.

The growth rates of the BVs (computed using the formula in section 1.2, here with an integration of forty minutes) associated with fast convection triggering inertia gravity waves differ greatly from the growth rates of the BVs associated with baroclinic and convective instabilities, as seen in Figure 5.7(*a*). Its values are so small (but not constant as Figure 5.7(*b*) demonstrates) because the vectors are only growing at the center of the disturbance and we measure the global growth. Hence the essentially zero values dampen the effects of the super growth at the center of the disturbance.

5.3 Summary

Molteni's (2003) SPEEDY model is a very successful simplification to general atmospheric circulations. It has several different types of instabilities with various saturation levels, making it a perfect model to test the behavior of bred vectors. Here we

see BVs are able to easily target three types of instabilities, baroclinic, convective, and inertia gravity waves triggered by convection, through proper selection of the breeding parameters. This result agrees with the results of S.-C. Yang *et al.* (2006b, 2008, 2009b) and Chikamoto *et al.* (2007) who used more complex models. Because BVs only require the use of the nonlinear model, they were the only vectors of the three kinds frequently computed to study dynamic instabilities that are currently feasible for this complex model. While we were unable to directly compute LVs, we can be fairly sure from the behavior of the BVs highlighting gravity waves that the leading LV exists for this weather model, contrary to the hypothesis of Toth and Kalnay (1997). Hence it may be worth the effort of finding the first few leading LVs in order to ascertain the information they can unlock about this simplified weather model.

Chapter 6 : Summary and Conclusions

Lyapunov vectors, singular vectors, and bred vectors are the three types of vectors normally used to study instability properties of dynamical systems. Each can provide the general shape and growth rates of the instabilities inherent within a particular system. This is extremely important for numerical weather predictions for the instabilities are a major source of error, along with model and observation errors, leading to the degradation of forecasts. Efficiently eradicating, or precisely measuring, any one of these errors would be tremendously beneficial, and LVs, SVs, and BVs are currently the most promising weapon against errors stemming from instabilities intrinsic to dynamical systems. Lyapunov and singular vectors locate instabilities within a system through the use of the linearized equations of the model. Bred vectors use the full nonlinear model. Their differences in computation lead to differences in their ability to effectively target particular instabilities, and this thesis explored these differences.

We began by expanding upon the work of Evans *et al.* (2004) and PK04 to reveal the growth rates of singular vectors and Lyapunov vectors can be used in the same manner as the growth rates of bred vectors to predict regime changes in a simple chaotic model. That is, fast growth implies a regime change, and the longer the BVs grow the longer the next regime will be. SVs are the most accurate when predicting regime changes in the Lorenz (1963) model. The LVs are also accurate in predicting regime changes. Not only are their local growth rates useful, but the correlation between LV1 and LV2 can also be used to predict regime changes, as the two become nearly orthogonal to one another in the center of multi-orbit regimes, and at the point when x

changes signs for single orbit regimes of the Lorenz model. Although LV1, fast scale BVs, and FSV1 all have slightly different behavior, they all coalesce to approximately the same subspace during periods of fast growth, which also correspond to regime changes. This is expected since all three describe the errors growing fastest in the past; ISVs are not expected to be similar to any of these as they describe the errors of perturbations mostly outside the attractor, growing fastest in the immediate future as they rotate back to the attractor (Pazó *et al.*, 2010).

In fact, in the Lorenz model, LV1, the leading Lyapunov vector, is approximately equal to (linear) bred vectors that have a small amplitude of 0.1 and are rescaled every 0.02 units, indicating that they both measure the same instabilities. LV1 has a large correlation with the (slightly) nonlinear bred vectors which have an initial perturbation of 1 and are rescaled every 0.08 time units; LV2 is highly correlated with both of these BVs as well, and as the BVs become more nonlinear (yet still dynamically significant) they coincide more with LV2 and less with LV1. Also, although LV2 has zero global growth, locally its growth is frequently faster than that of LV1's, and at these times the slightly nonlinear BV grows much closer to LV2.

The coupling of the nine-variable model, and the introduction of two very different time scales, to represent a toy atmosphere-ocean model, obscures some of the clear cut relationships the LVs, SVs, and BVs shared in the simple Lorenz model, so that the correlations of the LVs become useless as predictors, but some of the relationships found above still hold. The local growth rates of the LVs are still useful in making predictions in the model, with certain LVs being more closely related to different modes of growth within the model, although increased coupling degrades these relationships.

Thus the Lyapunov vectors associated with the extratropical subsystem are not as influenced by changes in the tropical and ocean subsystems because the extratropics are only weakly coupled to the tropics. In contrast the Lyapunov vectors associated with the strongly coupled ocean subsystem have times when they are strongly influenced by changes in the tropical subsystem and even changes in the extratropical subsystem (which the ocean is implicitly coupled to by its connection with the tropical subsystem). The slower mode LVs' inability to fully decouple the fast and slow subsystems may be a result of the fast changes of the extratropical subsystem being difficult to overcome or ignore. It may also be a deficiency of the algorithm to compute LVs which relies on linearized equations because these will always target the fastest growing errors. If the latter is the case, it is truly impressive that the vectors are able to detect the slower modes of growth as well as they do.

Regardless, LVs are not nearly as efficient at separating the fast and slow modes of the coupled system as the bred vectors are, and this is an important result. Through careful selection of perturbation size and rescaling interval, BVs are able to efficiently decouple and identify the fast and slow modes of growth in the nine-variable model. Thus not only are they much easier to compute than LVs, they are better predictors of slow mode growth, which agrees with the experience of S.-C. Yang *et al.* (2006b, 2008, 2009b) who derived the BVs associated with ENSO in fully coupled atmosphere-ocean global climate models (GCMs). Similarly, Chikamoto *et al.* (2007) were also able to derive the BVs associated with the Madden-Julian Oscillation as well as those associated with convective instabilities by using different BV amplitudes and rescaling periods.

SVs are not as useful as LVs or BVs in the coupled model with an extratropical subsystem. They are able to capture fast modes of growth, but are unable to decouple the slow modes from the fast modes in the same way the BVs, or even the LVs, are able to, failing to perceive their existence at all regardless of the optimization window used to compute them.

When the extratropical subsystem of the nine-variable model is replaced with a fast changing "convective subsystem", resulting in different frequencies for all three subsystems, the behaviors of the vectors change slightly again. The LVs retain the ability to separate all three subsystems, but there are some that are 'coupled.' They refuse to be dominated by either the tropical or ocean subsystems but instead manage to remain loyal to both. The length of the periods of growth of the 'coupled' vectors determine which subsystem the growth references. Thus long periods of growth correspond to changes within the ocean subsystem and shorter periods of growth correspond to changes within the tropical subsystem.

The BVs are still unable to completely perceive the existence of the tropical subsystem, which is still controlled by changes within the ocean subsystem, but the SVs can now distinguish between all three subsystems. There are even 'coupled' SVs whose growth rates correspond to changes within the tropical and ocean subsystems. The amount of coupling between the convective and tropical subsystems changed the number of SVs and LVs that corresponded to each subsystem, but it does not significantly change the behavior of the three types of vectors.

When studying the quasi-geostrophic model developed by Rotunno and Bao (1996), which is ruled by a single type of growth (baroclinic instability), it is evident that

there is a single leading LV since five initially random BVs merge into a single vector after a few days. Unfortunately, the SVs failed to converge within the same time period making it impossible to use the Wolfe-Samelson (2007) algorithm to compute the LVs. It is possible the SVs need an integration window long enough to test a significant portion of the phase space in order to allow for convergence. It is unlikely the algorithm of Ginelli *et al.* (2007) would fare better with this model since it also requires the convergence of a set of orthogonal vectors, although it is possible the QR decomposition would prove to be more robust and efficient than the singular vector decomposition WS07 is based upon. There have been minor comparisons of the two methods for obtaining LVs which are invariant under the linear flow in terms of theory (Kuptsov and Parlitz 2012) and computational costs (Ginelli *et al.* 2013), but no one has compared the two methods using a single model. Thus further testing is necessary to determine which of the two methods is best and under what circumstances.

Finally we come to the most realistic of the models examined here, the SPEEDY model of Molteni (2003). It has the most degrees of freedom and instabilities of several time scales, and is similar to modern global atmospheric models. Through careful selection of the breeding parameters we were able to identify baroclinicity, convection, and external inertia-gravity waves. The Lamb waves (equivalent to external inertia-gravity waves) are the fastest growing instabilities triggered by local tropical convection, propagating with the speed of sound, and the BVs associated with these waves quickly collapsed into a single global vector. This is most likely the leading LV for this model. Owing to SPEEDY being a reasonable approximation of atmospheric general circulation models (GCMs), this provides strong evidence of the existence of a single leading LV in

the earth's atmosphere-ocean system as promised by Oselecec's theorem (1968). The real earth's leading LV would thus coincide with external inertia-gravity waves, meaning it would not be of any use for the weather prediction ensembles for which bred vectors were initially created (Toth and Kalnay 1993).

These results have several significant implications for 'real life' atmospheric and oceanic models. The first is that each of the three vectors that have been used to study the dynamic behavior of unstable systems provides significant information, and, for the Lorenz three-variable model, the SVs are the best predictors of regime change. In contrast to LVs and SVs, BVs do not conserve their identity, but grow closer to the *locally* fastest growing LV, even when it is different from LV1, the leading LV. The BVs seem to follow the fastest local 'growth of opportunity,' which agrees with the experience in ensemble weather forecasting (Toth and Kalnay 1997). For the problem of instabilities that have different time scales, all three types of vectors can handle the fastest instabilities, but only BVs are able to completely separate the slow instabilities from the fast instabilities, and only if choosing long time scales and rescaling variables associated with the slow instabilities (PK04; S.-C. Yang *et al.*, 2006, 2008, 2009; Chikamoto *et al.* 2007; Hoffman *et al.* 2009).

Previously, only orthogonal LVs were computed for systems, typically using Benettin *et al.* (1980) or Shimada and Nagashima (1979). The work of Wolfe and Samelson (2007) and Ginelli *et al.* (2007) made it possible to compute Lyapunov vectors (often referred to as covariant or characteristic Lyapunov vectors or CLVs) that are invariant under the linearized flow and correspond to the Lyapunov exponents of Oseledec's multiplicative ergodic theorem (1968). Bosetti and Posch (2013), H.-l. Yang

et al. (2010), and Posch (2013) found (covariant or characteristic) LVs – all using the method of Ginelli *et al.* (2007) – are more physically meaningful than the orthogonal LVs found previously. Here we use the Wolfe–Samelson algorithm for computing LVs. It has proven to be very robust for simple models, and the results are promising for LVs' abilities to characterize instabilities of various sizes. The work of Ginelli *et al.* (2007) also demonstrates LVs are useful in identifying local stable and unstable subspaces in simple systems. Froyland *et al.* (2013) expanded the algorithms of Ginelli *et al.* (2007) and WS07 to compute LVs for complex models. Kuptsov and Parlitz (2012) developed an algorithm similar to WS07 without some of the redundant computations while also completing a theoretical comparison of the methods, but no one has tested the algorithms using models with as many degrees of freedom as the quasi-geostrophic or SPEEDY models. Their work suggests that further studies are still needed to test the usefulness of LVs as predictors and the exact manner in which the algorithms distinguish between specific instabilities within systems containing different modes of growth.

Of the three types of vectors, bred vectors are by far the easiest and cheapest to compute. They are also the most reliable, efficiently distinguishing between distinct modes of growth through appropriate selection of the perturbation amplitude and breeding window. The advantage of the BVs in identifying both the fast and the slow instabilities comes from the fact that they are computed with differences using the full nonlinear model. So for the limit of very small amplitude in the BVs' rescaling, they become the same as the leading LVs. However, when larger amplitudes are used for rescaling, the fast perturbations become saturated, and the BVs capture slower, larger amplitude instabilities. If the fast instabilities have larger amplitudes than the slow

instabilities, as it happens with the El Niño Southern Oscillations (ENSO) coupled atmosphere-ocean instabilities, modifying the rescaling amplitude does not lead to the BVs recovering the slow instabilities. In this case it is still possible to use BVs to recover ENSO by using rescaling intervals that are long enough that the fast weather noise becomes saturated. S.-C. Yang et al. (2006, 2008, 2009b) was thus able to recover BVs of the ENSO instabilities by rescaling once a month, too long for weather instabilities but short enough for ENSO. Our results within the SPEEDY model also provide evidence of a single leading LV for atmospheric models. However, this global leading LV, similar to external inertia-gravity waves propagating with the speed of sound, may be irrelevant to real world numerical weather prediction as far as the creation of ensemble members is concerned.

We have found that in simple models with one type of instability, LVs, SVs, and BVs provide the same information. If the BVs are computed with a small amplitude and short rescaling window they will equal the leading LV, which was used to determine the existence of the leading LV in the more complex QG and SPEEDY models. However, if the BVs are calculated with bigger amplitudes and longer windows, yet still relevant to the model, they will break free of the leading LV and align with the locally fastest growing vector. This is one of the reasons why BVs computed and used for ensembles in atmospheric models do not collapse into a single vector, as some atmospheric dynamics experts believed they would when Toth and Kalnay first developed them.

Another major reason BVs that are used for ensembles in weather prediction do not coalesce into a single vector is because there is no global leading Lyapunov vector for each type of instability. This is clearest in the SPEEDY model where the BVs associated

with baroclinic and convective instabilities refused to converge, but it is also apparent in the toy atmosphere-ocean model. Here the LVs never succeeded in fully decoupling the slow modes of growth from the fast modes of growth like the BVs were able to do. They always contained remnants of the fast modes of growth, evidenced by their growth rates which were often influenced by changes in the faster subsystems (see chapter 3). So take a large system like the atmosphere or ocean where energetic baroclinically unstable waves are generated in several regions of the world simultaneously. Because the scales of the instabilities are an order of magnitude smaller than the size of the atmosphere, the unstable waves are generated, grow until they saturate, and then decay independently in different regions. So it is not surprising that a global leading LV associated with baroclinic waves cannot form.

But does this mean LVs are useless? Unfortunately this thesis cannot definitively answer that question. Although there are more efficient algorithms for computing LVs, I do not have the computational resources to take advantage of them. It may be that the 'coupled' nature of LVs is not a hindrance but instead allows them to glean information from a complex system that we hitherto cannot obtain. Can LVs be determined that are associated with fast weather and slow coupled instabilities in a coupled atmosphere-ocean model? If they can be, and these vectors are truly characteristic of the system, then they should behave in a manner similar to the LVs studied here which can still be used as predictors for the systems. Even if they are not characteristic of the dynamics of the system, but instead attributes of the model, could they still be useful in ensemble forecasting? These are just a few of the many questions waiting to be answered.

Bibliography

Annan, J. D, 2004: On the orthogonality of bred vectors. *Mon. Wea. Rev.,* **132,** 843–9.

Benettin, G., L. Galgani, A, Giorgilli, and J. M. Strelcyn, 1980: Lyapunov characteristic exponents for smooth dynamical systems and for Hamiltonian systems: a method for computing all of them. *Meccanica,* **15,** 21–30.

Boffetta, G., P. Giuliani, G. Paladin, and A. Vulpiani, 1998: An extension of the Lyapunov analysis for the predictability problem. *J. Atmos. Sci.,* **125,** 3409–3416.

Bosetti, H. and H. A. Posch, 2013: Orthogonal versus covariant Lyapunov vectors for rough hard disc systems. *J. Phys A: Math. Theor.,* **46,** 254011.

Buizza, R., J. Tribbia, F. Molteni, and T. Palmer, 1993: Computation of optimal unstable structures for a numerical weather prediction model. *Tellus,* **45A,** 388-407.

Carrassi, A., M. Ghil, A. Trevisan, and F. Uboldi, 2008a: Data assimilation as a nonlinear dynamical systems problem: Stability and convergence of the prediction assimilation system. *Chaos,* **18,** 023112.

Carrassi, A., A. Trevisan, L. Descamps, O. Talagrand, and F. Uboldi, 2008b: Controlling instabilities along a 3DVAR analysis cycle by assimilating in the unstable subspace: a comparison with the EnKF. *Nonlin. Proc. Geophys.,* **15,** 503-521.

Carrassi, A., A. Trevisan, and F. Uboldi, 2007: Adaptive observations and assimilation in the unstable subspace by breeding on the data-assimilation system. *Tellus,* **59A,** 101-113.

Chikamoto, Y., H. Mukougawa, T. Kubota, H. Sato, A. Ito, and S. Maeda, 2007: Evidence of growing bred vector associated with the tropical intraseasonal oscillation. *Geophys. Res. Lett.*, **34,** L04806.

Corazza, M., E. Kalnay, D. J. Patil, S.-C. Yang, R. Morss, and co-authors, 2003: Use of the breeding technique to estimate the structure of the analysis "error of the day." *Nonlin. Proc. Geophys.*, **10,** 233-243.

Errico, R. M. and T. Vukicevic, 1992: Sensitivity analysis using an adjoint of the PSU-NCAR mesoscale model. *Mon. Wea. Rev.*, **120,** 1644–1660.

Evans, E., N. Bhatti, J. Kinney, L. Pann, M. Peña, S-C Yang, E. Kalnay, and J. Hansen, 2004: RISE undergraduates find the regime changes in Lorenz's model are predictable. *Bull. Am. Meteorol. Soc.,* 520–524.

Froyland, G., T. Hüls, G. P. Morriss, and T. M. Watson, 2013: Computing covariant Lyapunov vectors, Oseledets vectors, and dichotomy projectors: a comparative numerical study. *Phys. D,* **247,** 18–39.

Ginelli, F., H. Chaté, R. Livi, and A. Politi, 2013: Covariant Lyapunov vectors. *J. Phys. A: Math. Theor.*, **46,** 254005.

Ginelli, F., P. Poggi, A. Turchi, H. Chaté, R. Livi, and A. Politi, 2007: Characterizing dynamics with covariant Lyapunov vectors. *Phys. Rev. Lett.*, **99,** 130601.

Greybush, S. J., E. Kalnay, T. Miyoshi, K. Ide, and B. R. Hunt, 2011: Balance and ensemble Kalman filter localization techniques. *Mon. Wea. Rev.*, **139,** 511-522.

Harlim, J. and B. R. Hunt, 2007: Four-dimensional local ensemble transform Kalman filter: Numerical experiments with a global circulation model. *Tellus,* **59A,** 731-748.

Hoffman, M. J., E. Kalnay, J. A. Carton, and S.-C. Yang, 2009: Use of breeding to detect and explain instabilities in the global ocean. *Geophys. Res. Lett.*, **36,** L12608.

Holton, J., 2004: *An Introduction to Dynamic Meteorology Fourth Edition.* Burlington: Elsevier Academic Press, pp. 147-151.

Kobayashi, M. U. and Y. Saiki, 2014: Manifold structures of unstable periodic orbits and the appearance of periodic windows in chaotic systems. *Phys. Rev. E,* **89,** 022904.

Kuptsov, P. V., 2013: Violation of hyperbolicity via unstable dimension variability in a chain with local hyperbolic chaotic attractors. *J. Phys. A: Math. Theor.*, **46,** 254016.

Kuptsov, P. V. and U. Parlitz, 2012: Theory and computation of covariant Lyapunov vectors. *J. Nonlinear Sci.*, **22,** 727-762.

Legras, B. and R. Vautard, 1996: A guide to Liapunov vectors. *Proc. European Centre for Medium-Range Weather Forecasts Seminar on Predictability (Reading, UK)* vol I, pp 143–56.

Li, H., E. Kalnay, and T. Miyoshi, 2009a: Simultaneous estimation of covariance inflation and observation errors within an ensemble Kalman filter. *Quart. J. Roy. Meteorol. Soc.*, **135,** 523-533.

Li, H., E. Kalnay, T. Miyoshi, and C. M. Danforth, 2009b: Accounting for model errors in ensemble data assimilation. *Mon. Wea. Rev.*, **137,** 3407-3419.

Lorenz, E. N., 1963: Deterministic non-periodic flow *J. Atmos. Sci.*, **20,** 130–141.

Lorenz, E. N., 1965: A study of the predictability of a 28-variable atmospheric model. *Tellus*, **17A,** 321–333.

Lorenz, E. N., 1996: Predictability—a problem partly solved *Proc. European Centre for Medium-Range Weather Forecasts Seminar on Predictability (Reading, United Kingdom),* pp 1–18.

Miyoshi, T., 2005: Ensemble Kalman filter experiments with a primitive-equation global model. Ph.D. dissertation, University of Maryland, College Park. 197 pp.

Miyoshi, T., 2011: The Gaussian approach to adaptive covariance inflation and its implementation with the local ensemble transform Kalman filter. *Mon. Wea. Rev.*, **139,** 1519-1535.

Molteni, F. and T. N. Palmer, 1993: Predictability and finite-time instability of the northern winter circulation. *Quart. J. Roy. Meteorol. Soc.,* **119,** 269–98.

Norwood, A., E. Kalnay, K. Ide, S.-C. Yang, and C. Wolfe, 2013: Lyapunov, singular and bred vectors in a multi-scale system: an empirical exploration of vectors related to instabilities. *J. Phys A: Math Theor.,* **46,** 254021.

Oseledec, V., 1968: A multiplicative ergodic theorem. Lyapunov characteristic numbers for dynamical systems. *Trans. Moscow. Math. Soc.,* **19,** 197–231.

Palmer, T. N., R. Gelaro, J. Barkmeijer, and R. Buizza, 1998: Singular vectors, metrics, and adaptive observations. *J. Atmos. Sci.,* **55,** 633-653.

Patil, D. J., B. R. Hunt, E. Kalnay, J. Yorke, and E. Ott, 2001: Local low dimensionality of atmospheric dynamics. *Phys. Rev. Lett.,* **86,** 5878-5881.

Pazó, D., M. A. Rodríguez, and J. M. López, 2010: Spatio-temporal evolution of perturbations in ensembles initialized by bred, Lyapunov and singular vectors. *Tellus,* **62A,** 10–23.

Peña, M. and E. Kalnay, 2004: Separating fast and slow modes in coupled chaotic systems. *Nonlin. Proc. Geophys.,* **11,** 319–27.

Pires, C., R. Vautard, and O. Talagrand, 1996: On extending the limits of variational assimilation in nonlinear chaotic systems. *Tellus,* **48A,** 96-121.

Posch, H. A., 2013: Symmetry properties of orthogonal and covariant Lyapunov vectors and their exponents. *J Phys. A: Math. Theor.,* **46,** 254006.

Saiki, Y. and M. U. Kobayashi, 2010: Numerical identification of nonhyperbolicity of the Lorenz system through Lyapunov vectors. *JSIAM Lett.,* **2,** 107-110.

Shimada, I. and T. Nagashima, 1979: A numerical approach to ergodic problem of dissipative dynamical systems. *Prog. Theor. Phys.,* **61,** 1605-1615.

Snyder, C., T. M. Hamill, and S. B. Trier, 2003: Linear evolution of error covariances in a quasigeostrophic model. *Mon. Wea. Rev.,* **131,** 189-205.

Snyder, C. and A. Joly, 1998: Development of perturbations within growing baroclinic waves. *Q.J.R. Meteorol. Soc.,* **124,** 1961-1983.

Toth, Z. and E. Kalnay, 1993: Ensemble forecasting at NMC: the generation of perturbations. *Bull. Am. Meteorol. Soc.,* **74,** 2317–2330.

Toth, Z. and E. Kalnay, 1997: Ensemble forecasting at NCEP and the breeding method. *Mon.Wea. Rev.,* **125,** 3297–319.

Trevisan, A., M. D'Isidoro, and O. Talagrand, 2010: Four-dimensional variational assimilation in the unstable subspace (4DVAR-AUS) and the optimal subspace dimension. *Quart. J. Roy. Meteor. Soc.,* **136,** 487-496.

Trevisan, A. and R. Legnani, 1995: Transient error growth and local predictability: a study in the Lorenz system. *Tellus*, **47A,** 103–117.

Trevisan, A. and F. Pancotti, 1998: Periodic orbits, Lyapunov vectors, and singular vectors in the Lorenz system. *J. Atmos. Sci.*, **55,** 390–8.

Trevisan, A. and F. Uboldi, 2004: Assimilation of standard and targeted observations within the unstable subspace of the observation-analysis-forecast cycle system. *J. Atmos. Sci.*, **61,** 103-113.

Uboldi, F., A. Trevisan, and A. Carrassi, 2005: Developing a dynamically based assimilation method for targeted and standard observations. *Nonlin. Proc. Geophys.*, **12,** 149-156.

Wolfe, C. L. and R. M. Samelson, 2007: An efficient method for recovering Lyapunov vectors from singular vectors. *Tellus*, **59A,** 355–366.

Yang, H.-l. and G. Radons, 2010: Comparison between covariant and orthogonal LVs. *Phys. Rev. E*, **82,** 046204.

Yang, H.-l., K. A. Takeuchi, F. Ginelli, H. Chaté, and G. Radons, 2009: Hyperbolicity and the effective dimension of spatially extended dissipative systems. *Phys. Rev. Lett.*, **102,** 074102.

Yang, S.-C., 2005: Bred vectors in the NASA NSIPP Global Coupled Model and their application to coupled ensemble predictions and data assimilation. Ph.D. thesis. University of Maryland, College Park. 174 pp. [Available online at http://handle.net/1903/2477].

Yang, S.-C., D. Baker, H. Li, M. Huff, G. Nagpal, and co-authers, 2006a: Data assimilation as synchronization of truth and model: experiments with the 3-variable Lorenz system. *J. Atmos. Sci.*, **63,** 2340-2354.

Yang, S.-C., M. Cai, E. Kalnay, M. Rienecker, G. Yuan, and Z. Toth, 2006b: ENSO bred vectors in coupled ocean-atmosphere general circulation models. *J. Clim.*, **19,** 1422–1436.

Yang, S.-C., M. Corazza, A. Carrassi, E. Kalnay, and T. Miyoshi, 2009a: Comparison of local ensemble transform Kalman filter, 3DVAR, and 4DVAR in a quasigeostrophic model. *Mon. Wea. Rev.*, **137,** 693-709.

Yang, S.-C., E. Kalnay, M. Cai, and M. Rienecker, 2008: Bred vectors and tropical pacific forecast errors in the NASA coupled general circulation model *Mon. Wea. Rev.*, **136,** 1305–1326.

Yang, S.-C., E. Kalnay, and T. Enomoto, 2015: Ensemble Singular Vectors and their use as additive inflation in EnKF. *Tellus*, In press.

Yang, S.-C., C. Keppenne, M. Rienecker, and E. Kalnay, 2009b: Applications of coupled bred vectors to seasonal-to interannual forecasting and ocean data assimilation. *J. Clim.*, **22,** 2850–2870.